Quantum Quenches in Closed and Open Spin Chains: A Thesis in Two Parts

Jacob Robertson
Merton College
University of Oxford

A thesis submitted for the degree of
Doctor of Philosophy

Trinity 2024

Acknowledgements

Funding

This work was supported by the Engineering Physical Sciences Research Council UK, project reference 2397290, as part of the Oxford Doctoral Training Program supported by the grant EP/R513295/1.

Personal

During my DPhil I have relied on the friendship and encouragement of a great number of people, without whom I am sure this thesis would not have been written, and who it would be foolish to attempt to list all of. Nonetheless, allow me thank my friends Elisabeth Le Maistre, Jack McIntyre, Dylan Price, Daniel Sherlock and Julia Stadlmann for their role in keeping the institution that is board games night alive even after most of them graduated and went their separate ways; thanks also to Sarah Scripps, one of my oldest friends, who I was unexpectedly reunited with when she began a DPhil in 2023. Large thanks are also due to my office mates: Jonathan Classen-Howes, Jovan Jovanović and Minghao Li; who are always eager to take part in any discussion from physics to Balkan history or Chinese archaeology. Due thanks also go to all of my friends from Oxford University Quiz Society, including Oli Clarke, Alexander Gunasekera and Oliver Hargrave, alongside whom I was privileged to play at many tournaments. Of past OUQS committees I distinctly want to thank Ella Warde and Eliza Dean for all their help with room bookings which would otherwise have probably caused me to tear the rest of my hair out. I also wish to deeply thank my lovely partner Aarti Prajapati, who provided continual encouragement to me whilst writing this thesis.

An especially large debt of gratitude is owed to my DPhil brother, Riccardo Senese, with whom I have immensely enjoyed many long conversations as we tried to puzzle out some thorny problem or other, and who co-authored two of the papers on which this thesis is based. I am thankful to Aleksandra Ziółkowska for helpful discussions with her at the beginning of my DPhil when working on what would become Chapter 6. I am very grateful to Bruno Bertini for providing me with the

second Born approximation code used in Chapter 4. Next, I would like to give a sincere thanks to my supervisor Fabian Essler; his ability to cut to the core of any issue makes him a demanding but educational mentor. Over the course of my DPhil he has tirelessly worked to ensure my work was as good as it could be. Endless thanks go to all my family for their support, love and advice throughout not just these last years but my entire life. Lastly, I cannot adequately thank Leonie Woodland for being my firmest friend and for making my entire time at Oxford a blessing.

Abstract

This thesis is concerned with three studies of far from equilibrium dynamics in quantum spin chains. In all cases the nonequilibrium dynamics is generated by a protocol called a 'quantum quench', describing the time evolution after a sudden change in system parameters. Part A is concerned with closed systems, meaning those isolated from their environment and begins with Chapter 1, which introduces the quench protocol and motivates the study of quantum quenches through examples of its experimental relevance before providing a short survey of known theoretical results that will enable the reader to interpret the quenches in later chapters. Chapter 2 then introduces a paradigmatic spin chain — the transverse field Ising model (TFIM) — and details its solution, along with providing a worked elementary quench example, which shows that a class of local observables relax to stationary values following the quench.

The first chapter based on original research, Chapter 3, builds on this framework by considering the axial next-nearest neighbour Ising (ANNNI) model, an extension of the transverse field Ising model with an additional next-nearest neighbour Ising interaction. Whilst the TFIM is exactly solvable, the ANNNI is a generic quantum system and its behaviour far from equilibrium must be determined approximately. Quench dynamics in this system were recently used to investigate if signatures of proximate quantum critical points can be observed at early and intermediate times. Chapter 3 constructs a simple time-dependent mean-field theory that allows one to obtain a quantitatively accurate description of these quenches at short times and provides a simple framework for understanding the reported numerical results. In the process, this theory highlights fundamental limitations on detecting quantum critical points through quench dynamics. Moreover, the origin of the peculiar oscillatory behaviour seen in various observables is explained as arising from the formation of a long-lived bound state.

Chapter 4 continues the investigation into oscillations found in Chapter 3 by studying quench dynamics in systems that support kinematically protected gapped excitations at

zero temperature, a class of which the ANNNI is a member. An open question in this context is whether such oscillations will ultimately decay. I will argue that strong support for the decay hypothesis can be obtained by considering spin models that can be mapped to systems of weakly interacting fermions, which in turn are amenable to an analysis by standard methods based on the Bogoliubov–Born–Green–Kirkwood–Yvon (BBGKY) hierarchy. By performing such a systematic perturbative analysis in a representative model, Chapter 4 finds a time scale beyond which the oscillations start to decay.

Finally, in Part B I turn my attention to open quantum systems. Chapter 5 will contain a summary of the established physics involved with these, and in particular will introduce the Lindblad formalism applicable when such systems satisfy a Markov assumption as well as a 'superoperator' formalism for recasting Lindblad equations as (non-Hermitian) Schrödinger equations. Chapter 6 then calculates the full quench dynamics for a system described by a certain Lindblad equation for an initial product state. The Lindbladian in question is solved using an algebraic feature called 'operator-space fragmentation' which leads to exponentially many invariant subspaces. On each subspace the Lindblad dynamics projects to a model of free (non-Hermitian) fermions, which enables the solution.

This thesis is based on the following publications:

[1] Jacob H. Robertson and Fabian H. L. Essler, "Exact solution of a quantum asymmetric exclusion process with particle creation and annihilation",
J. Stat. Mech. 2021(10):103102, Oct 2021.

[2] Jacob H. Robertson, Riccardo Senese, and Fabian H. L. Essler. "A simple theory for quantum quenches in the ANNNI model",
SciPost Phys. 15:032, 2023.

[3] Jacob H. Robertson, Riccardo Senese, and Fabian H. L. Essler, "Decay of long-lived oscillations after quantum quenches in gapped interacting quantum systems",
Phys. Rev. A 109:032208, Mar 2024.

Quantum Quenches in Closed and Open Spin Chains

List of Figures

Part A

Closed Systems

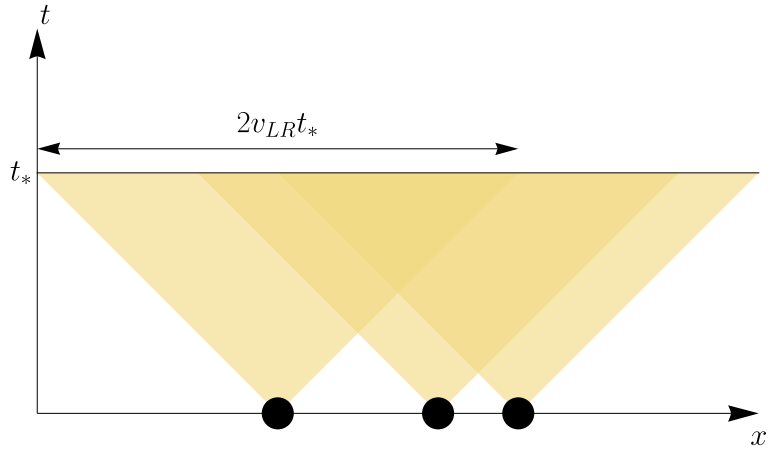

An intellect which at a certain moment would know all... for such an intellect nothing would be uncertain and the future just like the past could be present before its eyes.

A Philosophical Essay on Probabilities
Pierre Simon Laplace

1

Introduction to quench dynamics in closed systems

A pragmatic view of the purpose of theoretical physics is to predict, given the details of an experimental setup, what the results will be. A grandiose restatement would be to predict the future given the present. The difficulty of so-called 'fundamental physics' arises from the fact that the underlying laws of physics are not known, and must be guessed in such a way to agree with all previous experiments whilst explaining future experiments satisfactorily. This thesis is concerned with statistical physics, where these fundamental laws are known exactly but the challenge lies in being able to apply them to a large number of particles and successfully modelling the vast number of interactions between those constituents of the system. The intention of this thesis is to describe some of those edge cases where the future can indeed be, at least approximately, predicted and what we can learn from the result. The setting I will work in will be that of quantum mechanics, in which the art of predicting the future comes down to solving the Schrödinger equation

$$i\hbar\frac{\mathrm{d}}{\mathrm{d}t}|\psi\rangle = \hat{H}|\psi\rangle \ . \tag{1.1}$$

In Eq. (1.1) $\hbar$ is Planck's constant with dimensions of [Energy $\times$ Time], $|\psi\rangle$ is a vector in a complex Hilbert space $\mathcal{H}$ and $\hat{H} \in \mathrm{End}(\mathcal{H})$ is a Hermitian linear operator acting on $\mathcal{H}$ called the Hamiltonian that generates time evolution. I will work in units such that $\hbar = 1$ and consequently drop it from now on; this is equivalent to measuring time in units of the inverse of the problem's defining energy scale. I will also drop hats on operators unless additional clarification is needed. Given a complex

Hilbert space $\mathcal{H}$, an initial state $|\psi(t=0)\rangle$ and a Hamiltonian H, the Schrödinger equation is a well posed initial value problem. The Hermiticity of H ensures that it admits a spectral decomposition

$$H = \sum_{n=1}^{\dim(\mathcal{H})} E_n |n\rangle\langle n| \ , \tag{1.2}$$

where the eigenvalues E_n represent the allowed energies of the system and the energy eigenvectors $|n\rangle$ form a complete orthonormal set, that is,

$$\langle m|n\rangle = \delta_{mn} \ , \quad \sum_{n=1}^{\dim(\mathcal{H})} |n\rangle\langle n| = \mathbb{1}_{\mathcal{H}} \ . \tag{1.3}$$

In Eq. (1.3) δ_{mn} is the Kronecker delta, that equals 1 if $m = n$ and 0 otherwise, whilst $\mathbb{1}_{\mathcal{H}}$ is the identity on the Hilbert space. The Hermiticity of H and the linearity of Eq. (1.1) therefore allow one to 'solve' the time evolution problem, in the sense of writing the following spectral representation for $|\psi(t)\rangle$:

$$|\psi(t)\rangle = \sum_{n=1}^{\dim(\mathcal{H})} e^{-itE_n} \langle n|\psi(t=0)\rangle |n\rangle \ . \tag{1.4}$$

The difficulty in using Eq. (1.4) lies in the size of the sum. This thesis will be concerned with statistical mechanics of spin systems, where $\mathcal{H}$ is a tensor product of a local Hilbert space for each spin. If there are L such spins, then the Hilbert space is

$$\mathcal{H} = \bigotimes_{m=1}^{L} \mathcal{H}_m \ , \tag{1.5}$$

and consequently, if the local dimension is d (for a spin s, we have $d = 2s+1$), the total dimension of $\mathcal{H}$ is d^L. We are interested in many-body physics, i.e. $L \to \infty$, but even for relatively small L this means working in a vector space of enormously large dimensions. This direct approach therefore breaks down as one cannot even store the state $|\psi\rangle$ in memory, let alone extract physical predictions.

The rest of this chapter is divided into two sections. Section 1.1 gives motivations for studying quantum quenches in general, including a discussion of experimental platforms and known theoretical results. Section 1.2 then gives motivation for studying physics in one dimension and in particular gives a description of the matrix product state - a class of states that are very well suited to describing ground states of one dimensional systems without requiring exponentially many parameters to do so.

1.1 Quantum quenches

In order that the initial value problem described above be non-trivial, we will require that the initial state $|\psi(t=0)\rangle$ have a non-zero overlap with an exponentially large number of energy eigenstates of the Hamiltonian generating time evolution, otherwise Eq. (1.4) contains only a relatively small number of terms. The language we shall use is that of a *quantum quench*, where the initial state is chosen to be the ground state (or possibly a thermal state) of some initial Hamiltonian H_i whilst the time evolution is generated by a final Hamiltonian H_f. An important distinction is between *local* and *global* quenches, where in the former the operator $H_f - H_i$ has support only in a finite region. All the quenches in this thesis are global quantum quenches, which means that the initial state has a finite energy *density* relative to the ground state of the post-quench Hamiltonian. Often it is convenient to consider a parametrised family $H(\lambda)$, such that $H_{i/f} = H(\lambda_{i/f})$ and to reflect this I will often use the terminology of 'quenching' the parameter λ, and write $\lambda : \lambda_i \mapsto \lambda_f$ as a shorthand.

1.1.1 Motivation

The quantum quench is a simple protocol for accessing far from equilibrium physics that is experimentally accessible. An especially important question is that of "thermalisation": in what sense and how does an isolated quantum system relax? The quantum quench is ideal for investigating this question, stripping aside everything non-essential to it. Indeed, some Hamiltonians do *not* cause an initial nonequilibrium state to evolve to a thermal one. Subsection 1.1.3 describes the better known examples. Such behaviour can give rise to non-thermal states that may have exotic properties not possible in conventional equilibrium matter. In the case that the dynamics deviate only slightly from a non-thermalising Hamiltonian, they may still lead to very long-lived 'prethermal' states [4–6], before eventually reaching thermal equilibrium.

The main experimental platform for quench experiments are ultracold neutral atoms [7,8] which can have millions of (bosonic or fermionic) atoms contained in a magnetic or optical trap at "temperatures" measured in nanokelvin. Strictly speaking, this is a measure of kinetic energy and not temperature, which is ill-defined since these gases are not in equilibrium with a surrounding heat bath. The fact that they survive long enough for experiments despite their hot surroundings indicates how exquisitely isolated ultracold atoms are. Ultracold atomic systems can have coherence times of several seconds, several orders of magnitude longer than the typical dynamical timescales which are on the order of milliseconds. Ultracold atoms are now a relatively mature platform whose

toolbox includes quantum gas microscopes, which allow for the imaging of individual atoms [9, 10]; Feschbach resonances for tuning the inter-atom interaction strength using magnetic fields or laser light [11, 12]; and artificial gauge fields to allow the simulation of charged particles such as the electrons in a superconductor [8, 13]. Improvements to experiments are of course still needed. One notable problem is that whilst bosons can be efficiently cooled to very low temperature using forced evaporative cooling, applying the same technique to Fermi gases is less effective [14]. This is because evaporative cooling relies on high elastic scattering rates to bring a gas back into local equilibrium following the removal of the most energetic atoms. For fermions, the requirement of an antisymmetric wavefunction forces the s-wave two-body elastic scattering rate to be zero, and consequently, fermionic cooling lags behind that for bosons. Whilst a temperature of a few nanokelvin is an impressive feat of experimental work, the more meaningful quantity to consider is the ratio of the temperature to some energy scale in the simulated quantum system. For instance, in trying to simulate superconductivity the ratio of temperature to hopping energies T/t is about a factor of 10^3 larger than in cuprates [8]. For this purpose therefore, these 'cold fermionic gases' are still rather hot.

Several other quantum simulator platforms have also emerged [15], and those based on Rydberg atom arrays [16], superconducting quantum circuits [17, 18] and trapped atomic ions [19] all provide the ability to control 50 or more qubits with high fidelity and perform quantum quench experiments. Such analog quantum simulators represent a trade-off between the full programmability of a universal digital quantum computer and the availability of interactions 'native' to a platform that would require compilation into too many quantum gates to be feasible in the current era of noisy intermediate scale quantum (NISQ) computation [20]. At ~ 50 qubits, these experiments are able to outperform brute force classical computation which simply diagonalise the Hamiltonian, however they are still a long way from giving reliable information about the thermodynamic limit.

In order to interpret and validate the results from these experiments, as well as guide new experiments, a theory of nonequilibrium physics is highly desirable. In comparison to the description of quantum matter at equilibrium, for which several strong organising principles exist, far from equilibrium physics is much less explored. Nonetheless, there are several theoretical developments that are firmly established and which provide insights into nonequilibrium physics; the next subsection aims to give a biased selection of such tools that are useful for thinking about quantum quenches.

1.1.2 Survey of theoretical results

This subsection will briefly discuss theoretical results that are well established and form a core set of ideas applicable to a wide range of quenches.

The eigenstate thermalisation hypothesis (ETH) As stated above, an important question is whether an isolated quantum system will evolve to become thermal. A first observation is that thermal states are mixed, whilst unitary time evolution can only produce pure states from pure states. The key resolution is to introduce the *reduced density matrix* (RDM) of a local subsystem S, obtained by performing a partial trace over the remaining degrees of freedom of its environment E:

$$\rho_{\mathrm{S}} = \mathrm{Tr}_{\mathrm{E}}(\rho) \ , \tag{1.6}$$

where $\rho = |\psi\rangle\langle\psi|$ is the density matrix of the entire system and ρ_{S} is the RDM. The RDM is sufficient to calculate any expectation values for observables with support solely in S. When one speaks of a system becoming thermal, therefore, one is talking about only the RDM of sufficiently local subsystems, or equivalently of expectation values of local observables relaxing to their thermal values. The RDM is generically a mixed state even if ρ is pure, which removes the objection that unitary dynamics cannot produce a mixed state from a pure state.

The modern understanding of thermalisation is heavily guided by what has become known as the 'eigenstate thermalisation hypothesis' (ETH) [21–23]. ETH can be expressed as an ansatz on the matrix elements of local observables in terms of eigenstates of the post-quench Hamiltonian

$$\langle m|O|n\rangle = O(\bar{E})\delta_{mn} + f_O(\bar{E}, \omega_{m,n})e^{-S(\bar{E})/2}R_{mn} \ , \tag{1.7}$$

where $|m\rangle$ is an eigenstate of the post-quench Hamiltonian H_f with energy E_m, $\bar{E} = (E_m + E_n)/2$ is the mean energy of eigenstates and $\omega_{m,n} = E_m - E_n$ is the difference in energy between eigenstates. Lastly, $O(\bar{E}), f_O(\bar{E}, \omega_{mn}), S(\bar{E})$ are smooth functions and R_{mn} is a random matrix with zero mean and unit variance. The function $S(\bar{E})$ is generally expected to equal the thermodynamic entropy, which is extensive, and the second term is therefore exponentially suppressed at large system sizes. Eq. (1.7) can be interpreted as saying that expectation values in energy eigenstates give results equal to the thermodynamic prediction at that energy, plus random fluctuations that are exponentially small in the system size. The term 'eigenstate thermalisation' refers to the fact that one can therefore obtain statistical averages at temperature T by computing quantum mechanical expectation values

in any eigenstate of energy E, where E is chosen to equal the internal energy of the system at that temperature.

ETH is a sufficient condition for thermalisation in the sense that the infinite time average of the observable O relaxes to its thermal value, up to finite size corrections, and that temporal fluctuations around the time average vanish in the thermodynamic limit. Eq. (1.7) therefore implies that the RDM defined by Eq. (1.6) becomes thermal at late times, as promised. ETH has been numerically tested for many systems and is believed to hold true for the majority of chaotic quantum systems [24–27]. It is to be stressed that ETH is only expected to apply to local observables; certainly there exist some highly non-local observables such as projectors on to energy eigenstates $|n\rangle\langle n|$ that will never thermalise. A notable exception to ETH are so called 'integrable' models which have a much more intricate structure to their matrix elements [28]. Four known cases of violations of ETH, and consequently non-thermal behaviour, are briefly described in 1.1.3.

Lieb-Robinson bounds As originally proved by Lieb and Robinson [29], lattice spin systems can have a finite maximum speed at which information is propagated. This is analogous to the speed of light in relativistic theories, and leads to 'light cone' dynamics following a quantum quench [30]. We will consider k-local Hamiltonians of the form

$$H = \sum_i h_i \ , \ \|h_i\| < h_{\max} \ , \tag{1.8}$$

where $\|A\|$ is the operator norm of A and each h_i has support on the sites $i, i+1, \dots i+k-1$. The Lieb-Robinson bound then states that there exists a constant c, and velocity and length scales, v_{LR} and ξ respectively, such that

$$\|[A(t), B(0)]\| \leq c \min(|\operatorname{supp}(A_0)|, |\operatorname{supp}(B)|)\|A\|\|B\| \exp(-(L - v_{\mathrm{LR}}|t|)/\xi) \ , \tag{1.9}$$

where A, B are two operators with support at $t = 0$ in $\operatorname{supp}(A_0)$ and $\operatorname{supp}(B)$, respectively, and L denotes the minimum separation between these two regions. The constants c, v_{LR}, ξ depend on $h_{\max}$ (and on the lattice geometry) but not on L or t. The Heisenberg evolved operator $A(t)$ is defined by

$$\begin{aligned} A(t) =& \exp(iHt)A(0)\exp(-iHt) \ , \\ =& A(0) + it[H, A] - t^2/2![H[H, A]] + \dots \ . \end{aligned} \tag{1.10}$$

The Lieb-Robinson bound can be restated in terms of the rate of operator spreading following a quench. If $A(0)$ has support on one site, then, from Eq. (1.10), at time t, it will have support

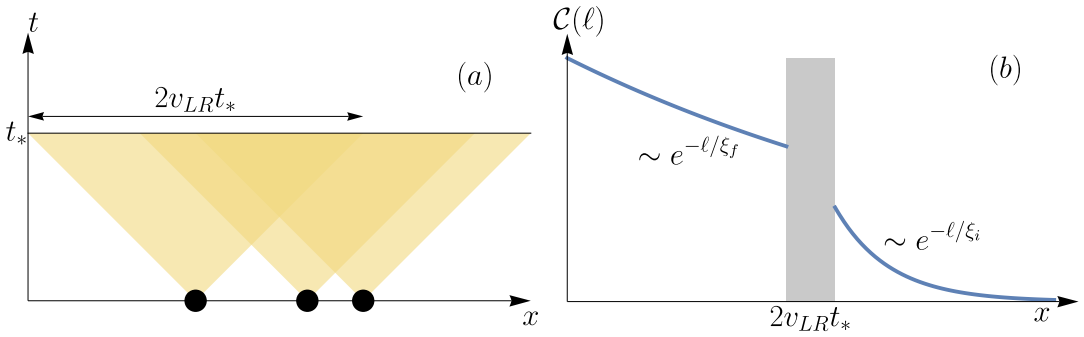

Figure 1.1: (a) Schematic illustration of the light cone picture. Three quasiparticles produced at different locations by a quench at $t = 0$ are shown, along with light cones showing the spatial regions influenced by the quasiparticles at a later time t_*. (b) Schematic depiction of what the light cone picture predicts for connected correlation functions $\mathcal{C}(\ell)$ at time t_*. Outside the light cone correlations decay with a pre-quench correlation length ξ_i; deep inside the light cone correlations may be expected to decay with some thermalised correlation length ξ_f. Around the light cone this argument ceases to hold and the behaviour may be more complex, hence the grey shaded out region. Compare (b) with Fig. 3.9.

throughout the entire spin chain, with each additional nested commutator adding contributions a further k sites away from the original support at $t = 0$. A result of the Lieb-Robinson bound however is that, if we define $A_\ell(t)$ as the restriction of $A(t)$ to sites within ℓ of the original support of $A(0)$, then we have

$$\|A_\ell(t) - A(t)\| \leq c|\operatorname{supp}(A_0)| \exp(-(\ell - v_{\mathrm{LR}}|t|)/\xi) \ . \tag{1.11}$$

In turn this implies, for initial states with exponentially decaying correlations, that equal time connected correlation functions

$$\langle A(t)B(t)\rangle - \langle A(t)\rangle\langle B(t)\rangle \ , \tag{1.12}$$

do not appreciably differ from their values at $t = 0$ following a quench until connected by a 'light cone' at time $t = L/(2v_{\mathrm{LR}})$. This is illustrated in Fig. 1.1. An important result of the light cone behaviour to bear in mind is that for finite systems there is a time after which the light cone spreading has traversed the entire length of the system. Such 'traversals' limit the usefulness of a finite size simulation to times $t < L/(2v_{\mathrm{LR}})$ [31, 32].

Cardy-Calabrese quasiparticle picture Complementary to the Lieb-Robinson bound is a picture of the post-quench state developed by Cardy and Calabrese in a landmark series of papers [33–36]. According to this picture, one should decompose the initial post-quench state in terms of the excitations of the post-quench Hamiltonian. In their papers they considered quenches

to conformal field theories, where the excitations are stable quasiparticles. For quenches to generic systems without stable quasiparticles one can still think of the initial state as a gas of approximate quasiparticles with a finite lifetime; Chapter 4 will stress that this is a useful viewpoint when said gas has a low density. This gives an intuitive viewpoint on the results obtained from the Lieb-Robinson bound, by considering that information is carried by the quasiparticles following the quench and that the Lieb-Robinson bound is a limit on these quasiparticles' velocity. Indeed, the Lieb-Robinson velocity can often be identified with the maximal group velocity of the excitation spectrum [37].

Linear growth of entanglement entropy A key quantity in modern many-body physics is the von Neumann (bipartite) entanglement entropy. This measures the quantum entanglement of a subsystem S with its environment E, defined through the RDM by

$$S_{\mathrm{vN}} = -\mathrm{Tr}_S(\rho_S \log \rho_S) \ . \tag{1.13}$$

For thermal states, it is generally expected that S_{vN} will be equal to the thermodynamic entropy and in particular be proportional to the volume of S. At zero temperature, this is no longer true. An early application of the Lieb-Robinson bounds [38] was to show that for gapped one dimensional Hamiltonians the entanglement entropy obeys an *area law*, meaning that it is proportional to the size of the boundary between S and E. This of course means that the entropy density $S_{\mathrm{vN}}/\,\mathrm{vol}(S)$, with $\mathrm{vol}(S)$ being the volume of the subsystem S, is zero, consistent with the third law of thermodynamics. Area laws in higher dimensions have turned out to be more difficult to prove but there have also been several results in this direction [39–42].

Following a global quantum quench from a ground state of a gapped system, the entanglement entropy grows from its initial area law value to, if the system reaches thermal equilibrium, a volume law. The question of how it does this has been the focus of much attention and it is generally believed that it increases linearly with time at some constant velocity v_{ent} until it saturates at the thermal value. In integrable systems, which possess well defined quasiparticle excitations, the argument is given by the Cardy-Calabrese picture: the entanglement of S with E is proportional to the number of quasiparticle pairs that were generated inside S by the quench and have reached E. In generic chaotic systems, a linear growth is also expected for different reasons [43, 44].

1.1.3 Absence of thermalisation

Whilst ETH predicts that generic quantum systems thermalise in the sense of time averages, there are several known ways to circumvent thermalisation following a quantum quench, which merit

a subsection of their own. The way that ETH is violated can be classified as 'strong' or 'weak' depending on whether a finite fraction of eigenstates obey ETH or not. Some authors also use the language of strong or weak 'ergodicity breaking', where the word ergodic refers to a specific property of classical systems that leads to thermal behaviour, but in the quantum case may be simply read as synonymous with the word 'thermal'. In a weakly non-ergodic system, there are a number of eigenstates that violate ETH that grows slower with system size than the number of eigenstates that satisfy ETH. Consequently the quench dynamics can seem thermal, unless the initial state has a high overlap with the non-ergodic eigenstates.

Yang-Baxter integrability Integrable models are a set of one dimensional models that have an extensive number of local conservation laws $I_1, I_2, \ldots$. There are therefore a large number of initial conditions possible for a quench such that the values of the conserved charges beyond energy and particle number are not consistent with the final Gibbs ensemble predicted by statistical mechanics

$$\rho = Z^{-1} \exp(-\beta(H - \mu N)) \ , \tag{1.14}$$

with β, μ fixed only by the initial energy and particle number density after the quench. Instead, one should introduce a separate Lagrange multiplier for each conserved quantity, giving rise to a *generalised Gibbs ensemble* (GGE) [45–48]

$$\rho_{\mathrm{GGE}} = Z^{-1} \exp(-\sum_{i}^{k} \lambda_i I_i) \ , \tag{1.15}$$

where the λ_i are chosen to ensure the GGE has the same expectation values for all conserved charges as the initial state and the sum should strictly run over all conserved charges but in practice may be truncated to run over the k charges with the highest degree of locality [47]. In interacting integrable models it may be required to additionally include quasilocal conserved quantities in the GGE description [48–50].

A 'typical' eigenstate in an integrable model will have expectation values that agree with the Gibbs ensemble [51]. However, since the structure of the off-diagonal elements differs from (1.7), integrable systems violate ETH strongly [28].

Despite needing to be finely tuned, experiments with ultracold atoms are able to realise integrable dynamics, with integrability breaking terms kept small enough to not impact on experimental timescales [52]. When studying quantum quenches where the time evolution is nearly integrable, the dominant (integrable) dynamics first results in *prethermalisation* to a GGE for an extended period

of time [4–6], whilst the weak interaction breaking terms result in the system becoming thermal at late times [53, 54].

Many body localisation A different form of ergodicity breaking is seen in *localised* systems, where eigenstates correspond to particles at fixed locations, generally due to the presence of strong disorder. The non-interacting case was established by Anderson [55] and the interacting case goes by the name many body localisation (MBL) [56, 57]. MBL is believed to cause strong violations of ETH due to the emergence of local integrals of motion, and in contrast to both integrable and generic chaotic systems, the entanglement entropy after a quench grows only logarithmically with time [58]. There is some controversy over whether MBL persists in the thermodynamic limit [59–63]. In this thesis I consider only clean, translationally invariant, systems and the phenomenology of MBL is therefore not present.

Hilbert space fragmentation Another class of models with non-ergodic dynamics are those exhibiting so-called Hilbert space fragmentation. This was initially discussed in certain spin chains with charge and dipole conservation [64, 65]. The excitations of these spin chains are 'fractons' with severely limited mobility — the Hilbert space of the models consists of an exponentially large set of dynamically disconnected sectors. This can be attributed to the presence of statistically local integrals of motion [66], a weaker versions of the local integrals of motion found in MBL systems. Hamiltonians displaying Hilbert space fragmentation do not require disorder, unlike MBL. Moreover, unlike integrable systems, they do not require fine tuned couplings, although adding additional interactions can weakly connect the originally disconnected sectors, leading to predictions of similar prethermal behaviour as in the weakly non-integrable case. Systems can be either weakly or strongly fragmented (and correspondingly violate ETH in a weak or strong way) depending on whether a randomly chosen state lies in the largest disconnected sector with unit probability or not.

Quantum many body scars The final failure of thermalisation this chapter will describe is an excellent case study in the importance of quantum quench experiments and theorists' role in exploring them. In [16], a 51 atom Rydberg simulator was demonstrated. Some of the experiments performed were quenches from either a translationally invariant state or a state invariant only under translation by two sites. The Hamiltonian simulated by the model was translationally invariant and disorder free, and local observables were measured following the quench. Surprisingly, whilst the translationally invariant initial state quickly became thermal, local observables oscillated in

expectation value for long times following the quench from the two-site translation invariant state. This was attributed in [67] to the presence of 'quantum many body scars' (QMBS) in a model spin-1/2 Hamiltonian very close to that realised by the experiment, the PXP model:

$$H_{\mathrm{PXP}} = \sum_i P_i \sigma^x_{i+1} P_{i+2} \ , \ P_i = (1 - \sigma^z_i)/2 \ , \tag{1.16}$$

each term of which acts on three sites by flipping the central spin if both its neighbours are spin down, and otherwise annihilating the state. In the spin description, the charge density wave state that the experiment started from is one of the Néel states

$$|\mathbb{Z}_2\rangle = |\uparrow\downarrow\uparrow\downarrow\ldots\rangle \ , \ |\mathbb{Z}_2'\rangle = |\downarrow\uparrow\downarrow\uparrow\ldots\rangle \ . \tag{1.17}$$

The explanation put forward for the oscillations in [67] is that there is a band of so called 'scar-states', which are eigenstates of the Hamiltonian but with anomalously high overlap with $|\mathbb{Z}_2\rangle$, see Fig. 1.2. Moreover, these states have approximately constant energy spacing between them, leading to coherent oscillations. These states are truly many body phenomena, since they are present throughout the entire many body spectrum of H_{PXP}, not just at low energies.

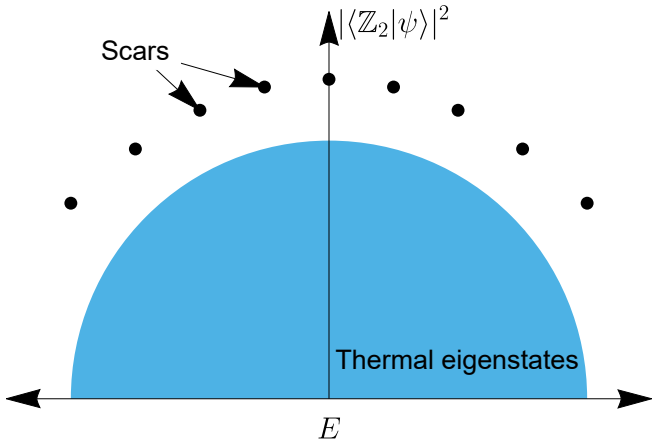

Figure 1.2: Cartoon of the overlap of Hamiltonian eigenstates in the PXP model with the initial $\mathbb{Z}_2$ invariant state. Non-scar eigenstates form a continuum of states with varying overlaps shown in blue. The scar states stand out by their anomalously large overlaps and are spread throughout the entire many body spectrum. Compare with Fig. 3(a) of [67].

QMBS has been extensively investigated in the years since that original Rydberg atom experiment [68–71]. QMBS systems are characterized by having non-thermal states embedded in the bulk of the spectrum, where the majority of states are thermal. In many models, such as the PXP model,

these are arranged into 'towers'. The non-thermal states are often sub-volume law states that can be written explicitly despite the Hamiltonian not being fully analytically diagonalisable, or otherwise possess low entanglement compared to the surrounding volume law states. These explicit non-thermal states violate ETH, and the violation is classed as weak because the ratio of non-thermal to thermal states vanishes in the thermodynamic limit. Nonetheless, the case of the PXP model shows that if the scar states turn out to have equally spaced energies, as well as if the total overlap with an initial state $|\psi_0\rangle$ does not vanish in the thermodynamic limit,

$$\lim_{L\to\infty} \sum_{\text{scars}} |\langle \text{scar}|\psi_0\rangle|^2 > 0 \ , \tag{1.18}$$

then unexpected, non-thermal, behaviour can result from a quench.

Chapter 4 discusses a class of Hamiltonians with a similar phenomenology after quenching to QMBS — for some quenches certain local observables oscillate for very long times whilst other choices of initial states or observables result in the oscillations rapidly decaying. However, that chapter will present an alternative explanation for the oscillations, argue that the the systems do thermalise, and give evidence for the oscillations having a finite lifetime. That is to say, Chapter 4 should be read partly as a warning not to jump to the conclusion of QMBS when observing oscillatory behaviour in either numerics or experiment.

1.2 Why one dimension?

The studies on quantum quenches contained in this thesis are all focused on one dimensional systems. One might complain that we live in three dimensions, and that this is therefore an unphysical situation to consider. However, ultracold atom experiments are able to access one dimensional physics by making the confining potential much steeper along two axes [72–74], whilst Rydberg, trapped ion and superconducting qubit simulators can all adopt largely arbitrary geometries. Even in solid state magnets, the magnetic ions can be arranged in weakly interacting chains such that one dimensional physics can be observed [75]. One dimensional physics is therefore very much experimentally relevant.

Quantum physics in one dimension does differ in some notable ways from higher dimensions [76]. Interactions in one dimension are effectively enhanced by the inability of particles to go around each other, which leads to a number of characteristic features of low dimensional quantum mechanics. Firstly, the Mermin-Wagner theorem [77] prevents the spontaneous symmetry breaking (SSB) of

continuous symmetries at finite temperature in one and two dimensions. Moreover, since one dimensional quantum systems can be identified with two dimensional classical systems, the former cannot support SSB of a continuous symmetry, even in the ground state. Quenches from an initial ordered state must therefore see that order melt in one dimension [78]. Secondly, the same strong fluctuations that destroy order also make naive mean-field theories of spins much less accurate in 1D [79], which prompts the theoretical question of how to provide more accurate approximate theories.

A further feature of low-dimensional physics is the breakdown of the usual boson/fermion dichotomy. In two dimensional quantum systems, particles called anyons with fractional statistics between that of bosons and fermions exist [80]. In one dimension, the technique of bosonisation allows problems involving hard-core bosons to be mapped to problems of fermions and vice versa [76]. Relatedly, the Jordan-Wigner transformation enables one dimensional spin chains to be recast as models of interacting fermions [81, 82]. In a few specific cases, one of which will be described in detail in Chapter 2, the fermion theory can even be non-interacting and therefore provide a full solution to the original spin problem. There are also a number of exactly solvable models in one dimension beyond non-interacting theories, these are the interacting Yang-Baxter integrable models, which provide a starting point for the analysis of nearby models. One dimensional physics therefore presents a fantastic opportunity to recast one Hamiltonian in new variables which might make a perturbative scheme more appropriate.

Another key reason to study one dimensional physics, even if one is interested in physics common to both three dimensions and low dimensions, is that powerful numerical tools are available and conventional numerical techniques are more powerful. For instance, (depending on what symmetries are able to be exploited) a computer might only be able to exactly diagonalise a system of around $\sim 16 - 25$ qubits before running out of RAM. For a one dimensional chain, this might be enough to extract some meaningful physical properties and compare their convergence with varying system size. A corresponding study in two dimensions, say on a square lattice, will naturally be much harder since one is limited to systems at most 4×4 or 5×5. Perturbative methods using plane wave basis sets will also be naturally much cheaper in one dimension, since the momentum space sums will be much smaller than their counterparts in a two or three dimensional calculation. However, the most powerful set of numerical tools available in one dimension are provided by matrix product state (MPS) algorithms, which are much more efficient than their higher dimensional counterparts.

1.2.1 Matrix product states

A huge advance in the ability to simulate one dimensional quantum systems has taken place over the last few decades due to the development of algorithms based on matrix product states [83]. Chapter 4 presents several numerical studies which use two such algorithms: density matrix renormalisation group (DMRG) [84, 85] and time evolving block decimation (TEBD) [86, 87]. Following a definition and brief discussion of the properties of an MPS, this subsection provides a brief overview of the physical intuition behind these algorithms; it is not intended as practical implementation advice, for which the reader is advised to read [83, 88].

A matrix product state generalises the notion of product state. In a product state, one has L sites with local Hilbert space dimension d (for instance, for spin 1/2 we have $d = 2$), with local basis states $|i_m\rangle_m$ and one simply considers the system to be in the unentangled state

$$|\psi\rangle = \sum_{i_1}\sum_{i_2}\cdots\sum_{i_L} C_{i_1}C_{i_2}\ldots C_{i_L}|i_1 i_2 \ldots i_L\rangle \ . \tag{1.19}$$

A product state is therefore specified by dL numbers, substantially fewer than the d^L needed to specify a general entangled state. Due to their lack of entanglement, product states are essentially classical. Matrix product states go beyond product states by allowing some entanglement, and (for periodic boundary conditions) have the form

$$|\psi_{\mathrm{MPS}}\rangle = \sum_{i_1}\sum_{i_2}\cdots\sum_{i_L} \mathrm{Tr}\left[A_1^{[i_1]}A_2^{[i_2]}\ldots A_L^{[i_L]}\right]|i_1 i_2 \ldots i_L\rangle \ , \tag{1.20}$$

here the matrices A_m are $\chi_m \times \chi_{m+1}$ matrices, where χ is called the bond dimension. If all the χ are equal, then this MPS requires $\chi^2 dL$ numbers to specify, which still evades the exponential scaling required to represent a fully general state. An MPS is an example of a more general class of states, called tensor network states (TNS) where the coefficients $C_{i_1 i_2 \ldots i_L}$ are expressed through contracting a set of tensors and leaving L uncontracted indices. This motivates a popular diagrammatic representation of a TNS shown in Fig. 1.3.

A key question is what is the entanglement entropy of an MPS state. It turns out that an MPS state is an area law state, so the size of the subsystem in question is not relevant, and the entropy is upper bounded by [89]

$$S_{\mathrm{MPS}} \leq 2\log\chi \ . \tag{1.21}$$

The MPS representation is so useful in 1D precisely because ground states of gapped Hamiltonians have area laws. Even non-area law states important in physics, such as ground states of critical

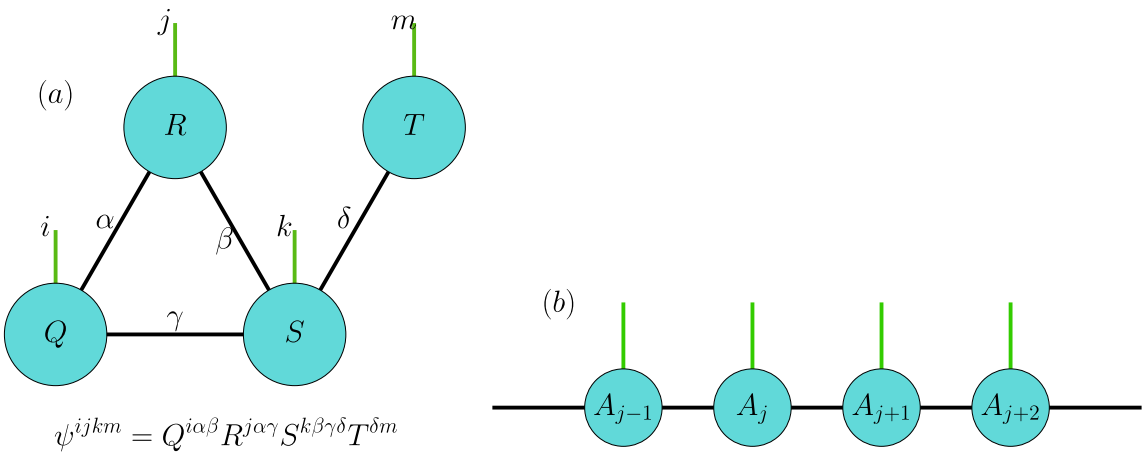

Figure 1.3: Two example tensor network states. (a) A tensor network representing a contraction of four tensors. Black lines show contracted indices and green lines show free indices. The expression below gives the traditional Einstein notation for this tensor, with the virtual indices labelled in Greek letters. (b) An MPS shown in this graphical language.

systems (which have logarithmic corrections to the area law) or low temperature thermal states, can have low enough entanglement entropy that choosing χ to be large allows for an accurate MPS representation. Where this fails, of course, is describing very high temperature or very far from equilibrium states. In particular, since entanglement entropy generically grows linearly following a quantum quench, the bond dimension χ required to faithfully represent the system grows *exponentially* with time.

DMRG When performing a quantum quench the first step is to characterise the initial state. When the initial state is the ground state of a one dimensional Hamiltonian, a highly efficient MPS algorithm is available, which goes by the name DMRG. The original DMRG algorithm is equivalent to variationally optimising the energy over the class of MPS states with some bond dimension χ; that is, one wants to minimise

$$C[A_1, \dots A_L] = \frac{\langle\psi|H|\psi\rangle}{\langle\psi|\psi\rangle} \ , \ |\psi\rangle = |\psi(A_1, \dots A_L)\rangle \ , \tag{1.22}$$

where $|\psi(A_1, \dots, A_L)\rangle$ is intended as the MPS state given by Eq. (1.20), with the A matrices considered as variational parameters. Equivalently, a Lagrange multiplier can be introduced and the quantity to be minimised chosen as

$$C'[A_1, \dots, A_L, \lambda] = \langle\psi|H|\psi\rangle - \lambda\langle\psi|\psi\rangle \ . \tag{1.23}$$

The utility of using MPS states as a variational class is that all the expectation values in these formulae can be easily computed. In contrast, in higher dimensions, calculating such tensor network contractions is a #P-complete problem [90]. Addressing this variational problem directly is very challenging since it is a highly nonlinear optimisation problem of many variables. However, an iterative procedure can be used, holding all but one A matrix fixed and optimising with respect to that A. The problem is then quadratic and easily solved and solvers then optimise each A matrix in turn, performing several such 'sweeps' of the system until the ground state energy converges. Various modifications to this are possible, including minimising the energy over two sites at once rather than one to avoid local minima of energy.

TEBD Having obtained an MPS representation of the initial state, I now turn my attention to the time evolution operator $U(t) = \exp(-itH_f)$. This is popularly computed using the Suzuki-Trotter decomposition [91] when H_f is the sum of local terms $H_f = \sum_{j=1}^{j=N} h_j$

$$U(\delta t) = \left(e^{-i\delta t h_1} e^{-i\delta t h_2} \dots e^{-i\delta t h_N}\right) + \mathcal{O}(\delta t^2) \ . \tag{1.24}$$

This is a first order Trotter decomposition, meaning that the error per step scales like δt^2, and so the error after $t/(\delta t)$ such steps may be expected to be $\mathcal{O}(\delta t)$. In practice one usually uses a second or higher order decomposition to avoid needing to make the time step δt prohibitively small. Each factor in $U(\delta t)$ acts only on a fixed number of sites (that is, if h_i acts on 2 sites then $\exp(-i\delta t h_i)$ also acts on 2 sites) and can be viewed as a quantum gate. The time evolution algorithm consists of applying each gate sequentially. Crucially, after every gate has been applied, the state ceases to be an MPS of bond dimension χ and we must project back on to the set of MPS states, as illustrated in Fig. 1.4.

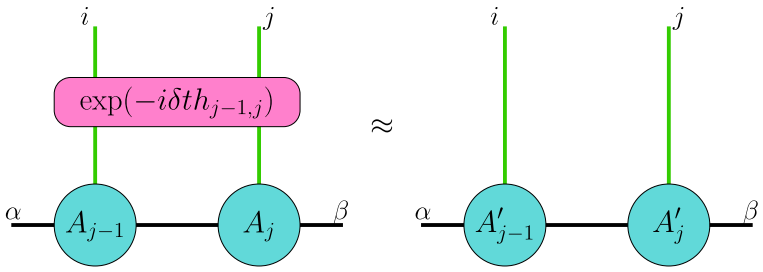

Figure 1.4: Graphical representation of a single TEBD update consisting of applying a gate and truncating to a low bond-dimension MPS.

To do this we first group the virtual and physical external legs in Fig. 1.4 into super-indices $I = (\alpha, i)$ and $J = (\beta, j)$ with dimension $d\chi$. Next, we make use of the singular value decomposition (SVD) for the resulting two index tensor

$$\begin{aligned} T^{IJ} =& U^{Ik}\Sigma^{kq}V^{qJ} \ , \\ =& \sum_{k=1}^{\chi} U^{Ik}\sigma_k V^{kJ} + \sum_{k=\chi+1}^{d\chi} U^{Ik}\sigma_k V^{kJ} \ , \\ \approx& [AB]^{IJ} \ , \\ A^{Ik} =& U^{Im}\sqrt{\tilde{\Sigma}}^{mk} \ , \ B^{kJ} = \sqrt{\tilde{\Sigma}}^{km} V^{mJ} \ , \ \tilde{\Sigma} = \mathrm{diag}(\sigma_1, \sigma_2, \ldots, \sigma_\chi) \ , \end{aligned} \tag{1.25}$$

where we have ordered the singular values $\sigma_1 > \sigma_2 \cdots > \sigma_{d\chi}$ and then discarded all but the largest χ values. The resulting tensor is now an MPS of bond dimension χ, and can have another two body gate applied to it.

TEBD therefore has two sources of error: trotterisation error and truncation error. The trotterisation error reflects how accurately the gate evolution reflects the true continuous time evolution. It is usually fairly easy to mitigate this by simply choosing a small enough Trotter step and perhaps using a high order integrator. The trotterisation errors are however particularly problematic for long ranged Hamiltonians, since then the number of gates applied in a single trotter step increases with the system size L. Other techniques are therefore more applicable to simulating long ranged models [92, 93]. Usually more problematic is the truncation error, which arises every time one uses an SVD to reduce the bond dimension. This prevents accurate simulation for times at which the entanglement generated following a quench has grown larger than can be represented by a fixed bond dimension MPS.

. . . So using all his strength,
Hephaestus loosed the chains. The pair of lovers
were free from their constraints, . . .

The Odyssey,
Homer (translated by Emily Wilson)

2

Anatomy of a free theory - the transverse field Ising model

This chapter will introduce the reader to the one dimensional transverse field Ising model (TFIM). This spin chain has the useful property of being directly mappable to a non-interacting theory of fermions [81,82], which enables many exact calculations to be performed. At the end of this chapter I consider one such quench calculation, with the result that local (in fermions) correlation functions decay according to a power law to stationary values following a field strength quench. The contents of this chapter are intended to be a brief introduction to known results; it is not original research. The techniques of this chapter will prepare the reader for Chapter 3, in which a quench is investigated in an extension of the TFIM known as the ANNNI model. Moreover, Chapter 4 investigates quenches in XXZ chains using the Jordan-Wigner technology described below and Chapter 6 describes the dynamics of an open system via the solution to a non-Hermitian extension to the TFIM.

In one dimension, the transverse Field Ising model (TFIM) for L sites with periodic boundary conditions is defined by the Hamiltonian

$$H_{\mathrm{TFIM}}(h) = -J\sum_{i}^{L-1}\sigma_i^x\sigma_{i+1}^x - J\sigma_L^x\sigma_1^x - h\sum_{i}^{L}\sigma_i^z \ . \tag{2.1}$$

Here, $\sigma^{x,z}$ are Pauli spin matrices satisfying the commutation relation

$$[\sigma_i^x, \sigma_j^y] = 2i\delta_{ij}\sigma^z \ , \tag{2.2}$$

and cyclic permutations thereof. The Kronecker delta δ_{ij} enforces that spins on different sites commute. The TFIM can be rewritten in terms of (spinless) fermions and the resulting theory is quadratic in fermions. The mapping that accomplishes this is the Jordan-Wigner transformation, which takes the following non-local form:

$$\begin{aligned} \sigma_i^+ &= \prod_{j<i}(1-2f_j^\dagger f_j) f_i \ , \\ \sigma_i^z &= 1 - 2f_i^\dagger f_i \ , \end{aligned} \tag{2.3}$$

Conceptually, the Jordan-Wigner transform represents the spin-up state $|\uparrow\rangle$ as an empty fermion orbital $|0\rangle$ and the spin-down state $|\downarrow\rangle$ by a filled orbital $|1\rangle$. The product factor is referred to as a 'string' and is necessary to ensure that the commutation relations (2.2) hold when the variables f_i are canonical fermions satisfying the anti-commutation relations

$$\{f_i^\dagger, f_j\} = \delta_{ij} \quad , \quad \{f_i, f_j\} = 0 \ . \tag{2.4}$$

Whilst the transformation is highly non-local for σ_i^+, products of spin operators with even numbers of raising/lowering operators are mapped to local operators in terms of the fermion variables. For instance one obtains:

$$\begin{aligned} \sigma_i^x \sigma_{i+1}^x &\mapsto (f_i^\dagger - f_i)(f_{i+1}^\dagger + f_{i+1}) \ , \\ \sigma_i^y \sigma_{i+1}^y &\mapsto (f_i^\dagger + f_i)(f_{i+1}^\dagger - f_{i+1}) \ , \\ \sigma_i^z \sigma_{i+1}^z &\mapsto 1 - 2(f_i^\dagger f_i + f_{i+1}^\dagger f_{i+1}) + 4 f_i^\dagger f_{i+1}^\dagger f_{i+1} f_i \ , \\ \sigma_i^x \sigma_{i+2}^x &\mapsto (f_i^\dagger - f_i)(1 - 2f_{i+1}^\dagger f_{i+1})(f_{i+2}^\dagger + f_{i+2}) \ , \\ \sigma_i^x \sigma_{i+1}^z \sigma_{i+2}^x &\mapsto (f_i^\dagger - f_i)(f_{i+1}^\dagger - f_{i+1}) \ . \end{aligned} \tag{2.5}$$

From this one sees that the Jordan-Wigner transform allows one to rewrite the TFIM Hamiltonian as

$$\begin{aligned} H_{\mathrm{TFIM}}(h) &\mapsto H_{\mathrm{Bulk}} + H_{\mathrm{Bdry}} \ , \\ H_{\mathrm{Bulk}} &= -J \sum_i^{L-1} \left(f_i^\dagger f_{i+1} + f_i^\dagger f_{i+1}^\dagger + \mathrm{h.c.} \right) + 2h \sum_i^L f_i^\dagger f_i - hL \ , \\ H_{\mathrm{Bdry}} &= -J(f_1^\dagger + f_1) \prod_{j=1}^{L-1} (1 - 2f_j^\dagger f_j)(f_L^\dagger + f_L) \ . \end{aligned} \tag{2.6}$$

The term H_{Bdry} comes from the periodic boundary conditions: defining the total fermion number operator $\hat{N} = \sum_i f_i^\dagger f_i$ and the fermion parity $\hat{P} = (-1)^{\hat{N}}$ we see that the term can be rewritten as

$$H_{\text{Bdry}} = J\hat{P}(f_L^\dagger - f_L)(f_1^\dagger + f_1) \ . \tag{2.7}$$

The fermion parity is, moreover, a constant of motion since it commutes with the Hamiltonian $[\hat{P}, \hat{H}] = 0$ and we are free to work in either the $\hat{P} = +1$ or $\hat{P} = -1$ sector. In the even parity sector, $\hat{P} = 1$ and we see that we can absorb H_{Bdry} into H_{Bulk} by extending the upper limit from $L-1$ to L and defining $f_{L+1} = -f_1$. That is, we adopt anti-periodic boundary conditions (also called Neveu-Schwarz boundary conditions). In the odd parity sector we simply take $f_{L+1} = f_1$, i.e. periodic boundary conditions (also called Ramond boundary conditions). The total Hamiltonian is a direct sum of two Hamiltonians acting on these spaces

$$\begin{aligned} H &= H_{\text{NS}} \oplus H_{\text{R}} \ , \\ H_{\text{NS}} &= -J\sum_i^L \left(c_i^\dagger c_{i+1} + c_i^\dagger c_{i+1}^\dagger + \text{hc} \right) + 2h\sum_i^L c_i^\dagger c_i - hL \quad (c_{L+1} = -c_1) \ , \\ H_{\text{R}} &= -J\sum_i^L \left(d_i^\dagger d_{i+1} + d_i^\dagger d_{i+1}^\dagger + \text{hc} \right) + 2h\sum_i^L d_i^\dagger d_i - hL \quad (d_{L+1} = d_1) \ . \end{aligned} \tag{2.8}$$

Here, I have labelled the canonical fermions c, d to stress that these are distinct from the original Jordan-Wigner fermions f since H_{NS} and H_{R} represent the Hamiltonian after projection onto sectors of definite fermion parity.

2.1 Diagonalisation and ground state

In Eq. (2.8), both H_{NS} and H_{R} are quadratic Hamiltonians and so may be solved by Bogoliubov transformation. Since we have translation invariance, we first introduce momentum space variables c_k, d_q by the Fourier transforms

$$\begin{aligned} c_m &= \frac{1}{\sqrt{L}}\sum_k e^{-ikm} c_k \ , \ k \in \frac{\pi}{L} + \frac{2\pi}{L} \times \left\{ -\left\lceil \frac{L-1}{2} \right\rceil, \ldots, \left\lfloor \frac{L-1}{2} \right\rfloor \right\} \ , \\ d_m &= \frac{1}{\sqrt{L}}\sum_q e^{-iqm} d_q \ , \ q \in \frac{2\pi}{L} \times \left\{ -\left\lceil \frac{L-1}{2} \right\rceil, \ldots, \left\lfloor \frac{L-1}{2} \right\rfloor \right\} \ , \end{aligned} \tag{2.9}$$

which explicitly have the property that $c_{m+L} = -c_m, d_{m+L} = d_m$. From now on, we assume that L is even for simplicity. Substituting these expressions into the real-space Hamiltonian and making use of

$$\sum_{m=1}^{L} e^{iqm} = L\delta_{q,0} \ , \tag{2.10}$$

gives the momentum space Hamiltonians

$$H_{\rm NS} = 2\sum_{k>0} \begin{pmatrix} c_k^\dagger & c_{-k} \end{pmatrix} \begin{pmatrix} h - J\cos k & iJ\sin k \\ -iJ\sin k & -(h - J\cos k) \end{pmatrix} \begin{pmatrix} c_k \\ c_{-k}^\dagger \end{pmatrix} + \tilde{E}_0^{\rm NS},$$
$$H_{\rm R} = 2\sum_{q>0} \begin{pmatrix} d_q^\dagger & d_{-q} \end{pmatrix} \begin{pmatrix} h - J\cos q & iJ\sin q \\ -iJ\sin q & -(h - J\cos q) \end{pmatrix} \begin{pmatrix} d_q \\ d_{-q}^\dagger \end{pmatrix} + h_0 + h_{-\pi} + \tilde{E}_0^{\rm R} \ . \tag{2.11}$$

where we have defined

$$\begin{aligned} \tilde{E}_0^{\rm NS} &= \sum_{k>0}(2h - 2J\cos k) - hL = 2h(L/2) - hL - 2J\sum_{k>0}\cos k = 0 \ , \\ \tilde{E}_0^{\rm R} &= \sum_{q>0}(2h - 2J\cos q) - hL = 2h(L/2-1) - hL - 2J\sum_{q>0}\cos q = -2h \ , \\ h_0 &= 2(h-J)d_0^\dagger d_0 \ , \\ h_{-\pi} &= 2(h+J)d_{-\pi}^\dagger d_{-\pi} \ . \end{aligned} \tag{2.12}$$

To diagonalise these quadratic Hamiltonians we now make use of a Bogoliubov transformation of the form

$$\begin{pmatrix} c_k \\ c_{-k}^\dagger \end{pmatrix} = e^{-i\theta_k\sigma_x/2} \begin{pmatrix} \alpha_k \\ \alpha_{-k}^\dagger \end{pmatrix} = \begin{pmatrix} \cos\frac{\theta_k}{2}\alpha_k - i\sin\frac{\theta_k}{2}\alpha_{-k}^\dagger \\ \cos\frac{\theta_k}{2}\alpha_{-k}^\dagger - i\sin\frac{\theta_k}{2}\alpha_k \end{pmatrix} \ , \tag{2.13}$$

with θ_k chosen to eliminate the anomalous $\alpha(k)\alpha(-k)$ terms. One finds that when θ_k satisfies

$$\cos\theta_k = \frac{h - J\cos k}{\sqrt{(h-J\cos k)^2 + (J\sin k)^2}} \ , \ \sin\theta_k = \frac{J\sin k}{\sqrt{(h-J\cos k)^2 + (J\sin k)^2}} \ , \tag{2.14}$$

the resulting Hamiltonian is equal to

$$H_{\rm NS} = \sum_k \epsilon(k)\alpha_k^\dagger\alpha_k + E_0^{\rm NS} \ , \tag{2.15}$$

and

$$\begin{aligned} \epsilon(k) &= 2\sqrt{J^2 + h^2 - 2hJ\cos k} \ , \\ E_0^{\rm NS} &= -\sum_{k>0}\epsilon(k) \ . \end{aligned} \tag{2.16}$$

Likewise, for the Ramond sector, we write

$$\begin{pmatrix} d_q \\ d_{-q}^\dagger \end{pmatrix} = e^{-i\theta_k\sigma_x/2} \begin{pmatrix} \beta_q \\ \beta_{-q}^\dagger \end{pmatrix} = \begin{pmatrix} \cos\frac{\theta_q}{2}\beta_q - i\sin\frac{\theta_q}{2}\beta_{-q}^\dagger \\ \cos\frac{\theta_q}{2}\beta_{-q}^\dagger - i\sin\frac{\theta_q}{2}\beta_q \end{pmatrix} \ (q \neq 0) \ , \tag{2.17}$$

and find

$$H_{\rm R} = 2(h-J)d_0^\dagger d_0 + \sum_{\substack{q\neq-\pi\\ q\neq 0}} \epsilon(q)\beta_q^\dagger\beta_q + 2(h+J)d_{-\pi}^\dagger d_{-\pi} + E_0^{\rm R} \ ,$$
$$E_0^{\rm R} = -2h - \sum_{q>0}\epsilon(q) \ . \tag{2.18}$$

2.1.1 Ground state

Notice that $\epsilon(k)$ is always positive and so the lowest energy state in the Neveu-Schwarz sector is the vacuum state defined by

$$\forall k : \alpha_k|0\rangle_{\rm NS}^h = 0 \ . \tag{2.19}$$

However, in the Ramond sector the $q=0$ contribution $h_0 = 2(h-J)d_0^\dagger d_0$ can have either sign. In particular, for $h > J$ the lowest energy state in the Ramond sector is also a simple vacuum state

$$\forall q : \beta_q|0\rangle_{\rm R}^{h>J} = 0 \ . \tag{2.20}$$

However, for $h < J$ the lowest Ramond state is instead given by

$$\forall q \neq 0 : \beta_q|0\rangle_{\rm R}^{h<J} = 0 \ , \beta_0^\dagger|0\rangle_{\rm R}^{h<J} = 0 \ , \tag{2.21}$$

that is, it is the previous vacuum, with an additional $q=0$ excitation. It therefore has odd fermion parity.

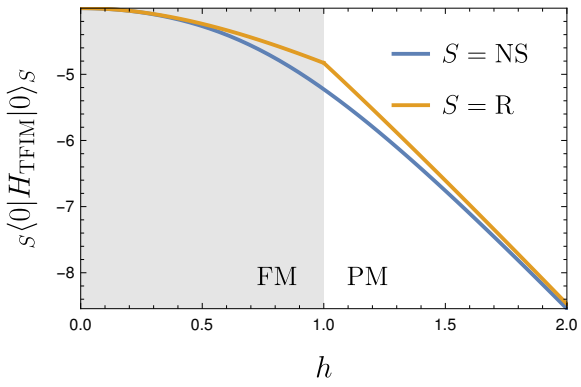

Figure 2.1: Vacuum energies in the Neveu-Schwarz and Ramond sectors, at $L = 4$ to emphasise the finite size effects.

The two regions $h < J$ and $h > J$ define two phases, a ferromagnet and a paramagnet, respectively. At large L the Neveu-Schwarz and Ramond vacua are degenerate in energy; however,

the Ramond vacuum has even fermion parity in the paramagnet and is thus unphysical. In the paramagnet the ground state is therefore $|0\rangle^h_{\rm NS}$. In the ferromagnet, the ground state is still $|0\rangle^h_{\rm NS}$ at finite size, and at large L the system undergoes spontaneous symmetry breaking and picks one of the states in the span of

$$\frac{1}{\sqrt{2}}\left(|0\rangle^h_{\rm NS} \pm |0\rangle^h_{\rm R}\right) \ . \tag{2.22}$$

Gaussian states

At this point it is worth a quick comment that part of the reason why free theories are so useful is because they give rise to *Gaussian* states. A fermionic density matrix is termed Gaussian if it can be written in the form

$$\rho = \mathcal{N}\exp(A_{mn}c^\dagger_m c_n + B_{mn}c_m c_n + D_{mn}c^\dagger_m c^\dagger_n) \ , \tag{2.23}$$

where for ρ to be Hermitian, one requires $A = A^\dagger$ and $B = D^\dagger$. Therefore, for any Hamiltonian H quadratic in fermions, all thermal states

$$\rho = Z^{-1}(\beta)\exp(-\beta H) \ , \tag{2.24}$$

are clearly Gaussian by construction. The ground states correspond to the limit $\beta \to \infty$ and are also Gaussian. In the case of a pure state, such as the ground states, an alternative definition of a Gaussian state is a state in the form

$$|\psi\rangle = \exp\left(T_{ij}c^\dagger_i c^\dagger_j\right)|0\rangle_0 = |0\rangle + T_{ij}c^\dagger_i c^\dagger_j|0\rangle_0 + \frac{1}{2}T_{ij}T_{mn}c^\dagger_i c^\dagger_j c^\dagger_m c^\dagger_n|0\rangle_0 + \dots \ , \tag{2.25}$$

where $|0\rangle_0$ is the original fermion vacuum state, defined by $c_m|0\rangle_0 = 0$ for all m. For instance , in the TFIM, the Neveu-Schwarz vacuum has even parity and is translationally invariant. It is therefore of the form

$$|0\rangle^h_{\rm NS} = |0\rangle_0 + \sum_{k>0} K(k)c^\dagger_k c^\dagger_{-k}|0\rangle_0 + (4 \text{ and higher fermion terms}) \ , \tag{2.26}$$

one can check (via a somewhat lengthy inductive argument that I relegate to App. A.1) that imposing $\alpha(k)|0\rangle^h_{\rm NS} = 0$ leads to the conclusion that the four and higher fermion terms must be of the factorised form implied by being a Gaussian state. Looking at the one fermion terms arising from the equation $\alpha(k)|0\rangle^h_{\rm NS} = 0$ meanwhile gives

$$\begin{aligned} 0 &= \left(i\sin\frac{\theta_k}{2} + K(k)\cos\frac{\theta_k}{2}\right)c_{-k}|0\rangle_0, \\ \implies K(k) &= -\frac{i}{2}\tan\frac{\theta_k}{2} \ . \end{aligned} \tag{2.27}$$

That is, the Bogoliubov fermion vacua are also Gaussian under this definition, as expected, and may be written compactly as

$$|0\rangle^h_{\rm NS} = \exp\left(-\frac{i}{2}\sum_{k>0}\tan\frac{\theta_k}{2}c^\dagger_k c^\dagger_{-k}\right)|0\rangle_0 \ . \tag{2.28}$$

2.1.2 Excitations

We now consider the excitation spectrum, first considering the paramagnet. After imposing fermion parity, the physical states are those that look like

$$|0\rangle^h_{\rm NS} \ , \ \beta^\dagger_q|0\rangle^h_{\rm R} \ , \ \alpha^\dagger_{k_1}\alpha^\dagger_{k_2}|0\rangle^h_{\rm NS} \ , \ \ldots \tag{2.29}$$

whilst states such as

$$|0\rangle^h_{\rm R} \ , \ \alpha_k|0\rangle^h_{\rm NS} \ , \ \beta^\dagger_{q_1}\beta^\dagger_{q_2}|0\rangle_{\rm R} \ , \ldots \tag{2.30}$$

are 'unphysical' (have no clear interpretation in the spin language). The excitations have a gap equal to

$$E_{\rm Gap} = \epsilon(h, q=0) + (E_0^{\rm R} - E_0^{\rm NS}) \ , \tag{2.31}$$

and the low energy eigenstates naturally arrange themselves into a 'one-particle' band with bandwidth $4J$. This description of the elementary excitations agrees with an intuitive picture at $J = 0$ where the system is simply non-interacting spins in an external field, and excitations look like individual spin flips with energy cost $2h$ per spin flip. Turning on J allows these spin flips to hop, causing the spin flip band to disperse.

In the ferromagnetic phase the physical states are

$$|0\rangle^h_{\rm NS} \ , \ |0\rangle^h_{\rm R} \ , \ \alpha^\dagger_{k_1}\alpha^\dagger_{k_2}|0\rangle^h_{\rm NS} \ , \ \beta^\dagger_{q_1}\beta^\dagger_{q_2}|0\rangle^h_{\rm R} \ , \ \ldots \ . \tag{2.32}$$

We therefore see that, in the ferromagnet, excited states must have an even number of excitations above the ground state. The low-lying states therefore form a continuum of two-particle states with width $8h$. Again, we can understand this from a simple limiting picture at $h = 0$ where the system is the classical Ising model and excitations are domain walls. These always occur in pairs, since the system has periodic boundary conditions, and adding a field allows the domain walls to hop and consequently their dispersion to broaden. This analysis allows one to understand the low energy spectrum of the TFIM as represented by the exact diagonalisation results in Fig. 2.2.

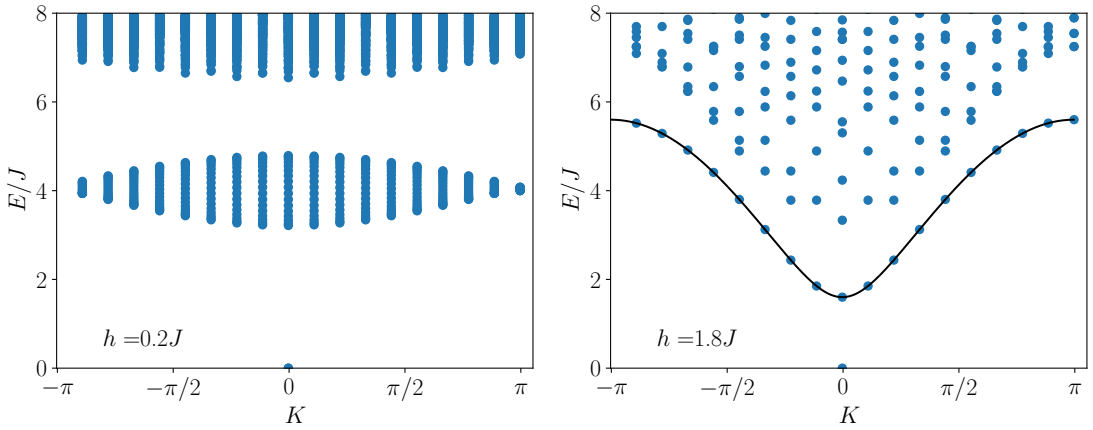

Figure 2.2: Excitations above the ground state for the TFIM in the ferromagnet ($h = 0.2J$) and the paramagnet ($h = 1.8J$). Horizontal axis is total momentum K whilst vertical axis shows energy above the ground state. Points are states found by exact diagonalisation (ED) on $L = 18$ sites using the Python package QuSpin [94, 95]. For $h = 1.8J$, the black line shows the expected one-particle dispersion $\epsilon(k)$ in the paramagnet.

2.2 Correlation functions - Wick's theorem

Aside from the fact that we can diagonalise free theories in a simple manner, they are also especially simple to work with because of Wick's theorem. This says that all $2n$-point correlation functions in a Gaussian state can be written in terms of two-point functions. Since the ground and thermal states of free theories are Gaussian, Wick's theorem can be leveraged. Wick's theorem is often proven by a rather laborious combinatorial proof requiring normal ordering, but there also exists a straightforward algebraic proof due to Gaudin [96]. For the correlation function of four fermionic operators A, B, C, D in a state ρ, this argument runs as follows. We first rewrite the desired four-point function

$$G_4^{ABCD} = \langle ABCD \rangle = \mathrm{Tr}\left[ABCD\rho\right] \ , \tag{2.33}$$

using the anticommutator $\{A, B\} = AB + BA$

$$\mathrm{Tr}\left[ABCD\rho\right] = \mathrm{Tr}\left[\{A,B\}CD\rho\right] - \mathrm{Tr}\left[B\{A,C\}D\rho\right] + \mathrm{Tr}\left[BC\{A,D\}\rho\right] - \mathrm{Tr}\left[BCD(A\rho)\right] \ . \tag{2.34}$$

Wick's theorem is then implied by two requirements on the operators A, B, C, D and the state ρ: firstly, that the anticommutators are c-numbers. Secondly that we can write $A\rho = x\rho A$ for some c-number x (that may depend on A and ρ). These hypotheses allow one to write

$$\mathrm{Tr}\left[ABCD\rho\right] = \frac{\{A,B\}}{1+x}\mathrm{Tr}\left[CD\rho\right] - \frac{\{A,C\}}{1+x}\mathrm{Tr}\left[BD\rho\right] + \frac{\{A,D\}}{1+x}\mathrm{Tr}\left[BC\rho\right] \ . \tag{2.35}$$

Applying the same argument to find the two-point function yields

$$\frac{\{A, B\}}{1+x} = \mathrm{Tr}\left[AB\rho\right] \ , \tag{2.36}$$

and therefore gives Wick's theorem

$$\langle ABCD\rangle = \langle AB\rangle\langle CD\rangle - \langle AC\rangle\langle BD\rangle + \langle AD\rangle\langle BC\rangle \ . \tag{2.37}$$

We are interested in multi-point functions of fermionic creation and annihilation operators, so the requirement that the commutators be c-numbers is automatic. It remains to show that $A\rho = x\rho A$ for a Gaussian density matrix. First, consider 'diagonal' Gaussian density matrices of the form

$$\rho = \frac{e^{-\beta\sum_k \epsilon_k c_k^\dagger c_k}}{Z(\beta)} \ , \tag{2.38}$$

where $Z(\beta)$ is a normalisation constant to force $\mathrm{Tr}[\rho] = 1$. For brevity denote $H = \sum_k \epsilon_k c_k^\dagger c_k$. Note that $(c_k^\dagger c_k)c_k = 0$ and $c_k(c_k^\dagger c_k) = c_k$. Then clearly we have:

$$\begin{aligned} e^{-\beta H} c_k =& c_k \ , \\ c_k e^{-\beta H} =& e^{-\beta\epsilon_k} c_k \ , \\ \therefore\, c_k\rho =& e^{-\beta\epsilon_k}\rho c_k \end{aligned} \tag{2.39}$$

so in this case $x = e^{-\beta\epsilon_k}$. This establishes Wick's theorem for all c_k and, as an easy corollary, all linear combinations thereof. Since Wick's theorem holds for all linear combinations of the c_k, we might just as well have started with a general Gaussian density matrix

$$\rho = Z(\beta)^{-1}\exp(-\beta c_k^\dagger A_{kq} c_q) \ , \tag{2.40}$$

from which the diagonal density matrix above is obtained by diagonalising A.

2.2.1 A Pfaffian formula

A useful result of Wick's theorem is that often once one has decomposed a $2n$-point function into two-point functions, the resulting expression can be recast as the determinant [81] or Pfaffian [97,98] of some matrix and therefore can be efficiently computed. In particular we have

Theorem For $2n$ Majorana fermions $a_1 \dots a_{2n}$ satisfying $a_i^2 = \mathbb{1}$ and $\{a_i, a_j\} = \delta_{ij}$, the $2n$-point function is given by

$$\langle a_1 a_2 \dots a_{2n} \rangle = \mathrm{Pf}(G) \ , \tag{2.41}$$

where G is the skew-symmetric matrix with elements $G_{ij} = \langle a_i a_j \rangle - \delta_{ij}$ and $\mathrm{Pf}(A)$ denotes the Pfaffian of the skew-symmetric matrix A.

Proof *We will prove this by induction on n. For the case $n = 1$ the desired matrix is*

$$G = \begin{pmatrix} 0 & \langle a_1 a_2 \rangle \\ \langle a_2 a_1 \rangle & 0 \end{pmatrix} = \begin{pmatrix} 0 & \langle a_1 a_2 \rangle \\ -\langle a_1 a_2 \rangle & \end{pmatrix} \ . \tag{2.42}$$

The Pfaffian $\mathrm{Pf}(A)$ *satisfies*

$$\mathrm{Pf} \begin{pmatrix} 0 & a \\ -a & 0 \end{pmatrix} = a \ , \tag{2.43}$$

which establies the base case $n = 1$. Then, in an abbreviated notation, Wick's theorem gives the desired $2n$-point function as

$$\begin{aligned} \langle 123 \dots 2n \rangle &= \langle 12 \rangle \langle 3 \dots 2n \rangle - \langle 13 \rangle \langle 24 \dots 2n \rangle + \dots \ , \\ &= \sum_{j=2} (-1)^j \langle 1j \rangle \langle \not{1} 23 \dots j-1 \not{j} j+1 \dots 2n \rangle \end{aligned} \tag{2.44}$$

where the crossed out terms are excluded from the $(2n-2)$-point functions. This is to be compared with the Laplace expansion for the Pfaffian

$$\mathrm{Pf}(A) = \sum_{j=2}^{2n} (-1)^j A_{1j} \, \mathrm{Pf}(\hat{A}_{1j}) \ , \tag{2.45}$$

where $\hat{A}_{1j}$ is the matrix formed by deleting the 1st and jth row and column from A. Since $j \neq 1$ we have $G_{1j} = \langle 1j \rangle$ and by our induction hypthesis $\mathrm{Pf}(\hat{G}_{1j}) = \langle \not{1} 23 \dots j-1 \not{j} j+1 \dots 2n \rangle$, which completes the proof.

Note that using the Laplace expansion for the Pfaffian, or that for the determinant, gives an extremely costly $\mathcal{O}(n!)$ calculation method. Fortunately, the determinant can also be computed efficiently using Gaussian elimination. For the Pfaffian, Gaussian elimination based methods can also be used [99], or, if one does not care about the sign, one can make use of $\mathrm{Pf}(A)^2 = \det(A)$. We will make use of this formula in Section 3.4.2 to compute long ranged equal time correlation functions of $\langle \sigma_m^x \sigma_{m+\ell}^x \rangle$ type in the ANNNI model from knowledge of the Jordan-Wigner fermion two point functions.

2.3 A quantum quench

Being a free theory also enables quantum quench calculations to be analytically carried out for the TFIM that would otherwise not be possible. Several sophisticated methods for calculating both equal and non-equal time correlation functions of spin variables have been found [47, 100–104]. Here however, we focus on the simplest question of what happens to local fermionic observables following a quench — in particular, this means that the following simple calculation does not cover the evolution of the order parameter $\langle\sigma^x(t)\rangle$.

Consider quenching the field from h_i to h_f. Before and after the quench the Hamiltonian can be diagonalised to give a set of modes $\alpha_{i/f}(k)$ such that

$$H_i = \sum_k \epsilon_i(k)\alpha_i^\dagger(k)\alpha_i(k) \ , \ H_f = \sum_k \epsilon_f(k)\alpha_f^\dagger(k)\alpha_f(k) \ . \tag{2.46}$$

These are related to the original fermions by

$$\begin{pmatrix} c(k) \\ c^\dagger(-k) \end{pmatrix} = \exp\left(\frac{i\theta_i}{2}\sigma^x\right)\begin{pmatrix} \alpha_i(k) \\ \alpha_i^\dagger(-k) \end{pmatrix} = \exp\left(\frac{i\theta_f}{2}\sigma^x\right)\begin{pmatrix} \alpha_f(k) \\ \alpha_f^\dagger(-k) \end{pmatrix} \ , \tag{2.47}$$

and therefore the pre- and post-quench modes are related linearly by

$$\alpha_f(k) = \cos\frac{\theta_f-\theta_i}{2}\alpha_i(k) + i\sin\frac{\theta_f-\theta_i}{2}\alpha_i^\dagger(-k) \ . \tag{2.48}$$

Moreover, the time evolution is very simple for two-point functions of the $\alpha_f(k)$ modes, being given by

$$\begin{aligned} \langle\alpha_f^\dagger(k)\alpha_f(k)\rangle(t) =& \langle\alpha_f^\dagger(k)\alpha_f(k)\rangle(t=0) \ , \\ \langle\alpha_f^\dagger(k)\alpha_f^\dagger(-k)\rangle(t) =& e^{-2i\epsilon_f(k)t}\langle\alpha_f^\dagger(k)\alpha_f^\dagger(-k)\rangle(t=0) \ . \end{aligned} \tag{2.49}$$

For simplicity, consider a quench from the ground state of H_i, defined by

$$\begin{aligned} &\langle\alpha_i^\dagger(k)\alpha_i(k)\rangle = 0 = \langle\alpha_i(k)\alpha_i(-k)\rangle \ , \\ &\langle\alpha_i(k)\alpha_i^\dagger(k')\rangle = \delta_{kk'} \ . \end{aligned} \tag{2.50}$$

These translate into

$$\begin{aligned} \langle\alpha_f^\dagger(k)\alpha_f(k)\rangle =& \frac{1}{2}\left(\cos(\theta_f-\theta_i)-1\right) \ , \\ \langle\alpha_f^\dagger(k)\alpha_f^\dagger(-k)\rangle =& -\frac{i}{2}\sin(\theta_f-\theta_i)e^{-2i\epsilon_f(k)t} \ . \end{aligned} \tag{2.51}$$

As stressed earlier, we are interested in local observables. To this end, consider a local fermionic two-point function

$$G(a) = \langle c_m^\dagger c_{m+a} \rangle = \int_{-\pi}^{\pi} \frac{\mathrm{d}k}{2\pi} e^{-iak} \langle c_k^\dagger c_k \rangle \ . \tag{2.52}$$

The desired momentum space function is

$$\langle c_k^\dagger c_k \rangle(t) = (1 + \cos\theta_f)\langle \alpha_f^\dagger(k)\alpha_f(k)\rangle(t) + \sin\theta_f \, \mathrm{Im}\langle \alpha_f^\dagger(k)\alpha_f^\dagger(-k)\rangle(t) \ , \tag{2.53}$$

and consequently the real space Green's function is

$$G(a) = \frac{1}{2}\int_{-\pi}^{\pi} \frac{\mathrm{d}k}{2\pi} e^{-ika} \Big((1+\cos\theta_f)(\cos(\theta_f - \theta_i) - 1) - \sin\theta_f \sin(\theta_f - \theta_i)\cos(2\epsilon_f(k)t) \Big) \ . \tag{2.54}$$

In particular, note that the time dependence consists of a sum of oscillating components spanning a continuous band of frequencies. At late times, the time-dependent term may be approximated using a stationary phase argument: the dispersion relation $\epsilon_f(k)$ has stationary points at $0, \pm\pi$. At these values, the amplitude however is zero since $\sin\theta_f(k = 0, \pi) = 0$. The leading order stationary phase result, which would scale like $t^{-1/2}$, is therefore zero and the time dependent part is given asymptotically by the next term, which is $\mathcal{O}(t^{-3/2})$. We therefore find that local fermionic observables relax to stationary values

$$G(a) = \text{const} + \mathcal{O}(t^{-3/2}). \tag{2.55}$$

This conclusion of power law decay (the specific exponent depending on the operator considered) to stationary values extends to all $2n$-point functions by Wick's theorem. However, quantities like the order parameter $\langle \sigma^x(t) \rangle$, which have non-local representations in terms of Jordan-Wigner fermions, are not covered.

I like talking to Rabbit. He talks about sensible things. He doesn't use long, difficult words, like Owl. He uses short, easy words, like "What about lunch?"

The House at Pooh Corner
A. A. Milne

3

A simple theory for quantum quenches in the ANNNI model

Having introduced the TFIM as an exactly solvable free model in the previous chapter, a natural progression is to consider quenches in an interacting extension of it. This chapter is based on [2], in which we analysed quantum quenches in the anisotropic next-nearest neighbour Ising (ANNNI) model, an interacting generalisation of the TFIM. The immediate motivation of that work was to investigate a proposal in Refs. [105,106] to use intermediate time dynamics to detect quantum critical points. Those works studied the effects of quantum phase transitions (an equilibrium phenomenon) on the nonequilibrium quench dynamics, first in a non-interacting system and then in interacting systems. This chapter revisits the interacting study, using a tool known as self-consistent time-dependent mean-field theory (SCTDMFT), which perturbatively includes the effect of interactions on top of the exact quench dynamics known from the solution to the TFIM.

3.1 Introduction

Quantum phase transitions (QPT) provide a key framework for our understanding of equilibrium phases of correlated quantum matter [82]. More recently physical properties in the vicinity of quantum critical points in out-of-equilibrium settings have been investigated theoretically [36, 107, 108] and in ultra-cold atom experiments [109–111]. An interesting question that has been raised is

whether it is possible to detect the location of QPTs, and associated physical properties, through the dynamics at short and intermediate times after a quantum quench [105,106,112–115]. In Ref. [106], Haldar et al. proposed a set of generalised susceptibilities that quantify the sensitivity of the time evolution and stationary values of local observables to changes in the quench protocol. Based on numerical studies in the axial next-nearest neighbour Ising model (ANNNI), the authors concluded that such susceptibilities can indeed provide signatures of a proximate QPT not only in the stationary regime but already at short/intermediate times. An important question is how general this approach is, and what its limitations are. In order to address these issues we show that the findings of Ref. [106] for the ANNNI model can be understood in terms of a simple (time-dependent) mean-field theory. This approach provides a clear insight into the window of applicability of any approach using generalised susceptibilities to search for the location of critical points. En route we clarify the origin of interesting oscillatory behaviours of local observables observed in Ref. [106].

The outline of this chapter is as follows. In Section 3.2 we introduce the ANNNI model and describe the quench protocol we consider. In Section 3.3 we then construct a mean-field description of the stationary state under the assumption that the system thermalises. We argue that mean-field theory in this stationary state provides a convenient tool to evaluate if the critical phenomena being accessed are truly quantum critical. In Section 3.4 we construct a time-dependent self-consistent mean-field description of the time evolution. Within this approximation the density matrix is Gaussian at all times and Wick's theorem may be employed to calculate any correlation function. This method is expected to be quantitatively accurate for short times as long as the initial state is itself Gaussian. In Section 3.5 we show that non-equal time correlation functions are easily accessible with this method and use it to compute the transverse component of the generalised dynamical structure factor following a quench in the ANNNI, demonstrating that this object contains information about the spectrum of the post-quench Hamiltonian.

3.2 Definition of the model and quench protocol

The ANNNI model is a well studied non-integrable model with competing interactions, see e.g. [116–119]. The model extends the transverse field Ising model by adding a next-nearest neighbour Ising exchange, which we take to have the opposite sign to the nearest-neighbour Ising interaction

$$H(h,\kappa) = -J\sum_{i}^{L}\sigma_i^x\sigma_{i+1}^x - h\sum_{i}^{L}\sigma_i^z + \kappa\sum_{i}^{L}\sigma_i^x\sigma_{i+2}^x \ . \tag{3.1}$$

Here σ_j^α are the usual Pauli matrices on sites j of a ring of circumference L. As discussed in Chapter 2, the Hamiltonian (3.1) can be mapped to a model of spinless lattice fermions. Whilst the discussion of Ramond/Neveu-Schwarz boundary conditions of that chapter does a priori apply here, in what follows we only consider operators which have even fermion parity. For our purposes, therefore, it is sufficient to consider only the Neveu-Schwarz sector. For simplicity we only consider even system sizes L. The Hamiltonian then reads

$$\begin{aligned} H(h,\kappa) = &- J\sum_j \left(c_j^\dagger c_{j+1} + c_j^\dagger c_{j+1}^\dagger + \text{h.c.}\right) + \kappa \sum_j (c_j^\dagger c_{j+2} + c_j^\dagger c_{j+2}^\dagger + \text{h.c.}) + 2h\sum_j c_j^\dagger c_j \\ &+ 2\kappa \sum_j \left(c_j c_{j+1}^\dagger c_{j+1} c_{j+2}^\dagger - c_j^\dagger c_{j+1}^\dagger c_{j+1} c_{j+2}^\dagger + \text{h.c.}\right) \ . \end{aligned} \tag{3.2}$$

The next-nearest neighbour spin-spin interaction is seen to give rise to a quartic interaction amongst the fermions, making the model non-integrable. The Hamiltonian (3.1) has a global $\mathbb{Z}_2 \otimes \mathbb{Z}_2$ symmetry corresponding to rotations around the z-axis by π,which is broken spontaneously in the ferromagnetic phase, and site parity $\sigma_n^\alpha \mapsto \sigma_{-n}^\alpha$. The latter remains unbroken in the situations we consider and enforces $t_{ij} \equiv \langle c_i^\dagger c_j \rangle = t_{ji} \in \mathbb{R}$ (see Appendix A.2), while the former translates into fermion number parity.

The ground state phase diagram of the ANNNI model for $\kappa < J/2$ is shown in Fig. 3.1 [117, 120–122]. For $\kappa > J/2$ the phase diagram is substantially more complicated, but, like Ref. [106], we

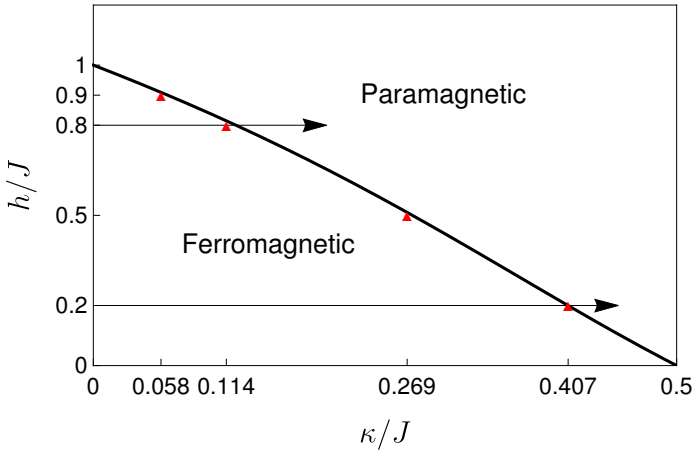

Figure 3.1: Ground state phase diagram of the ANNNI model for $0 < \kappa/J < 1/2$ - the solid curve is the boundary obtained by second order perturbation theory (3.3), red triangles indicate the critical points found by our self-consistent mean-field theory at select fields. There exist other phases at $\kappa > J/2$. Arrows indicate the quenches performed in this work.

restrict our analysis to the ferromagnet-paramagnet transition. At $\kappa = 0$ the model (3.1) reduces

to the transverse field Ising model (TFIM) and is exactly solvable, with a quantum phase transition at $h = J$. For $\kappa > 0$ a second order phase transition in the Ising universality class separates a ferromagnetically ordered phase from a paramagnetic one. For $\kappa < J/2$ and small values of h the locus of the critical line can be determined by second order perturbation theory, which yields [116]

$$J - 2\kappa_c = h_c - \frac{1}{2J}\frac{\kappa_c h_c^2}{J - \kappa_c} \ . \tag{3.3}$$

In terms of the spins the transition is characterised by the order parameter $\langle \sigma_j^x \rangle$ taking a non-zero value in the ferromagnetic phase. In terms of the fermions this is a non-local (string) operator and the transition is topological [123]. Our analysis of quench dynamics close to quantum critical points in one dimension therefore pertains to both topological transitions and conventional transitions with local order parameters. Our mean-field analysis developed below may be expected to work rather well for small κ/J as it is exact along the line $\kappa = 0$. Moreover, since the (equilibrium) mean-field theory we describe below is via a free fermion whose critical scaling limit is a relativistic Majorana fermion [124], we correctly account for the symmetry and critical exponents of the Ising transition. Hence, our mean-field theory is expected to give a quantitatively accurate description of the ANNNI model in the region $h \approx J$ and $\kappa \approx 0$. Conversely, mean-field theory cannot be expected to give a reasonable description either deep into the paramagnetic phase or for the other transitions. We therefore do not investigate the rest of the phase diagram in this chapter.

In what follows we consider quantum quenches from initial thermal states of the TFIM with transverse field h_i and inverse temperature β, i.e. our initial density matrix is

$$\rho(t = 0) = \frac{\exp\big(-\beta H(h_i, 0)\big)}{\mathrm{Tr}\exp\big(-\beta H(h_i, 0)\big)} \ . \tag{3.4}$$

Including thermal states at finite temperatures rather than only ground states is useful as it allows us to tune the energy density of the stationary state reached at late times in a simple manner. We then consider the time evolution induced by the ANNNI Hamiltonian $H(h_f, \kappa)$, i.e.

$$\rho(t > 0) = e^{-iH(h_f,\kappa)t}\rho(t = 0)e^{iH(h_f,\kappa)t} \ . \tag{3.5}$$

We will restrict ourselves to the case $h_i = h_f \equiv h$ and quenches with $\kappa < J/2$. To simplify notations we also set $J = 1$. As the ANNNI model is non-integrable when both h and κ are non-zero we expect the model to thermalise [107, 125], i.e. in the thermodynamic limit the system should locally relax to a thermal stationary state described by an effective temperature that is set by the energy density of the initial state

$$e_0 = \lim_{L\to\infty} \frac{1}{L}\mathrm{Tr}\Big(\rho(t = 0)H(h_f, \kappa)\Big). \tag{3.6}$$

In our setup the correlation length typically starts off small as a result of a large pre-quench gap, while at late times the system settles into a thermal state at a low effective temperature in the vicinity of a quantum critical point. Hence, the correlation length in the stationary state is typically much larger than in the initial state. Intuitively, therefore, the physics should be that of a system whose correlation length grows following the quench.

3.3 Mean-field theory for the stationary state

Since the ANNNI model is believed to thermalise and has no local conservation laws other than the total energy, we expect local observables $\mathcal{O}$ to reach their Gibbs ensemble values at late times after a quantum quench

$$\langle \mathcal{O} \rangle(t) \overset{t=\infty}{\longrightarrow} Z^{-1} \mathrm{Tr}[e^{-\beta_f H(h_f,\kappa)} \mathcal{O}] \ . \tag{3.7}$$

Here Z is the partition function and β_f the inverse effective temperature, set by the initial energy density (3.6) generated by the quench protocol. For sufficiently small values of κ this thermal state should be amenable to a description in terms of a simple self-consistent mean-field theory of spinless fermions

$$Z^{-1} \mathrm{Tr}[e^{-\beta_f H} \mathcal{O}] \approx Z_{\mathrm{MFT}}^{-1} \mathrm{Tr}[e^{-\beta_{\mathrm{MFT}} H_{\mathrm{MFT}}} \mathcal{O}] \ , \tag{3.8}$$

where

$$H_{\mathrm{MFT}} = \sum_i \sum_{a=0}^{2} \left\{ J_{\mathrm{Eff}}^{(a)} (c_i^\dagger c_{i+a} + \mathrm{hc}) + (\Delta_{\mathrm{Eff}}^{(a)} c_i^\dagger c_{i+a}^\dagger + \mathrm{hc}) \right\} + E_0 \ . \tag{3.9}$$

This mean-field theory is the result of requiring that Wick's theorem holds, or equivalently that higher cumulants vanish. The effective couplings $J_{\mathrm{Eff}}^{(a)}$ and $\Delta_{\mathrm{Eff}}^{(a)}$ and the constant E_0 are generated by decoupling the quartic interaction terms self-consistently via

$$ABCD \mapsto \langle AB \rangle_{\mathrm{MFT}} CD + AB \langle CD \rangle_{\mathrm{MFT}} - \langle AB \rangle_{\mathrm{MFT}} \langle CD \rangle_{\mathrm{MFT}} + \text{all other Wick contractions} \ , \tag{3.10}$$

where

$$\langle \mathcal{O} \rangle_{\mathrm{MFT}} \equiv Z_{\mathrm{MFT}}^{-1} \mathrm{Tr}[e^{-\beta_{\mathrm{MFT}} H_{\mathrm{MFT}}} \mathcal{O}] \ . \tag{3.11}$$

Defining the (self-consistent) expectation values

$$\begin{aligned} t_a &\equiv \langle c_j^\dagger c_{j+a} \rangle_{\mathrm{MFT}} \ , \quad a = 0, 1, 2 \ , \\ \Delta_b &\equiv \langle c_j^\dagger c_{j+b}^\dagger \rangle_{\mathrm{MFT}} \ , \quad b = 1, 2 \ , \end{aligned} \tag{3.12}$$

we have

$$\begin{aligned} J^{(0)}_{\text{Eff}} &= h - 2\kappa(t_2 + \operatorname{Re}\Delta_2) \ , \\ J^{(1)}_{\text{Eff}} &= -(J - 4\kappa(t_1 + \operatorname{Re}\Delta_1)) \ , \quad \Delta^{(1)}_{\text{Eff}} = -(J - 4\kappa(t_1 + \Delta_1^*)) \ , \\ J^{(2)}_{\text{Eff}} &= \kappa(1 - 2t_0) \ , \qquad\qquad\quad \Delta^{(2)}_{\text{Eff}} = \kappa(1 - 2t_0) \ , \\ E_0 &= -hL - 4L\kappa(|\Delta_1|^2 + t_1^2 - t_0 t_2 + 2\operatorname{Re}\Delta_1 t_1 - \operatorname{Re}\Delta_2 t_0) \quad . \end{aligned} \tag{3.13}$$

Note that $J^{(1)}_{\text{Eff}} \neq \Delta^{(1)}_{\text{Eff}}$. In order to fully specify our self-consistent mean-field theory we require the self-consistent values of the five mean-fields as well as the value of the inverse effective temperature β_{MFT}, which is fixed by the condition that the energy density in the stationary state is the same as in the initial state (3.6), i.e.

$$e_0 = \lim_{L\to\infty} \frac{\langle H_{\text{MFT}} \rangle_{\text{MFT}}}{L} \ . \tag{3.14}$$

The various self-consistency equations are most easily solved in momentum space. As stated above, it is sufficient to work in the Neveu-Schwarz sector for even system sizes L, so that

$$c_k \equiv \frac{1}{\sqrt{L}} \sum_m e^{ikm} c_m \ , \qquad k \in \left\{ 2\pi \frac{n + 1/2}{L} \ , \ n = -\frac{L}{2}, \dots, \frac{L}{2} - 1 \right\} \ . \tag{3.15}$$

The mean-field Hamiltonian then becomes

$$\begin{aligned} H_{\text{MFT}} &= \sum_{k>0} A_k (c_k^\dagger c_k - c_{-k}^\dagger c_{-k}) + i B_k (c_k^\dagger c_{-k}^\dagger) - i B_k^* (c_{-k} c_k) + \text{const} \ , \\ A_k &= 2 \sum_{a=0}^{2} J^{(a)}_{\text{Eff}} \cos ak \ , \qquad B_k = 2 \sum_{a=1}^{2} \Delta^{(a)}_{\text{Eff}} \sin ak \ . \end{aligned} \tag{3.16}$$

We remark that in equilibrium not just the t_a but also the Δ_b are in fact real despite the absence of a unitary symmetry enforcing this, see Appendix A.2. This in turn makes it possible to diagonalise the Hamiltonian by a one-parameter Bogoliubov transformation

$$b_\kappa(k) = \cos \frac{\theta_\kappa(k)}{2} c(k) - i \sin \frac{\theta_\kappa(k)}{2} c^\dagger(-k) \ , \qquad e^{i\theta_\kappa(k)} = \frac{A_k - iB_k}{\sqrt{A_k^2 + B_k^2}} \ , \tag{3.17}$$

which gives [1]

$$H_{\text{MFT}} = \sum_{k>0} \varepsilon_\kappa(k) b_\kappa^\dagger(k) b_\kappa(k) + \text{const} \ , \qquad \varepsilon_\kappa(k) = \sqrt{A_k^2 + |B_k|^2} . \tag{3.18}$$

[1] Here we write $|B_k|^2$ which gives the correct dispersion for complex B_k, as it will be out-of-equilibrium, although the form of the required canonical transformation in (3.17) will be more complicated.

The self-consistency conditions on the mean-fields are given by calculating the expectation values using (3.11)

$$t_a = \frac{1}{L}\sum_k e^{-iak}\langle c_k^\dagger c_k\rangle_{\rm MFT} = \frac{1}{L}\sum_{k>0}\cos ak\left(1-\cos\theta_\kappa(k)\tanh\frac{\beta_{\rm MFT}\varepsilon_\kappa(k)}{2}\right)\,, \tag{3.19}$$

$$\Delta_a = \frac{1}{L}\sum_k e^{-iak}\langle c_k^\dagger c_{-k}^\dagger\rangle_{\rm MFT} = \frac{1}{L}\sum_{k>0}\sin ak\sin\theta_\kappa(k)\tanh\frac{\beta_{\rm MFT}\varepsilon_\kappa(k)}{2}\,, \tag{3.20}$$

while the equation fixing the effective temperature (3.6) takes the form

$$\begin{aligned}&4\kappa\left((t_1+\Delta_1)^2-(t_0-1/2)(t_2+\Delta_2)\right)_{\kappa=0}+h-\frac{1}{L}\sum_{k>0}\varepsilon_{\kappa=0}(k)\tanh\frac{\beta_i\varepsilon_{\kappa=0}(k)}{2}\\ &=E_0+J_{\rm Eff}^{(0)}-\frac{1}{L}\sum_{k>0}\varepsilon_\kappa(k)\tanh\frac{\beta_{\rm MFT}\varepsilon(k)}{2}.\end{aligned} \tag{3.21}$$

The initial energy density given by the left hand side of (3.21) is a constant for fixed values of κ and h; however, the right hand side depends upon the values of the mean-fields and thus this equation must be solved self-consistently along with the other conditions on the mean-fields.

Eqs. (3.19)-(3.21) need to be solved numerically, where the Bogoliubov angles are defined by Eq. (3.17) and Eq. (3.13). The solutions can be directly compared to numerical results obtained in Ref. [106] via a numerical linked cluster expansion [126, 127]. In Fig. 3.2, we plot the mean-field

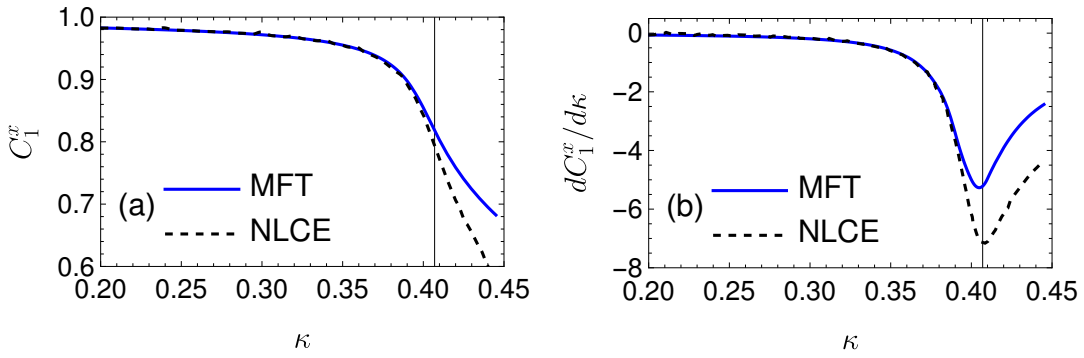

Figure 3.2: (a) $C_1^x = 2(t_1+\Delta_2)$ in the thermal state reached at late times after a quench from the TFIM ground state at $h = 0.2$ as a function of κ. The solid blue line is the result obtained from our self-consistent mean-field theory and the dashed black line shows numerical linked cluster expansion (NLCE) results extracted from [106]. (b) Same comparison as (a) but for $\chi_1 = \partial_\kappa C_1^x(\kappa)$. The vertical lines indicate κ_c.

results for the longitudinal nearest-neighbour correlator

$$C_1^x \equiv \langle\sigma_i^x\sigma_{i+1}^x\rangle = 2(t_1+\mathrm{Re}\,\Delta_1)\,, \tag{3.22}$$

in the (thermal) steady state following a quench from the ground state of the TFIM with $h = 0.2$ along with the susceptibility $\mathrm{d}C_1^x/\mathrm{d}\kappa$ defined using an ensemble of quenches. We see that the agreement of our mean-field analysis with the numerical results of Ref. [106] is excellent, up to fairly large values of κ. We observe similarly good agreement with the transverse magnetisation $m^z \equiv \langle \sigma_j^z \rangle$ and the next-nearest neighbour longitudinal correlator $C_2^x \equiv \langle \sigma_i^x \sigma_{i+2}^x \rangle$. In Fig. 3.3 we compare the self-consistent inverse temperature β_{MFT} to numerical results of Ref. [106]. We observe excellent agreement essentially over the full range of κ considered.

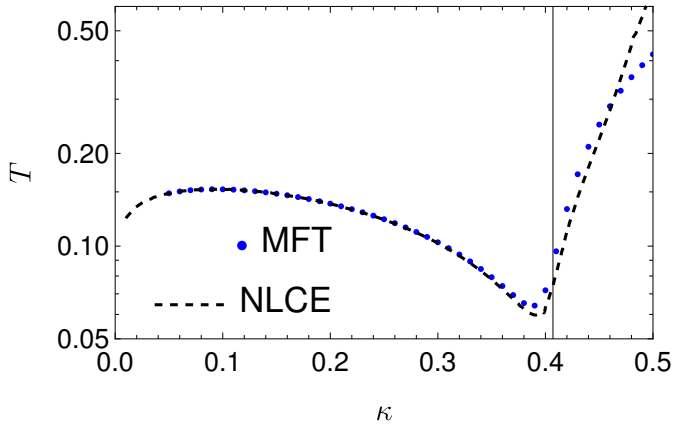

Figure 3.3: Comparison of $T = \beta_{\mathrm{MFT}}^{-1}$ to effective temperatures reported in [106]. The dashed black curve shows the NLCE results reported in Fig. 8 of [106], while the blue data points are the values found by our self-consistent mean-field theory. The vertical line indicates κ_c.

Given the good agreement with state-of-the-art numerical results, we conclude that our self-consistent fermionic mean-field theory provides a good description of the steady state reached at late times after the quenches considered.

3.3.1 Scaling regime at finite energy densities

The key objective of Ref. [106] was to establish that quantum quenches can be used to locate the positions of quantum phase transitions in some parameter space. An important question is to what extent the observed signatures are indeed associated with the scaling behaviour induced by the proximate quantum critical point. To answer this question by purely numerical methods would require the analysis of the long distance behaviour of correlation functions or entanglement entropies of large subsystems, in order to ascertain whether they display scaling behaviour characteristic of the proximate quantum critical point. Our mean-field theory gives us a much simpler way of answering

this question: as the field theory describing the quantum critical point is a gapless relativistic Majorana fermion the scaling regime extends at most to energies per particle at which the mean-field dispersion is still to a good approximation linear. These considerations set an energy cut-off for the field theory. In Fig. 3.4, we plot the mean-field dispersion relation (3.18) and compare it to the respective effective temperatures. We see from Fig. 3.4(c,d) that, when h is close to 1 and κ

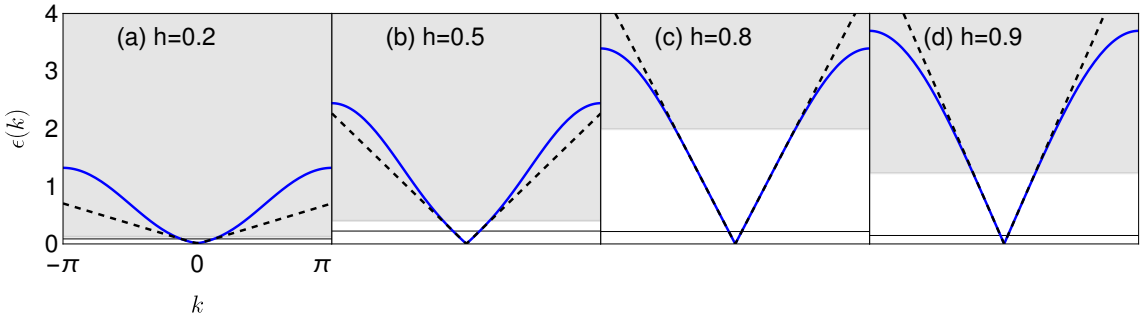

Figure 3.4: Effective dispersion relations in the steady state following a quench with (a) $h = 0.2$, $\kappa = 0.407 \approx \kappa_c$, (b) $h = 0.5$, $\kappa = 0.269 \approx \kappa_c$, (c) $h = 0.8$, $\kappa = 0.114 \approx \kappa_c$, (d) $h = 0.9$, $\kappa = 0.058 \approx \kappa_c$. The black horizontal line is the effective temperature $T = \beta_{\mathrm{MFT}}^{-1}$. The dashed black line is a fit to $\varepsilon_{\mathrm{fit}}(k) = \sqrt{\varepsilon_\kappa(0)^2 + v_{\mathrm{fit}}^2 k^2}$ and the gray shaded region indicates the regime of energy densities where spectral nonlinearities become significant and corrections to scaling limit behaviour can no longer be expected to be negligible.

is small, the scale over which the dispersion is linear is much larger than the effective temperature. This implies that for these quenches the steady state is in fact in the scaling regime of the Ising transition and properties of the underlying quantum critical point are readily accessible.

By contrast in Fig. 3.4(a,b) we show the mean-field dispersion relation (3.18) in the steady state for quenches with small h and large κ can be fitted with a relativistic dispersion only for a small energy window. Here the scale over which the Majorana dispersion is linear is very small and of the same order of magnitude as the effective temperature. This means that for these quenches the steady state is *outside* the scaling regime of the Ising transition, and so we cannot actually glean any useful information about the underlying quantum critical point using quench dynamics.

We expect the fact that the cut-off decreases for smaller values of h to be an accurate prediction of the mean-field theory presented here in light of the good agreement with the numerics seen in Fig. 3.2. The point that the energy density needs to be sufficiently below the cut-off scale of the quantum critical point one is trying to probe is of course very general.

3.4 Self-consistent time-dependent mean-field theory (SCTDMFT)

Following Refs [128–134], we now turn to the dynamics after our quantum quenches in the framework of a self-consistent time-dependent Gaussian approximation. This amounts to considering time evolution with a time-dependent mean-field Hamiltonian

$$H_{\mathrm{MFT}}(t) = \sum_i \sum_{a=0}^{2} \left\{ J^{(a)}_{\mathrm{Eff}}(t)(c_i^\dagger c_{i+a} + \mathrm{hc}) + (\Delta^{(a)}_{\mathrm{Eff}}(t) c_i^\dagger c_{i+a}^\dagger + \mathrm{hc}) \right\} + E_0(t) \ , \tag{3.23}$$

where the time-dependent couplings are given by the time-dependent analogs of (3.13), i.e.

$$\begin{aligned} t_a(t) &= \mathrm{Tr}\Big(\rho_{\mathrm{MFT}}(t) c_j^\dagger c_{j+a}\Big) \ , \quad a = 0, 1, 2 \ , \\ \Delta_b(t) &= \mathrm{Tr}\Big(\rho_{\mathrm{MFT}}(t) c_j^\dagger c_{j+b}^\dagger\Big) \ , \quad b = 1, 2 \ , \\ \rho_{\mathrm{MFT}}(t) &= \left\{ \mathcal{T} e^{-i\int_0^t H_{\mathrm{MFT}}(t')\mathrm{d}t'} \right\} \rho(t=0) \left\{ \mathcal{T} e^{-i\int_0^t H_{\mathrm{MFT}}(t')\mathrm{d}t'} \right\}^\dagger \ . \end{aligned} \tag{3.24}$$

Here $\mathcal{T}$ denotes time ordering; the initial density matrix $\rho(t=0)$ (3.4) is by construction Gaussian and concomitantly so is $\rho_{\mathrm{MFT}}(t)$. This is the essence of the SCTDMFT, which by construction is expected to work best at short times. This is because it is based on the assumption that all higher cumulants vanish, which is strictly true at time $t = 0$. At short times the higher cumulants will become non-zero, but their growth is expected to be slow for small κ.

At late times SCTDMFT, is not expected to work well in general [53, 54] and in some models is known to describe relaxation towards a "prethermalisation plateau" [135–137]. This can be described by a deformation of a Generalised Gibbs ensemble rather than the Gibbs ensemble that describes the thermalised steady state. The studies of Refs. [53, 54], in which the accuracy of the SCTDMFT was assessed in detail, focused on initial states that led to non-trivial dynamics even in the absence of interactions. In such settings the prethermalisation plateau is generally well separated from the corresponding thermal expectation values, and as a result SCTDMFT cannot describe the late time behaviour, even qualitatively.

However, following Ref. [106], here we consider initial states for which there is no dynamics without quenching the interaction strength. This is the scenario investigated by [135, 138, 139]. As a result the system still prethermalises, but now for local quantities the prethermalisation plateau is quite close to the corresponding thermal expectation values. Given that the prethermalisation plateau is reached at early times where SCTDMFT works well, the expectation is that the difference to the Gibbs value at small κ is of order $\mathcal{O}(\kappa^2)$. Hence, SCTDMFT can be viewed as providing a

reasonable account of the late time behaviour (as long as the quench parameter κ is small enough, which must be checked numerically). We elaborate on this point below by comparing the late-time behaviour in SCTDMFT to the expected equilibrium values.

As a consequence of the translation invariance of the problem, the time-evolved Gaussian density matrix $\rho_{\mathrm{MFT}}(t)$ is fully characterised by the two momentum space two-point averages

$$\tilde{t}_k(t) = \mathrm{Tr}\Big(\rho_{\mathrm{MFT}}(t)\ c_k^\dagger c_k\Big)\ , \qquad \tilde{\Delta}_k(t) = \mathrm{Tr}\Big(\rho_{\mathrm{MFT}}(t)\ c_k^\dagger c_{-k}^\dagger\Big). \tag{3.25}$$

The self-consistent equations of motion for these k space two-point functions can be obtained using the Heisenberg equations of motion associated to the (now time-dependent) analog of the momentum space Hamiltonian (3.16). The result is

$$\begin{aligned} \frac{\mathrm{d}\tilde{\Delta}_k(t)}{\mathrm{d}t} =& 2iA_k(t)\tilde{\Delta}_k(t) + B_k^*\Big[1 - 2\tilde{t}_k(t)\Big] \\ \frac{\mathrm{d}\tilde{t}_k(t)}{\mathrm{d}t} =& 2\,\mathrm{Re}\left(B_k(t)\tilde{\Delta}_k(t)\right)\ , \end{aligned} \tag{3.26}$$

where

$$A_k = 2\sum_{a=0}^{2} J_{\mathrm{Eff}}^{(a)}(t)\cos ak\ , \qquad B_k = 2\sum_{b=1}^{2}\Delta_{\mathrm{Eff}}^{(b)}(t)\sin ak\ . \tag{3.27}$$

We now integrate the equations (3.26) using a second-order midpoint scheme with a time step of 10^{-3}, which we choose to ensure that the mean-fields are converged with respect to the time step. At each time step we must update the real space mean-fields t_a and Δ_b using $\tilde{t}_k$ and $\tilde{\Delta}_k$

$$t_a = \frac{1}{L}\sum_k \tilde{t}_k(t)e^{-ika}\ , \qquad \Delta_b = \frac{1}{L}\sum_k \tilde{\Delta}_k(t)e^{-ikb}\ . \tag{3.28}$$

Physical quantities such as spin-spin correlation functions can then be calculated in terms of (sums of products of) the fermionic two-point functions.

3.4.1 Short and intermediate-time behaviour of local correlation functions

In Fig. 3.5, we compare the results of the above SCTDMFT approximation to iTEBD results taken from [106], which are believed to be essentially numerically exact. For small values of κ compared to the critical value κ_c we find excellent agreement over the entire time range accessible to iTEBD. For larger values of κ the agreement is still very good at short times, but gets worse at late times.

While Ref. [106] focused on spin correlations, the time evolution of the fermionic two-point functions is of interest as well, in particular in relation to the question of detecting topological

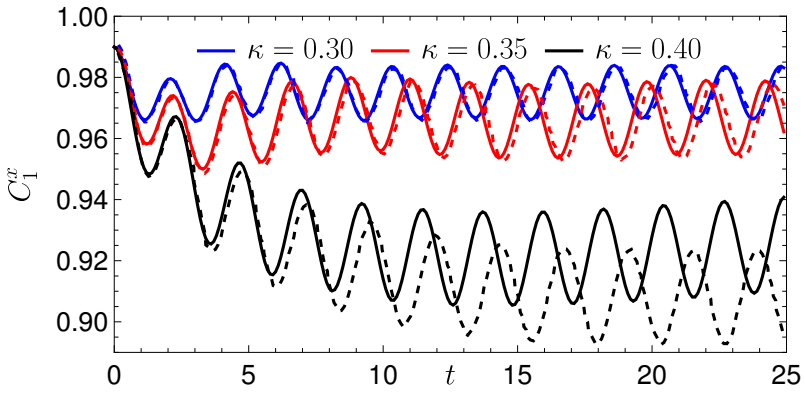

Figure 3.5: Comparison of SCTDMFT results for $C_1^x(t)$ to iTEBD results taken from [106] for a quench from the ground state at $h = 0.2, \kappa = 0$ to $\kappa > 0$. Here the solid lines are SCTDMFT results for $L = 2000$ and the dashed lines in the respective color are iTEBD. The agreement is seen to be very good except for near the critical point ($\kappa_c \approx 0.407$).

transitions by quench dynamics. In Fig. 3.6, we present results obtained by SCTDMFT for $t_1(t)$ and $\mathrm{Re}(\Delta_1(t))$ following quenches from the ground state of $H(h, \kappa = 0)$ with $h = 0.2, 0.8$ to $\kappa = 0.05, 0.20$. We observe the following:

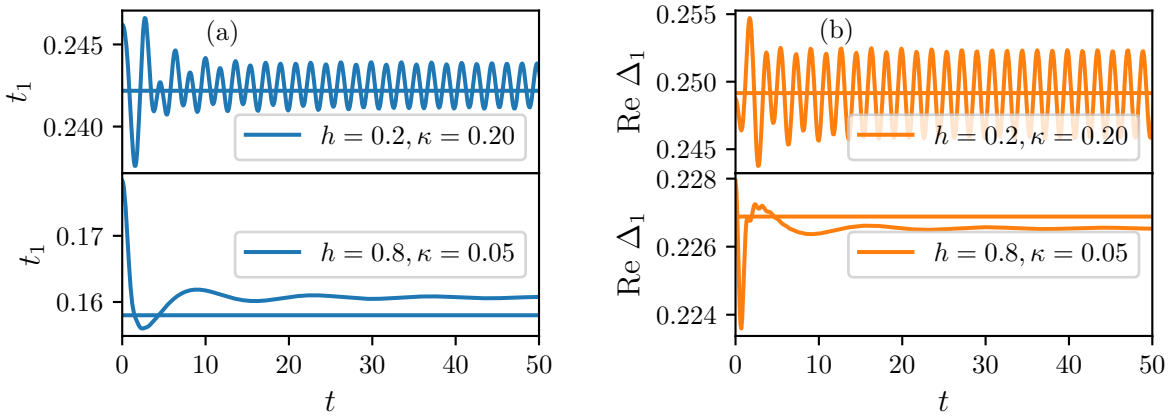

Figure 3.6: Nearest neighbour fermion two-point functions $t_1(t)$, $\mathrm{Re}\,\Delta_1(t)$ after quenches from the ground state of $H(h, \kappa = 0)$ with $h = 0.2$ and $h = 0.8$ to $H(h, \kappa)$. Horizontal lines indicate the stationary values found in Section 3.3.

- For quenches with small transverse fields h there are persistent oscillations around a constant value, which is in good agreement with the corresponding expectation value after thermalisation.

- For quenches at large fields h there are no long-lived oscillations. Instead the expectation values relax to stationary values that differ from the ones predicted (in mean-field theory) by thermalisation, by an amount that we find scales as $\mathcal{O}(\kappa^2)$ as expected.

An explanation of the oscillatory behaviour is provided below in Section 3.4.3.

As suggested in [106], a signature of the proximate quantum phase transition can be obtained by processing data for the expectation value of a local observable for an ensemble of quenches at a fixed time t after the quench. In Fig. 3.7 we show results for $C_1^x(t)$ and $dC_1^x(t)/d\kappa$ for an ensemble of quenches starting in the ground state of $H(h, \kappa = 0)$ and quenching to $H(h, \kappa)$ for $h = 0.2, 0.8$ and a wide range of κ values.

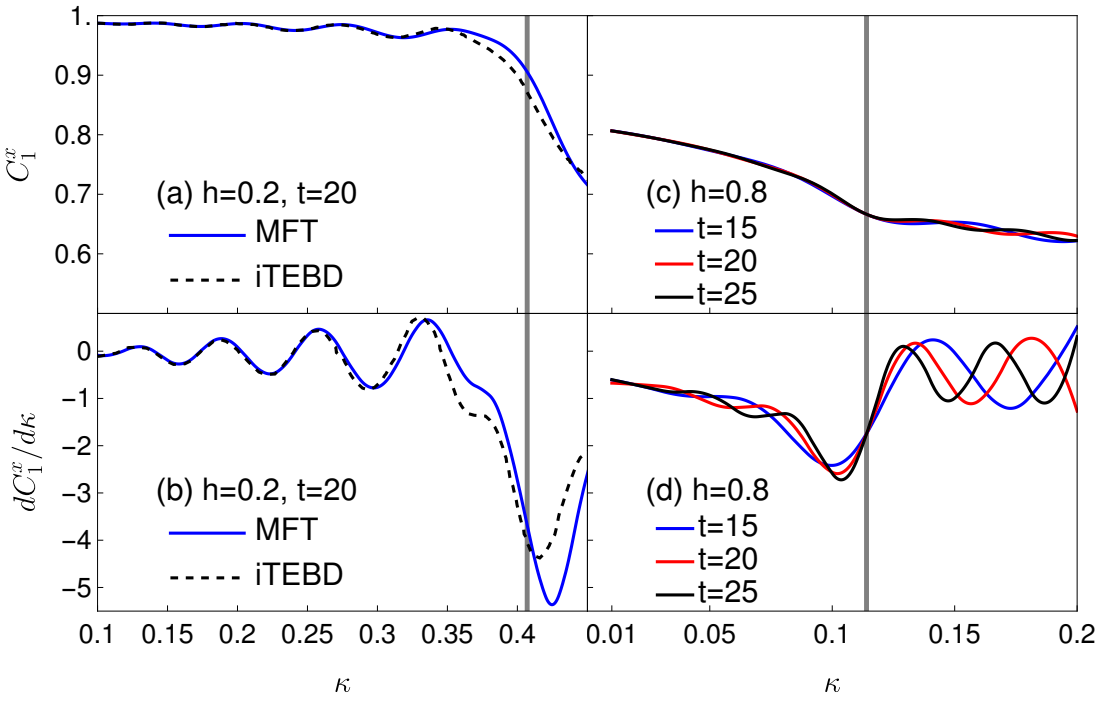

Figure 3.7: Performing quenches from $H(h, 0)$ to $H(h, \kappa)$ we build a picture of observables as a function of final κ. (a-b) Comparison with iTEBD data taken from [106] for $h = 0.2$ ($\kappa_c \approx 0.407$, indicated by thick gray line). (c-d) Equivalent calculation at $h = 0.8$ ($\kappa_c \approx 0.114$). All quench calculations are performed starting from the ground state and with a system size $L = 2000$.

In Fig. 3.7(a-b), we find very good agreement between our SCTDMFT results and the iTEBD simulations of Ref. [106] for $h = 0.2$ and in Fig. 3.7(c-d) we show the results for $h = 0.8$. The generalised susceptibility $\mathrm{d}C_1^x/\mathrm{d}\kappa$ in Fig. 3.7(b,d) shows a strong dip even at the relatively early time $t = 20$ around the critical value κ_c. Intuitively one expects that the reason for this strong

response to the varying post-quench parameters is that the correlation length at time $t = 20$ is already large and the system "feels" the proximity of the QPT; this implies a large correlation length and consequently a strong linear response of the system, reflected in the dips in generalised susceptibilities. We return to this point in the next section where, in Fig. 3.9, we extract correlation lengths for the nonequilibrium state of the system following the quench for $h = 0.8$ and find that the correlation length has grown from $\xi \approx 1.9$ at $t = 0$ to $\xi \approx 12$ at $t = 20$. Conversely, in cases where the correlation length is short, we do not expect the susceptibility to be large. This is indeed the case for small values of κ in Fig. 3.7. In Fig. 3.8 we show the time evolution of the generalised

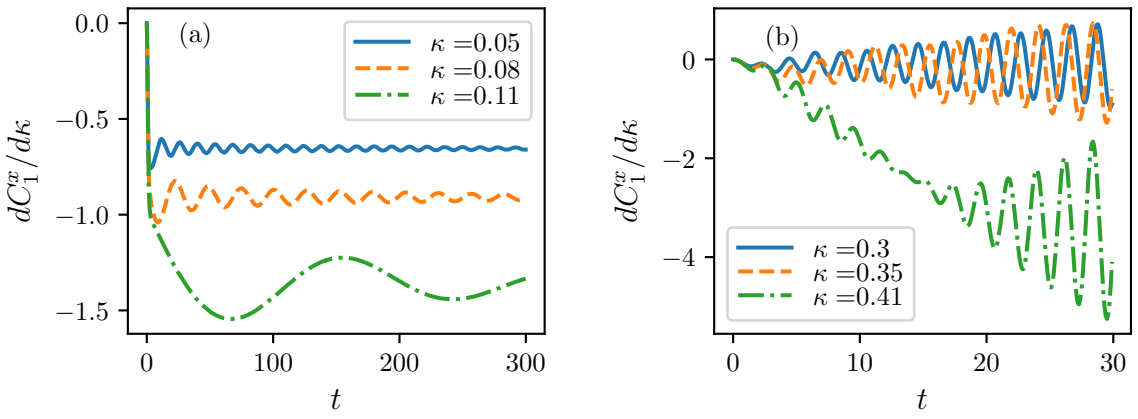

Figure 3.8: Short time dynamics of the generalised susceptibility for quenches from an initial thermal state with $\beta = 2.0$ and (a) $h = 0.8$ ($\kappa_c \approx 0.114$) and (b) $h = 0.2$ ($\kappa_c \approx 0.407$) on a system with $L = 2000$.

susceptibilities. Fig. 3.8 shows , for two values of h, quench data for various κ, including near the critical value κ_c. For κ far from κ_c we observe a quick relaxation to a plateau, whilst for κ close to the QPT we observe a longer relaxation time. Fig. 3.8(b) features growing oscillations due to a 'beat' phenomenon when numerically differentiating between the different quench data with slightly different persistent oscillation frequencies.

3.4.2 Growth of the correlation length in time

As we have noted above, the correlation length grows in time for many of the quenches we consider. To show this explicitly we focus on the connected order-parameter two-point function

$$C^x_{c,\ell}(t) = \underbrace{\mathrm{Tr}\left[\rho_{\mathrm{MFT}}(t)\ \sigma^x_n \sigma^x_{n+\ell}\right]}_{C^x_\ell(t)} - \left(\mathrm{Tr}\left[\rho_{\mathrm{MFT}}(t)\ \sigma^x_n\right]\right)^2, \tag{3.29}$$

as it is easier to extract a correlation length for than for the corresponding expression with σ_j^z. Since the order parameter expectation value is itself difficult to calculate even in the TFIM [103, 104], we follow Ref. [140] in using the Lieb-Robinson bound [29] to express the connected correlator as

$$C^x_{c,\ell}(t) = C^x_\ell(t) - C^x_R(t) \ , \quad R \gg v_{\max} t, \tag{3.30}$$

where $v_{\max}$ is the Lieb-Robinson velocity. In our self-consistent mean-field approximation we can use Wick's theorem to express $C^x_\ell(t)$ as a block-Toeplitz Pfaffian [141]

$$C^x_\ell(t) = \mathrm{Pf} \begin{pmatrix} G_0(t) & G_1(t) & \dots & G_{\ell-1}(t) \\ -G_1^T(t) & \ddots & \ddots & \vdots \\ \vdots & \ddots & \ddots & \vdots \\ -G_{\ell-1}^T(t) & \dots & \dots & G_0(t) \end{pmatrix} \ , \tag{3.31}$$

where

$$G_n(t) = 2 \begin{pmatrix} i \operatorname{Im} \Delta_n(t) & \operatorname{Re}(t_{1-n}(t) + \Delta_{1+n}(t)) - \frac{1}{2}\delta_{0,n+1} \\ -\operatorname{Re}(t_{1-n}(t) + \Delta_{1-n}(t)) + \frac{1}{2}\delta_{0,1-n} & i \operatorname{Im} \Delta_n(t) \end{pmatrix} \ . \tag{3.32}$$

We note that if we replace the time-dependent Gaussian density matrix by a thermal equilibrium state, Eq. (3.31) reduces to a determinant because $\Delta_n \in \mathbb{R}$.

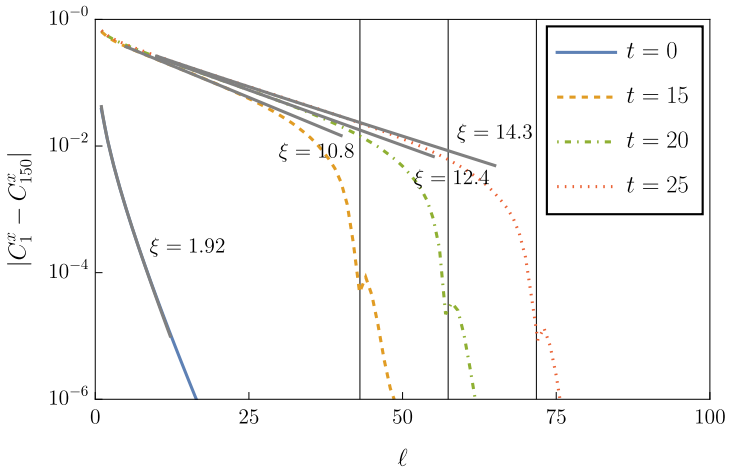

Figure 3.9: Connected order-parameter two-point function $C^x_{c,\ell}(t)$ for a quench from the ground state of the TFIM at $h = 0.8$ to the ANNNI with $h = 0.8, \kappa = 0.11$ ($\kappa_c \approx 0.114$). Vertical lines indicate the light cone distance at $t = 15, 20, 25$ using the maximal group velocity of the effective dispersion in the steady state. Gray lines indicate fits to functions of the form $C^x_{c,\mathrm{fit}} = a\ell^{-\nu} \exp(-\ell/\xi)$ where ξ is the fitted correlation length. Compare with Fig. 1.1.

In Fig. 3.9 we show the connected order-parameter two-point function for a quench from the ground state of the TFIM with $h = 0.8$ and turning on next-nearest neighbour interactions of

strength $\kappa = 0.11$. This is close to the critical value for this field, $\kappa_c(h = 0.8) \approx 0.114$. In the initial state the connected correlator displays exponential decay with a correlation length $\xi(0) \approx 1.9$. Extracting correlation lengths at $t > 0$ is complicated by the fact that the connected correlator for outside the "light cone" remains unchanged and we are therefore restricted to separations $\ell < 2v_{\max}t$, where $v_{\max}$ is the maximal propagation velocity [33,34,107]. On the other hand, in order to extract a correlation length $\xi(t)$ we require that $\ell \gg \xi(t)$. This causes us to be unable to convincingly fit correlation lengths for short times (other than $t = 0$ which is an equilibrium state by design), although we obtain relatively good fits to the exponential behaviour at times $t \geq 20$ which show the correlation length has grown to about $\xi(25) \approx 14.3$.

3.4.3 Oscillations in the low energy-density regime

A striking feature seen in Figs. 3.5, 3.6, 3.8 are the high-frequency oscillations in local observables for quenches at reasonably small h which do not appear to decay in time in the mean-field theory. These do not occur in quenches in the TFIM and hence seem to be a result of fermion interactions. We stress that these oscillations were previously observed in the iTEBD simulations of Ref. [106] and are not an artifact of the mean-field approximation. Importantly they are observed in quenches that result in small energy densities compared to the fermion gap, which puts us in a regime where we are dealing with the nonequilibrium dynamics of a very dilute gas of fermions. This suggests that these oscillations could be related to the formation of long lived bound states of (pairs of) fermions, *cf.* Refs [142–146]. A simple limiting case in which this bound state formation can be seen is $h = 0$. Here excitations are highly degenerate domain-wall states, whilst the antiferromagnetic next-nearest neighbour term partially lifts this degeneracy by introducing an energy penalty of 4κ when the domain-walls are on exactly neighbouring bonds. That is, at $h = 0$ the next-nearest neighbour interaction produces a spin-flip (anti-)bound state. In order to investigate the possibility of these bound states persisting to the non-zero values of h we consider, we have determined the spectrum of low-lying excitations of the ANNNI model by exact diagonalisation using the QuSpin [94] package on $L = 24$ sites. These results provide useful information for physical properties at finite energy densities that are small compared to the excitation gap over the ground state. As in the ferromagnetic phase of the TFIM, the lowest excitations can then be thought of as a continuum of pairs of ferromagnetic domain-walls. This is indeed observed in the exact diagonalisation results in Fig. 3.10. In addition we observe a bosonic bound state of two domain-walls that occurs at energies

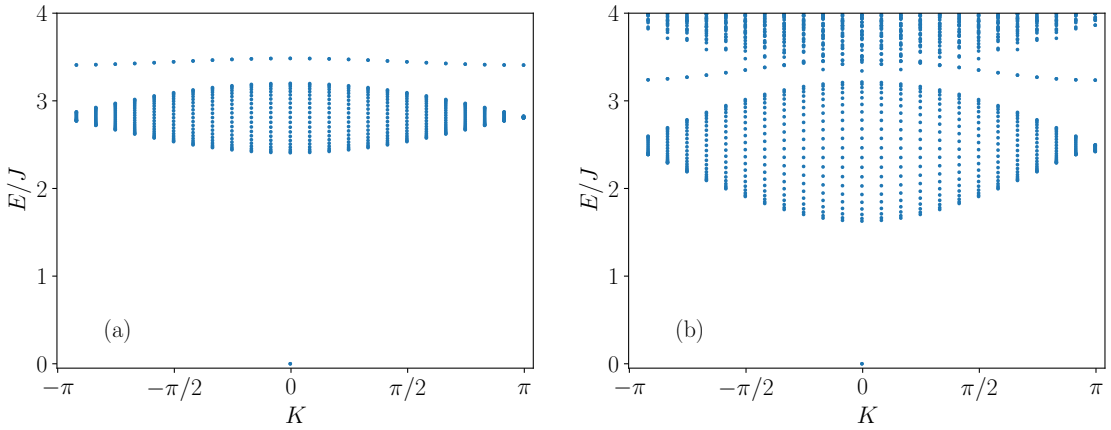

Figure 3.10: Spectrum of the ANNNI Hamiltonian for (a) $h = 0.1$, $\kappa = 0.15$ and (b) $h = 0.2$, $\kappa = 0.2$ from exact diagonalisation using QuSpin [94] on $L = 24$ sites. As physical states have even fermion parity, the lowest excited states are the two domain-wall continuum and a sharp bosonic mode corresponding to the anti-bound state. For $h = 0.2, \kappa = 0.2$ the four-particle continuum is low enough in energy to be visible on this scale.

above the two domain-wall continuum. With regards to the oscillations observed in local observables after some of our quenches we note the following:

- The bound state energy at $k = 0$ agrees with the oscillation frequency observed after the quantum quenches.
- For reasonably large values of h, the bound state ceases to exist around $k = 0$. It can be seen from a Lehmann representation that only excited states with $k = 0$ contribute to the dynamics when performing quenches from translationally invariant states as we do here. As such this is consistent with the fact that when we perform quenches with larger h we do not see persistent oscillations.

An important caveat is that in the quench set-up we are dealing with there is a small, but finite, energy density above the ground state and thus in the thermodynamic limit the system is in fact at an energy infinitely above what is pictured in Fig. 3.10. There, the bound states always "sit" on top of multi domain-wall excitations and are not expected to be stable. However, as the density of domain-walls is very small the lifetime of the bound state can be very large compared to the time scale we observe in our quenches. We believe that this is indeed the case.

A rough estimate of the decay time of the bound states can be obtained by thinking in the quasiparticle picture described above. If there were truly a single bound state, then energy and

momentum conservation would prevent it from decaying; however, the decay is allowed due a background density of domain-walls that the bound state may scatter from. A semi-classical approach to compute the scattering time is to reason in terms of the quasiparticle picture [31, 142, 147]. To do this we introduce the mean-free-path of the domain-walls

$$\lambda_{\text{mfp}} = \frac{E_g}{\varepsilon} \ , \tag{3.33}$$

where ε is the energy density *relative to the ground state after the quench* and E_g the quasiparticle gap. If the mean-free-path is larger than the system size $\lambda_{\text{mfp}} > L$, then the state has in expectation fewer than one quasi-particle in the entire system and the system does not require a many-body description and the bound states will have nothing to scatter from. Even for thermodynamically large systems however, if we consider times less than

$$2v_{\text{max}}t \lesssim \lambda_{\text{mfp}} \ , \tag{3.34}$$

where v_{max} is the Lieb-Robinson velocity of the domain-wall excitations, we may consider the bound state quasiparticles as having little interaction with the domain-wall background. We now estimate

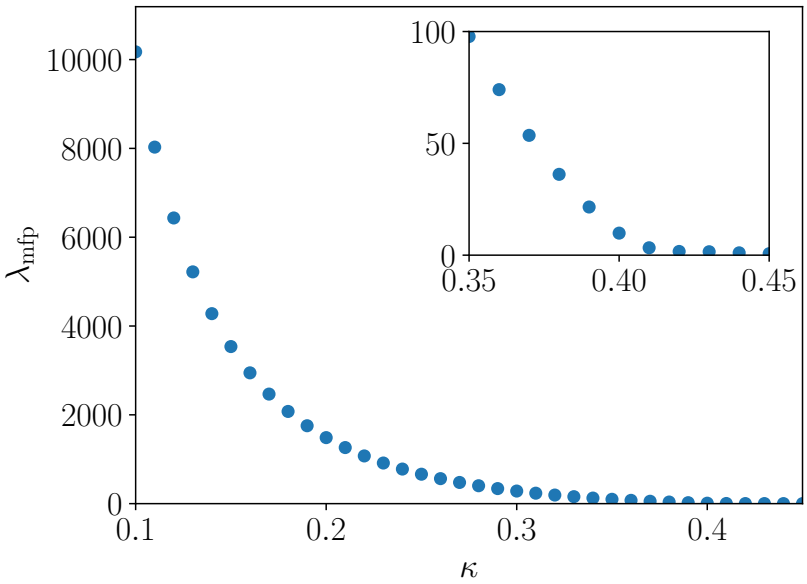

Figure 3.11: Mean-free-path of the quasiparticles generated by quantum quenches from the TFIM ground state at transverse field $h = 0.2$ to the ANNNI model with $0.1 < \kappa < 0.45$ ($\kappa_c \approx= 0.407$).

all the relevant quantities in the case of interest. The post-quench energy density e_0 defined in (3.14) may be calculated using Wick's theorem. The energy density ε appearing in Eq. (3.33) is however

not the e_0 of (3.14), but rather one must subtract the ground state energy density of the ANNNI, which is not known analytically. We estimate the latter by exact diagonalisation for $L = 18$ sites, for which it is essentially converged. The resulting mean-free-path for quenches from the ground state of the TFIM with $h = 0.2$ to the ANNNI model with $0.1 < \kappa < 0.45$ is shown in Fig. 3.11. We see that for these quenches the mean-free-path is extremely large unless κ is very close to the QPT. The time range accessible to us in our SCTDMFT analysis is limited by finite-size effects, which strongly influence observables after the traversal time $L/(2v_{\max})$ [31, 32, 107]. To access very late times without encountering finite-size effects therefore requires larger system sizes and more memory. In order to test whether or not the oscillations eventually decay in mean-field theory we instead change our initial density matrix in a way that reduces the mean-free-path, e.g. for a quench with $h = 0.1$ and $\kappa = 0.15$ from an initial temperature $\beta = 2.0$, we estimate that the mean-free-path should be roughly 50 sites and the scattering time about $t_s \sim 56$, see Table (3.1). Nonetheless there is no visible damping in the mean-field theory up to very late times ($t = 10^3$), see Fig. 3.12. We

$e_0(\beta = 2.0)$	$e_{\mathrm{GS}}(h = 0.1, \kappa = 0.15)$	ε	$2E_g$	λ_{mfp}	$v_{\max}$	t_s
-0.82739	-0.85295	0.02556	2.410	47.14	0.4187	56.29

Table 3.1: Post-quench energy density e_0 obtained from Eq. (3.14), ground state energy density e_{GS} and two particle gap estimated with ED on $L = 20$ sites. Lieb-Robinson velocity is estimated as the maximal group velocity for the dispersion $\epsilon_\kappa(k)$ given in Eq. (3.18) using the values of the mean-fields at $t = 100$.

conclude that in SCTDMFT the oscillations are *undamped* while we expect in an exact theory they would decay.

3.5 Non-equal time correlation functions

A natural question is whether the existence of a bound state can be detected more directly in the quench setup. One proposal in the literature is to use certain Fourier transforms of equal time correlation functions [148, 149], but these do not provide useful insights in our case. In thermal equilibrium, it is well established that dynamical response functions give detailed information about the particle content of the theory. An obvious question then is to what extent their nonequilibrium analogs can be used to do the same. In order to address this question we now determine certain non-equal time correlation functions in our SCTDMFT. We do not attempt to address the problem of calculating non-equal time two-point functions of the order parameter, as this is difficult even for

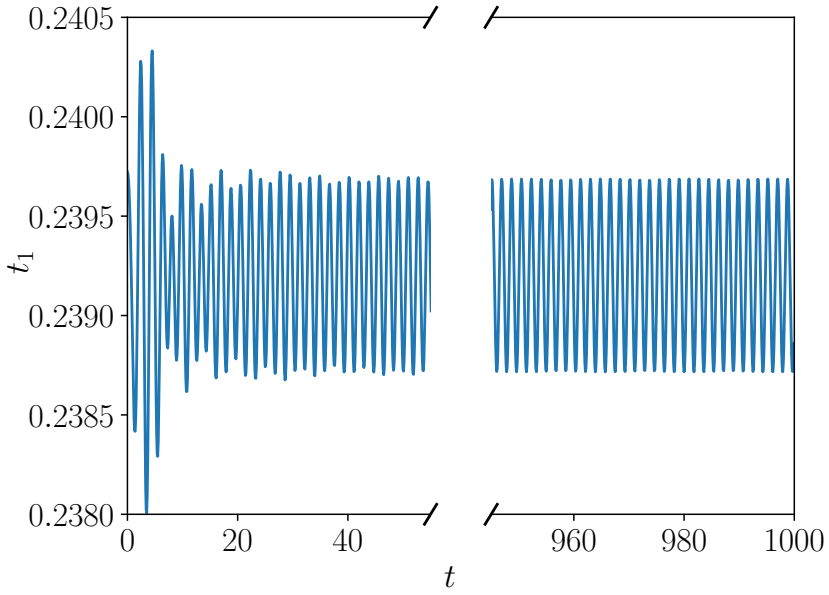

Figure 3.12: Time evolution of the mean-field t_1 following a quench from $\beta = 2.0$, $h = 0.1, \kappa = 0.15$.

the transverse field Ising chain itself [102, 104]. In MFT the Heisenberg equations of motion for the fermion operators c_k are linear

$$\frac{\mathrm{d}}{\mathrm{d}t}c_k(t) = i[H_{\mathrm{MFT}}(t), c_k(t)] = -iA_k(t)c_k(t) + B_k c^\dagger_{-k}(t) \ , \tag{3.35}$$

and can be solved by a time-dependent Bogoliubov transformation

$$c_k(t) = \alpha_k(t)c_k(0) + \beta_k(t)c^\dagger_{-k}(0) \ , \tag{3.36}$$

where the time-dependent coefficients are solutions to

$$\frac{\mathrm{d}\alpha_k(t)}{\mathrm{d}t} = -iA_k(t)\alpha_k(t) + B_k(t)\beta^*_{-k}(t) \ , \qquad \frac{\mathrm{d}\beta_k(t)}{\mathrm{d}t} = -iA_k(t)\beta_k(t) + B_k(t)\alpha^*_{-k}(t) \ . \tag{3.37}$$

As we are dealing with a Gaussian theory all non-equal time correlation functions are then expressible in terms of the two non-equal time Green's functions given by

$$\begin{aligned} G_k(t,t') = \langle c^\dagger_k(t)c_k(t')\rangle =& \alpha^*_k(t)\alpha_k(t')f_k + \alpha^*_k(t)\beta_k(t')g_k \\ &+ \beta^*_k(t)\alpha_k(t')g^*_k + \beta^*_k(t)\beta_k(t')(1-f_{-k}) = G_{-k}(t,t') \ , \end{aligned} \tag{3.38}$$

$$\begin{aligned} \tilde{G}_k(t,t') = \langle c^\dagger_k(t)c^\dagger_{-k}(t')\rangle =& \alpha^*_k(t)\alpha^*_{-k}(t')g_k + \alpha^*_k(t)\beta^*_{-k}(t')f_{-k} \\ &+ \beta^*_k(t)\alpha^*_{-k}(t')(1-f_k) + \beta^*_k(t)\beta^*_{-k}(t')g^* = -\tilde{G}_{-k}(t,t') \ , \end{aligned} \tag{3.39}$$

where expectation values are always taken with respect to $\rho(t=0)$, i.e. $\langle\mathcal{O}\rangle = \mathrm{Tr}[\rho(t=0)\mathcal{O}]$. The final equalities hold due to the parity symmetry and f_k, g_k encode the initial conditions

$$f_k = G_k(0,0), \qquad g_k = \tilde{G}_k(0,0)\ . \tag{3.40}$$

As an example of the use of these formulas we consider the nonequilibrium analog of the density response function

$$\chi_{\rho\rho}(r,t,t') = \frac{1}{L^2}\sum_{k_1,\ldots k_4} e^{i(k_1-k_2)r}\langle[c^\dagger_{k_1}(t)c_{k_2}(t), c^\dagger_{k_3}(t')c_{k_4}(t')]\rangle\ . \tag{3.41}$$

After Fourier transforming in the spatial co-ordinate this takes the following form in SCTDMFT

$$\begin{aligned}\tilde{\chi}(q,t,t') = \frac{1}{L}\sum_k \Big\{ &\tilde{G}_k(t,t')\tilde{G}^*_{k-q}(t',t) - \tilde{G}_k(t',t)\tilde{G}^*_{k-q}(t,t') \\ &+ G_k(t,t')\left(\alpha^*_{k-q}(t')\alpha_{k-q}(t) + \beta^*_{k-q}(t')\beta_{k-q}(t)\right) \\ &- \left(\alpha^*_k(t)\alpha_k(t') + \beta^*_k(t)\beta_k(t')\right) G_{k-q}(t',t)\Big\}\ .\end{aligned} \tag{3.42}$$

We note that $\chi(q,t,t')$ is in principle measurable via linear-response measurements, see Appendix A.3. Employing a Lehmann representation suggests that spectral properties of the post-quench Hamiltonian should be inferrable by taking appropriate "Fourier transforms" in time. In practice we consider

$$\chi_{t_f}(q,\omega) = \int_0^{t_f} dt'\ \tilde{\chi}(q,t_f,t')\ e^{i\omega t'}. \tag{3.43}$$

The imaginary part of this generalised dynamical susceptibility is shown in Fig. 3.13 for a quench from $\kappa = 0$ to $\kappa = 0.15$ and initial inverse temperature $\beta = 1.0$. These parameters correspond to those in Fig. 3.10(a), which has a clear bound state, except at elevated temperature. The single time correlation functions still show characteristic oscillations and so we believe there is a bound state still at this increased temperature. In Fig. 3.13, we can clearly identify the continuum of two-domain-wall excitations but there is no evidence for a bound state above it. In order to capture the latter, one has to go beyond the SCTDMFT.

3.6 Conclusion

This chapter has formulated both equilibrium (at finite energy density) and time-dependent mean-field descriptions for quantum quenches in the ANNNI model starting from a Gaussian state. We first used this to compute properties of the expected stationary state following a quantum quench, assuming that the system looks thermal again at late times and then used the time-dependent

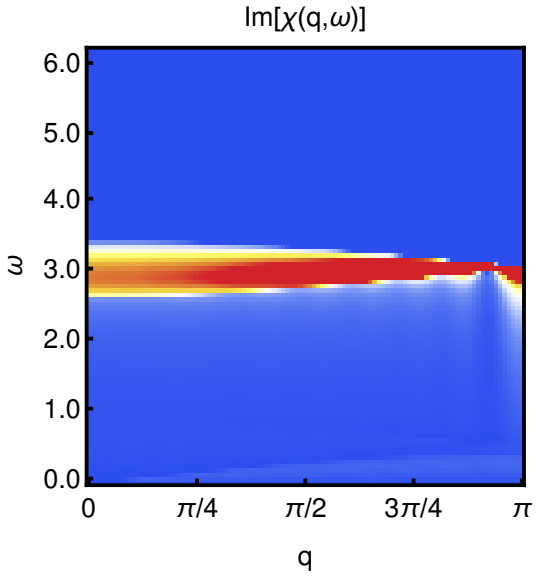

Figure 3.13: Out-of-equilibrium density-density susceptibility calculated for the mean-field theory with $L = 200, h = 0.1, \kappa = 0.15, \beta = 1.0$

formulation to probe the approach to stationarity. Comparisons, in both the stationary and time-dependent cases, with the numerical results of Ref. [106] show that this simple description is fairly accurate even for large next-nearest neighbour interactions close to the critical value. Importantly it fully reproduces the signatures of the equilibrium phase transition previously found numerically. Our approach makes it clear that the observed signatures are associated with the growth of the correlation length following a quantum quench and sheds light on the applicability of this mechanism for detecting quantum phase transitions in general. The analysis of this chapter makes it clear that to truly see quantum critical behaviour the quench must not produce an energy density higher than the cutoff for the critical scaling theory, however the appearance of soft modes can still produce signatures of the phase transition in the susceptibilities for one point functions. Our theory is based on a fermionic description with a topological transition and so it is clear that topological as well as conventional transitions may be detected in this manner. Moreover, we give an explanation for a potentially puzzling feature of the real time dynamics, namely long lived oscillations, by showing that the oscillation frequency is the mass of a bound state in the interacting theory.

Finally, we showed that self-consistent time-dependent mean-field theory can partially capture the presence of this bound state due to the characteristic oscillations caused in equal time correlation functions. However, when used to compute non-equal time correlation functions that are expected

to show spectral properties, the mean-field theory fails to capture the bound state. The expected fate of the oscillations is not fully clear from this study — in mean-field theory they persist for all times simulated with no signs of damping. This is in conflict with intuition from statistical physics and ETH which states that in a chaotic system such as the ANNNI model local observables should have their expectation values relax to stationary values at late times. A thorough investigation of the intermediate time behaviour is therefore of interest, which the next chapter will attempt to shed light on.

Turning and turning in the widening gyre
The falcon cannot hear the falconer;
Things fall apart; the centre cannot hold;

The Second Coming
W. B. Yeats

4

Persistent oscillations in gapped chains and their decay

This chapter will be based on [3], which aims to answer the question that arose in the previous chapter as to whether the oscillations in equal time observables decay at late times. To do so, this chapter will discuss the mechanism for the origin of the oscillations and argue it is generic to quenches in gapped spin chains with kinematically protected modes such as those arising from bound states. This being the case, this chapter will abandon the ANNNI model to focus on a simpler paradigmatic example of such oscillations using a systematic perturbative analysis. This analysis will show that mean-field theory captures the oscillations but not their decay, whilst the next order in perturbation theory causes them to decay. This is in good agreement with the fully non-perturbative results available to us via MPS calculations, but provides the ability to investigate much later times.

4.1 Introduction

Following a quantum quench, local observables are expected to relax to stationary values in generic models as a result of ETH [21–23]. The presence of long lived oscillations of local observables in an experiment with a 51-atom Rydberg simulator [16] led to the theoretical development of the concept of quantum many body scars (QMBS) [67]: non-thermal states embedded deep in the spectrum of otherwise quantum chaotic models. An apparently related phenomenon to QMBS

has been observed in quenches in certain spin chains, referred to as 'weak thermalisation' in [150]. Various authors [142–144, 146, 150–155] have noted that for the Ising chain in a tilted field following a quench, there are long lived oscillations at frequencies corresponding to the masses of 'meson' bound states. Similar oscillations were observed in the Potts model [156]. These studies were unable to simulate late enough times to conclude if the oscillations decayed or not, although arguments for their eventual decay have been given in [142]. In the latter work it is moreover argued that such oscillations should be generic to quantum systems with a quasiparticle gap and isolated bands such as produced by bound states. The requirements for systems to have such long lived oscillations at bound state masses seem very general. This is in stark contrast to the usual understanding of QMBS as arising from highly unusual algebraic properties such as exact eigenstates in the form of low bond dimension matrix product states.

The fate of oscillations at late times is however controversial: oscillations in the post-quench dynamics of observables in quantum field theories were predicted by Delfino and collaborators in [157, 158] and subsequently in [159, 160] it was argued that they persist for arbitrarily long times.

The Ising chain in a tilted field is unusual, in the sense that the perturbation that leads to the formation of meson bound states is non-local with respect to the fermionic elementary excitations of the transverse field Ising chain. This precludes the analysis of particle decay by standard perturbative approaches. In light of this fact, it is important to identify models that exhibit the same phenomenology, but can be studied by such methods. The ANNNI model studied in Chapter 3 is one such example, with a non-confining (contact) potential that binds the elementary domain-wall excitations into a spin flip. In this chapter we give two quench setups that we consider to be particularly simple examples of such behaviour. The first is a quantum quench in integer spin antiferromagnetic chains, which possess a gapped single particle (magnon) mode according to Haldane's conjecture [161, 162]. This model very cleanly demonstrates that the phenomenology is due neither to confinement, nor indeed to bound states, but simply due to the system possessing a kinematically protected, gapped quasiparticle excitation. However, as integer spin antiferromagnets are strongly interacting systems we are restricted to purely numerical investigations of the nonequilibrium dynamics of this model by matrix product state methods. Secondly, we present and analyse in detail a novel example of these long lived oscillations in a model with weak interactions that has the simplifying feature of exhibiting a $\mathsf{U}(1)$ symmetry associated with particle number conservation: a dimerised XXZ chain in a staggered magnetic field. In the scaling limit, the low-lying excitations

of this model can be understood in terms of solitons, antisolitons and a bound state known as a 'breather' which can give rise to long lived oscillations after quantum quenches.

Many other mechanisms for producing long lived oscillations are possible in quantum systems that should be differentiated from the case we discuss. We have already mentioned exact quantum many body scars, which can cause infinite lifetime oscillations if the initial state has large overlap with scar states lying in the middle of the spectrum. There are also Bloch oscillations of domains in the tilted field Ising model at low domain-wall density and related models of Rydberg atoms [163, 164]. Long lived oscillations can also occur in the electric field strength in lattice gauge theories that are related to quantum many body scars [165, 166]. Finally, in the presence of a $\mathsf{U}(1)$ symmetry undamped oscillations can occur when one considers observables that connect neighbouring charge sectors and applies a Zeeman field that splits all sectors by the same energy difference [167, 168].

The organisation of this chapter is as follows: in Section 4.2 we describe the mechanism that can give rise to long lived oscillations in models with kinematically protected single-particle excitations before giving a simple numerical case study of such behaviour in the spin-1 bilinear biquadratic (BLBQ) chain in Section 4.2.1. The spin-1 chain provides a clear example of the phenomenology we are interested in, however it is always strongly interacting. In contrast, the ANNNI and related Ising models can be mapped to fermionic chains for which the interaction can be considered perturbatively. However the lack of a $\mathsf{U}(1)$ symmetry (and in the case of a tilted field, long-ranged interactions between fermions) significantly complicates the application of standard methods based on the BBGKY hierarchy [169–171]. In Section 4.2.2 we address this problem by introducing a dimerised XXZ chain in a staggered magnetic field, which exhibits a $\mathsf{U}(1)$ symmetry as well as long-lived oscillations of observables after quantum quenches. In Section 4.3 we present two different approximations based on the BBGKY hierarchy — a self-consistent time-dependent mean-field theory (SCTDMFT) and the Second Born approximation [53, 54] — to study the quench dynamics of local observables.

4.2 Oscillations at "early" times

The physics underlying the oscillations explored within this chapter arises from two key requirements, these are:

1. The existence of a kinematically protected mode, i.e. a quasiparticle with a gapped dispersion $\epsilon(q) \geq \Delta_{\text{ex}}$ such that there is some region in the energy-momentum plane that has no other energy eigenstates.

2. Initial density matrices $\rho(t=0)$ such that the energy density deposited into the system by the quench (relative to the post-quench ground state energy $E_{\rm GS}$) is small compared to the spectral gap of the post-quench Hamiltonian

$$\epsilon_{\rm Quench} = \lim_{L\to\infty} \frac{1}{L}\left(\mathrm{Tr}\big[\rho(t=0)H\big] - E_{\rm GS}\right) \ll \Delta_{\rm ex}. \tag{4.1}$$

If the above requirements are met the physics can be viewed in terms of a dilute gas of long lived particles, whose scattering is to a good approximation purely elastic, *cf.* [101,172–178]. The possible emergence of long lived oscillations can then be understood by considering the linear response regime of ground state quenches. This is equivalent to the approach of Refs. [157–160]. To that end we consider an initial state $|\psi_0\rangle$ that is the ground state of a Hamiltonian H_0, and time-evolve with $H = H_0 + \lambda V$. Here V is a global operator that is assumed to be translationally invariant (as is H_0). By construction both H_0 and H feature kinematically protected gapped single-particle excitations. Linear response theory then gives

$$\begin{aligned}
\langle\psi_0|\mathcal{O}(t)|\psi_0\rangle &\approx \langle\psi_0|\mathcal{O}|\psi_0\rangle - i\lambda\int_0^t dt'\ \chi_{\mathcal{O}V}(t,t')\ ,\\
\chi_{\mathcal{O}V}(t,t') &= \langle\psi_0|[\mathcal{O}_I(t), V_I(t')]|\psi_0\rangle,\\
\mathcal{O}_I(t) &\equiv e^{iH_0t}\mathcal{O}e^{-iH_0t}\ .
\end{aligned} \tag{4.2}$$

The response function $\chi_{\mathcal{O}V}(t,t')$ can be expressed in terms of a Lehmann representation using the eigenstates of H_0, which gives

$$\chi_{\mathcal{O}V}(t,t') = \sum_n e^{i(t-t')(E_0-E_n)}\langle\psi_0|\mathcal{O}|\psi_n\rangle\langle\psi_n|V|\psi_0\rangle - \text{c.c.} \tag{4.3}$$

We now consider perturbations V and operators $\mathcal{O}$ that have non-vanishing matrix elements between the ground state and the kinematically protected gapped excitation. As by construction we are dealing with a ground state calculation the contribution of this excited state will provide the dominant contribution to the linear response function for large t

$$\langle\psi_0|\mathcal{O}(t)|\psi_0\rangle \approx \langle\psi_0|\mathcal{O}|\psi_0\rangle + 2\lambda\sum_k \mathrm{Re}\frac{e^{-it\bar\epsilon(k)}-1}{\bar\epsilon(k)}F_{\mathcal{O}}(k)F_V^*(k) + \ldots \tag{4.4}$$

where $F_{\mathcal{O}}(k) = \langle\psi_0|\mathcal{O}|k\rangle$ is the matrix element of the operator $\mathcal{O}$ between the ground state of H_0 and the single quasiparticle excitation of H_0 with momentum k and dispersion $\bar\epsilon(k)$. As V is by assumption a global, translationally invariant operator the only non-zero matrix element is with the zero-momentum single-particle state

$$F_V(k) \propto \delta_{k,0}\ , \tag{4.5}$$

which establishes that in linear response theory we obtain persistent oscillations with frequency $\bar{\epsilon}(0)$, *cf.* Refs [157–160]. If, instead, either V or the initial state has invariance only under translations by two sites, the matrix element will select out momenta $k = 0$ and $k = \pi$. In this case oscillations will occur at two frequencies, $\bar{\epsilon}(0), \bar{\epsilon}(\pi)$, as long as the kinematically protected mode exists at these momenta. The approach of [157–160] can be straightforwardly modified by expanding the initial state in terms of the eigenstates of the post-quench Hamiltonian using perturbation theory. This gives

$$\langle\psi_0|\mathcal{O}(t)|\psi_0\rangle \approx \langle\psi_0|\mathcal{O}|\psi_0\rangle + 2\lambda \sum_k \mathrm{Re}\frac{e^{-it\epsilon(k)}-1}{\epsilon(k)}\widetilde{F}_{\mathcal{O}}(k)\widetilde{F}^*_V(k) + \ldots \tag{4.6}$$

Here $\epsilon(k)$ is the dispersion of the kinematically protected mode in H (rather than H_0) and $\widetilde{F}_{\mathcal{O}}(k) = \langle 0|\mathcal{O}|\widetilde{k}\rangle$ is the matrix element of the operator $\mathcal{O}$ between the ground state of H and the single quasiparticle excitation of H with momentum k. This way of approaching the problem is important for some of the cases considered below, in which H has a kinematically protected single-particle mode, but H_0 does not. In these cases the small perturbation λV leads to the creation of a bound state, which is a non-perturbative effect. In these cases it turns out that the perturbation theory around H as sketched above gives a (qualitatively) correct description of the observed dynamics.

The question we want to address is what happens outside the linear response regime. Linear response theory is usually expected to describe the short-time regime for very small but finite values of λ, but fail at late times. The question of its regime of applicability is related to the properties of nonlinear response functions, which have recently been analysed in the class of systems discussed here [179] and shown to acquire late-time divergences in some cases.

The linear response viewpoint summarised above obscures the fact that the quench deposits a finite energy density into the system. A complementary viewpoint on long lived oscillations is obtained by employing a spectral representation in terms of energy eigenstates of the post-quench Hamiltonian

$$\mathrm{Tr}\big[\mathcal{O}\rho(t)\big] = \sum_{m,n} e^{i(E_m - E_n)t}\langle m|\mathcal{O}|n\rangle\langle n|\rho(t=0)|m\rangle \ . \tag{4.7}$$

Assuming that the operator $\mathcal{O}$ connects states with quasiparticle numbers that differ by one, oscillations with frequency Δ_{ex} may ensue for the following reason. In the gas phase, energy eigenstates can be viewed as scattering states of the stable quasiparticles and adding a single quasiparticle with momentum q to an energy eigenstate (approximately) leads to an energy eigenstate that differs in energy and momentum by $\epsilon(q)$. If ρ is translationally invariant, then the only non-zero contributions to the sum occur at $q = 0$. As this process works for all energy eigenstates at the (low) energy

density of interest (which is set by the factor $\langle n|\rho(t=0)|m\rangle$), one may expect long lived oscillations in the expectation value (4.7) to occur.

We stress that the oscillations produced by the mechanism outlined above are not a finite-size effect but can persist in the thermodynamic limit. For all examples discussed below we have verified that varying the system size does not affect the amplitude or frequency of the oscillations observed. This is very different to the oscillations reported in [180], which indeed are finite-size effects.

4.2.1 Haldane-gap chains

As a first example of a model that exhibits undamped oscillations after quantum quenches in the linear response regime we consider the antiferromagnetic bilinear-biquadratic (BLBQ) chain. This is a family of spin-1 chains described by [181–183]

$$H(\gamma) = J \sum_{i}^{L-1} \left[(\boldsymbol{S}_i \cdot \boldsymbol{S}_{i+1}) + \gamma \, (\boldsymbol{S}_i \cdot \boldsymbol{S}_{i+1})^2 \right] \ . \tag{4.8}$$

For $\gamma = 0$ the model reduces to the spin-1 Heisenberg antiferromagnet whilst for $\gamma = 1/3$ it is the AKLT chain [184], whose ground state is an exact MPS with bond dimension $\chi = 2$.

Both values of γ lie within the gapped 'Haldane gap phase' [162] $-1 < \gamma < 1$. At $\gamma = 1$ the model is the $SU(3)$ symmetric Lai-Sutherland model which is gapless [185, 186]. In Fig. 4.1 we plot the low-energy spectrum obtained by exact diagonalisation (ED) on $L = 16$ sites and periodic boundary conditions for $\gamma = 0.25$ which is representative of the Haldane phase, with a gap of $\Delta_{\rm ex}(\pi) \approx 0.62J$ and group velocity $v \approx 1.26J$.

The ground state is at $k = 0$ and there is a gap to a triplet band of magnons with energy minimum at $k = \pi$.

Consider first global quenches where a finite energy density is generated by quenching the ratio of exchange constants $\gamma \to \gamma'$. For the Hamiltonian (4.8) the ground state has momentum $k = 0$ but the Haldane gap is at $k = \pi$, with the magnon mode only persisting in a region of the Brillouin zone around this that does not extend to $k = 0$. For such a quench both the Hamiltonian and the initial state are translationally invariant, so local operators cannot "access" single magnon excitations in the way described above because $\rho_{nm} = \langle n|\rho(t=0)|m\rangle = 0$ for energy eigenstates that differ by a single magnon, as they differ in momentum. As a result there are no long lived oscillations for translationally invariant initial states. On the other hand these considerations suggest a way out: we need to choose an initial state that is invariant only under translations by two sites, which can be

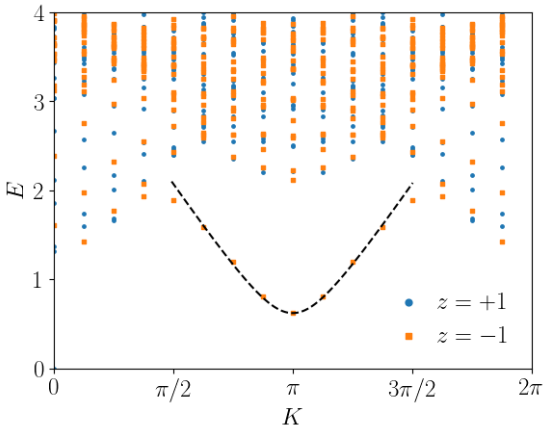

Figure 4.1: Spectrum of the BLBQ Hamiltonian (4.8) found with QuSpin [94, 95] for $L = 16$ sites and $\gamma = 0.25$, within the magnetisation sector with $S^z_{\text{Tot}} = 0$. States are coloured by their charge under a $\mathbb{Z}_2$ spin-flip symmetry $S^z \mapsto -S^z$, $|\psi\rangle \mapsto z|\psi\rangle$. Dashed line is a fit around $k = \pi$ to a functional form $\epsilon(k) = \sqrt{\Delta^2_{\text{ex}} + v^2(k-\pi)^2}$.

achieved simply by choosing the pre-quench Hamiltonian to have an additional staggered magnetic field

$$H_{\text{pre}} = H(\gamma_i) + h_s \sum_m (-1)^m S^z_m \ . \tag{4.9}$$

H_{pre} now has a ground state that is invariant only under translation by two sites and $\rho_{nm} \neq 0$ and so, as discussed in the previous section, we therefore expect to see oscillations at $\epsilon(\pi)$ (the magnon does not extend to $k = 0$ so this will be the only frequency present). As a numerical test of these ideas in the BLBQ chain, we perform a quench using the ITensor [187] library, which enables us to use DMRG to compute an approximation to the ground state of $H(\gamma_i, h_s)$, and then to time evolve the state according to $H(\gamma_f, 0)$ using time evolving block decimation (TEBD). Here and elsewhere, the time window in which we plot TEBD data is determined such that the TEBD results do not change when suitably increasing the bond dimension; in Figs. 2,3 we have plotted data for $\chi = 400$ and ensured no change in the corresponding plots for $\chi = 600$.

The results are shown in Fig. 4.2 for two quenches of different strengths. For the weaker quench we see that there are oscillations in the quantity $\langle S^z_{L/2} \rangle$ with little to no visible damping, whilst the evolution of $\langle S^z_{L/2} S^z_{L/2+1} \rangle$ is strongly damped. In light of the previous section, this is to be understood as due to a discrete spin-flip symmetry as follows: the oscillations can only occur when the matrix element $\langle \text{GS}|\mathcal{O}|\text{QP}(k)\rangle \neq 0$ where $|\text{QP}(k)\rangle$ is the quasiparticle at momentum k and $|\text{GS}\rangle$ is the ground state of the post-quench Hamiltonian. For the BLBQ chain the ground state

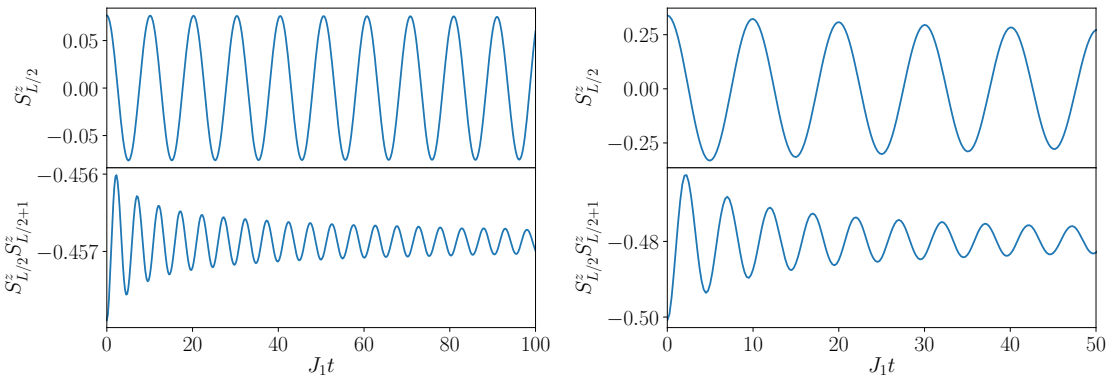

Figure 4.2: Result of a quantum quench keeping $\gamma = 0.25$ and quenching the initial staggered field $h_{s,i} \mapsto 0$. Left: $h_{s,i} = 0.01$, producing an energy per site of $\epsilon_{\text{Quench}} \approx 3.8 \times 10^{-4} J$, equivalent to an equilibrium temperature $T \approx 0.12J$. Right: $h_{s,i} = 0.05$, energy per site $\epsilon_{\text{Quench}} \approx 7.86 \times 10^{-3} J$, corresponding to an equilibrium temperature of $T \approx 0.23J$. Equilibrium temperatures determined using ED on 12 sites, TEBD numerics performed with $L = 400$ sites and a bond dimension of $\chi = 400$. The final time is window is determined by requiring that the results do not change on increasing the bond dimension to $\chi = 600$.

is invariant under $S^z \mapsto -S^z$ but the magnon mode is odd under this symmetry. Therefore, the matrix elements are only non-zero when the observable is $\mathbb{Z}_2$ odd, such as S^z itself, and conversely the oscillations decay rapidly when the observable is $\mathbb{Z}_2$ even. The oscillations in the magnetisation have frequency ω very close to the magnon gap at $k = \pi$ as expected

$$\omega \approx \ 0.62102\ldots J \ , \qquad \Delta_{\text{ex}}(\pi) \approx 0.62096 J \ . \tag{4.10}$$

Fig. 4.2 also shows a somewhat larger quench from $h_s = 0.05$, which still has an energy per site well below the gap. The average inter-particle distance after this quench is approximately

$$\ell = \Delta_{\text{ex}}/\epsilon_{\text{Quench}} \approx 79 \ . \tag{4.11}$$

From the perspective of a low density gas of quasiparticles, the finite lifetime of the oscillations is caused by scattering events [155]. Therefore one would not expect to see appreciable decay at times $vt \lesssim \ell$. From ED we estimate that the group velocity is roughly $v \approx 1.26J$, and so the slight decay by $Jt = 50$ makes sense within the quasiparticle gas picture. Conversely, for the shallower quench from $h_{s,i} = 0.01$ the mean-free-path is $\ell \approx 1600$ and thus the lack of decay is also consistent with this rough estimate. For even larger quenches than $h_{s,i} = 0.05$ we find that, as expected on the basis of our quasiparticle gas picture, the decay becomes more easily visible at short times.

The quenches in Haldane-gapped models explored above yield several insights: the first is that for weak quenches oscillatory behaviour results as predicted [157–160] when there is a quasiparticle mode. This confirms that such oscillations are unrelated to the formation of bound states or of confinement, except inasmuch as they provide a mechanism for kinematically protected quasiparticles to exist. It also highlights the importance of symmetries which can cause the relevant matrix elements to be zero and relaxation to be consequently much faster. Perhaps most importantly we have evidence that the oscillations do decay, which was suggested in previous studies [144, 146] but not observed in the models considered therein. Our findings also show that in the case studied above the regime of validity of the perturbative approach used in [157–160] is limited to short times.

4.2.2 Dimerised XXZ model

Generally the quasiparticle gas can consist of several species, for instance in models with "elementary" quasiparticle excitations as well as (multi-particle) bound states. We have already mentioned two examples of this situation - the Ising model with both longitudinal and transverse field [143, 144, 146, 158] and the Ising model with transverse field only, but additional next-nearest neighbour Ising interactions [2]. Neither of these lattice models analysed in the context of persistent oscillations exhibits a $\mathsf{U}(1)$ symmetry associated with particle number conservation, which greatly complicates the application of perturbative approaches based on the BBGKY hierarchy or the flow equation approach [53, 54, 135–139, 188]. In order to study the fate of these oscillations at very late times we therefore introduce a spin-1/2 dimerised XXZ model in a staggered field, which can be mapped to a model of spinless interacting fermions with particle number conservation. This enables us to apply the equations of motion techniques developed in [53, 54]. This model features elementary fermionic excitations as well as bosonic two-particle bound states. Moreover, in the appropriate scaling limit the model reduces to the sine-Gordon quantum field theory in the attractive regime. The Hamiltonian of our model is

$$H(\Delta,\alpha,h_s) = -\frac{J}{2}\sum_{m=0}^{L-1}[1+\alpha(-1)^m][S_m^+S_{m+1}^- + \text{h.c.}] + \Delta J\sum_m S_m^zS_{m+1}^z + h_sJ\sum_m(-1)^mS_m^z \ . \tag{4.12}$$

Here α tunes the degree of dimerisation in the XY plane and h_s is a staggered applied field. For $\alpha = h_s = 0$ and $|\Delta| < 1$ the model reduces to the integrable spin-1/2 XXZ chain in the massless Luttinger liquid phase, whilst non-zero values of α, h_s break the integrability and open a gap in the zero magnetisation sector. A Jordan-Wigner transformation maps the Hamiltonian (4.12) to one of

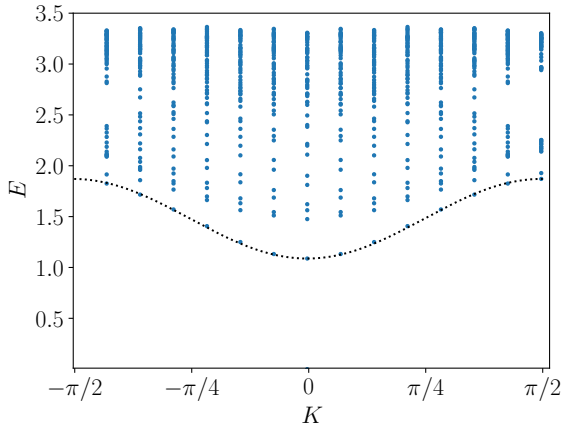

Figure 4.3: Low energy spectrum of the Hamiltonian (4.12) in the $S^z_{\text{Tot}} = 0$ sector for $\alpha = 0.4, h = 0.2, \Delta = 0.65$, calculated for $L = 28$ spins. The dotted black curve is a fit of the bound state to $\epsilon(k) = M - \frac{v}{2}(\cos 2k - 1)$ where $v \approx 0.78$ is the maximal group velocity.

interacting spinless fermions with interaction strength Δ. As in the case of the BLBQ chain, discrete symmetries play a role in allowing or disallowing persistent oscillations. When only one of α, h_s is present in (4.12) there is a discrete spatial $\mathbb{Z}_2$ symmetry corresponding to reflection across a bond or site, respectively. We will elaborate the importance of retaining both parameters after presenting data from quenches.

Rotational symmetry about the z axis corresponds to $\mathsf{U}(1)$ particle number conservation in the fermionic variables. In the low energy limit, the Hamiltonian (4.12) for $|\Delta| < 1$ reduces to a sine-Gordon model [189], whose low-lying excitations for $\Delta > 0$ are solitons, antisolitons and soliton-antisoliton bound states known as 'breathers'. In the lattice model we determine the spectrum of low-lying excitations in the $S^z_{\text{Tot}} = 0$ sector by exact diagonalisation, *cf.* Fig. 4.3. We can see that throughout the Brillouin zone there is a bound state visible below a continuum of states. The bound state is kinematically protected and therefore stable. This establishes that our model fulfils the first of our requirements.

We investigate the time evolution using both TEBD, which is capable of exactly describing the evolution of states with sufficiently low entanglement, and perturbative methods which are valid at small Δ. The latter is needed because following a quench the entanglement entropy generically grows linearly in time [43, 44, 190]. As such the true time evolved state quickly leaves the manifold of states that can be accurately described by matrix product states with finite bond dimensions. We adopt open boundary conditions when performing TEBD numerics; when working with the equivalent

fermionic model it suffices to work in the sector with fixed fermion number and we adopt periodic boundary conditions out of convenience. We also ensure that our system sizes are sufficiently large to rule out finite-size effects such as traversals [107] on the time scales we are interested in.

To ensure a long window of applicability of the perturbative approaches [53, 54] we consider quantum quenches from an initial thermal state of the non-interacting model $\rho(0, \alpha, h_s, \beta)$, where

$$\rho(\Delta, \alpha, h_s, \beta) = \frac{\exp\left(-\beta H(\Delta, \alpha, h_s)\right)}{\mathrm{Tr}\left[\exp\left(-\beta H(\Delta, \alpha, h_s)\right)\right]} \ . \tag{4.13}$$

As the perturbative approaches expand around thermal states of free Hamiltonians, they are able to describe states with volume law entanglement, unlike MPS methods. Instead, they are limited by their assumption that higher particle cumulants are negligible. This is then time evolved using the Schrödinger equation for $H(\Delta, \alpha', h_s')$. We focus on expectation values of local observables such as the staggered magnetisation within a unit cell and nearest-neighbour spin-bilinears

$$\begin{aligned} m_s &= \langle\psi(t)|S^z_{2n} - S^z_{2n+1}|\psi(t)\rangle, \\ S^{\alpha\alpha}_{m,m+1} &= \langle S^\alpha_m S^\alpha_{m+1}\rangle \ . \end{aligned} \tag{4.14}$$

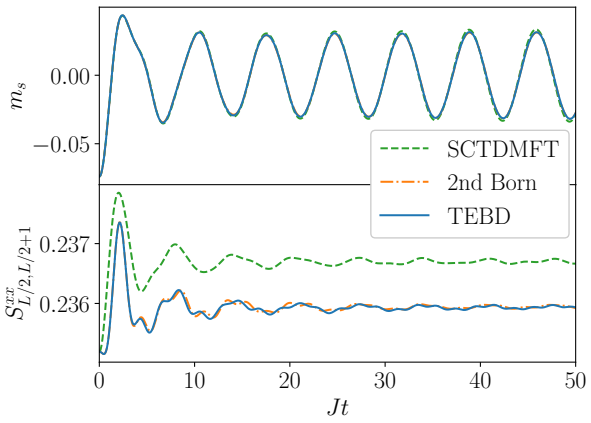

Figure 4.4: Time evolution following a quench from the ground state with $\Delta : 0 \mapsto 0.2, h_s : 0.1 \mapsto 0$ and $\alpha_s = 0.4$ before and after the quench. Upper: staggered magnetisation, showing persistent oscillations. Lower: Time evolution of $\langle S^x_m S^x_{m+1}\rangle$ where $m = L/2$. Calculations use $L = 400$ sites and a maximum bond dimension of $\chi = 1000$ for the TEBD.

We plot these quantities in Fig. 4.4, computed using TEBD on $L = 400$ sites with the ITensor [187] library and two approximate calculations: self-consistent time-dependent mean-field theory and the second Born Approximation, both detailed in Section 4.3. Fig. 4.4 shows the case where

the time evolution has a $\mathbb{Z}_2$ symmetry (reflection in a bond as $h'_s = 0$) but the initial state does not. In this case, the staggered magnetisation initially has a non-zero value and then oscillates about the thermal value of 0. The frequency agrees with the energy difference between the post-quench ground state and the bound state, which have opposite $\mathbb{Z}_2$ parities and are thus connected by the $\mathbb{Z}_2$ odd operator m_s^z. Conversely, $S^{xx}_{m,m+1}$ is the expectation value of a $\mathbb{Z}_2$ even operator and thus has decaying expectation value at late times. We note that in the bottom panel of Fig. 4.4 the SCTDMFT does not appear to accurately capture the early time evolution, this is despite the fact that SCTDMFT is expected to be accurate at early times. We have checked that the difference between it and the second Born approximation scales like $\mathcal{O}(\Delta^2)$ and so this deviation indicates that for the observable in question the $\mathcal{O}(\Delta)$ contribution is either very small or absent.

4.3 Decay of oscillations in the staggered XXZ model at late times

We now turn to the "intermediate" time regime. This is no longer accessible to TEBD for the reasons set out above, but can be studied by appropriate truncation schemes of the BBGKY hierarchy. The correct degrees of freedom for such a perturbative analysis of (4.12) are fermions rather than spins. Applying a Jordan-Wigner transformation to the Hamiltonian gives

$$H(\Delta, \alpha, h_s) = -\frac{J}{2}\sum_{m=0}^{L-1}(1+\alpha(-1)^m)(c_m^\dagger c_{m+1} + \text{h.c}) - h_s\sum_m (-1)^m n_m + \Delta\sum_m n_m n_{m+1}\ , \quad (4.15)$$

where c_n are spinless fermions and $n_m = c_m^\dagger c_m$. We work at half filling such that for an even (odd) number of cells Neveu-Schwarz (Ramond) boundary conditions are appropriate. The following subsections briefly consider this model at order Δ^0, Δ^1 and Δ^2 in perturbation theory.

4.3.1 Free limit – $\mathcal{O}(\Delta^0)$

Quenches at the non-interacting point may be analysed by the methods of Sec. 2.3 and will have no long lived oscillations due to the absence of an interaction term to produce the responsible breather bound state. It is nonetheless useful to record in this section what the ground state looks like in the free limit, as well as what the modes are in this limit, since they provide the starting point for any perturbative analysis.

The presence of the staggering causes the states at k and $k+\pi$ to hybridise into two states which we denote (k, μ) with $\mu = 0, 1$. The result is that the free part of the Hamiltonian is diagonalised

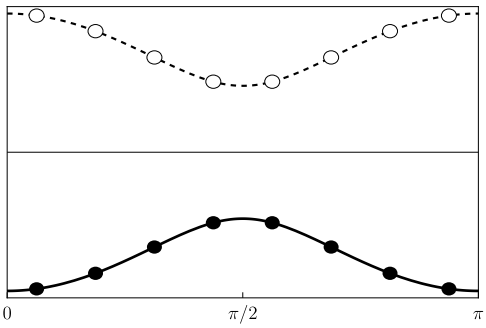

Figure 4.5: Dispersion at $\Delta = 0$, with the ground state indicated. Filled circles indicate states that are occupied and empty circles ones that are unoccupied, drawn at $L = 16$ for clarity. Note that $k = \pi/2$ is not an allowed single particle state for any finite system size.

with the canonical transformation:

$$c_m = \sqrt{\frac{2}{L}} \sum_{0 \leq k < \pi} \sum_{\mu=0,1} e^{-ikm} \gamma_{m,\mu}(k) b_\mu(k) \ , \tag{4.16}$$

where the Bogoliubov co-efficients $\gamma_\mu(k)$ are

$$\begin{aligned} \gamma_{2m,0} &= -e^{-i\varphi_k} \sin\frac{\theta_k}{2} \ , \gamma_{2m-1,0} = \cos\frac{\theta_k}{2} \ , \\ \gamma_{2m,1} &= e^{-i\varphi_k} \cos\frac{\theta_k}{2} \ , \ \gamma_{2m-1,1} = \sin\frac{\theta_k}{2} \ , \end{aligned} \tag{4.17}$$

here the two Bogoliubov angles φ_k and θ_k are given by

$$\begin{aligned} \cos\frac{\theta_k}{2} &= \sqrt{\frac{\epsilon_k + h_s}{2\epsilon_k}} \ , \ \sin\frac{\theta_k}{2} = \sqrt{\frac{\epsilon_k - h_s}{2\epsilon_k}} \ , \\ e^{-i\varphi_k(\alpha)} &= \frac{-\cos k + i\alpha \sin k}{\sqrt{\cos^2 k + \alpha^2 \sin^2 k}} \ , \end{aligned} \tag{4.18}$$

where ϵ_k is the dispersion of the free part of the Hamiltonian and equal to

$$\epsilon_\pm(k) = \pm\sqrt{\alpha^2 J^2 + h_s^2 + (1-\alpha^2) J^2 \cos^2 k} \ . \tag{4.19}$$

The ground state is then a Fermi sea where the entire $(-)$ band is filled and the $(+)$ band is empty, illustrated in Figure 4.5. In the next subsection, we will discover that ED gives a poorly converged result for the gap at small Δ. The picture of the ground state at $\Delta = 0$ shown in Figure 4.5 helps explain this as follows. In the thermodynamic limit the minimum energy excitation corresponds to a hole in the filled band at $k = \pi/2$ and a particle in the empty upper band at $k = \pi/2$, with a corresponding gap of $E_{\text{gap}}(\infty) = 2\epsilon_+(\pi/2) = 2\sqrt{\alpha^2 J^2 + h_s^2}$. However, if the number of unit cells $L/2$ is even then we must work in the Neveu-Schwarz sector and so have anti-periodic boundary

conditions with $k = (2n+1)\pi/L$, which never equals exactly $\pi/2$. Likewise for an odd number of unit cells we work in the Ramond sector where $k = 2n\pi/L \neq \pi/2$. For finite L the gap is therefore

$$E_{\text{gap}}(L) = 2\epsilon_+\left(\frac{\pi}{2} + \frac{\pi}{L}\right) = E_{\text{gap}}(\infty) + \delta E_{\text{gap}}(L) \ , \tag{4.20}$$

for large L the finite size effects become

$$\delta E_{\text{gap}}(L) = \frac{\mathrm{d}^2\epsilon}{\mathrm{d}k^2}\Big|_{k=\pi/2}\frac{\pi^2}{L^2} = J\frac{1-\alpha^2}{\sqrt{\alpha^2+h_s^2}}\frac{\pi^2}{L^2} \ . \tag{4.21}$$

4.3.2 Self-consistent time-dependent mean-field theory (SCTDMFT)

The same steps as were taken in Section 3.4 can now be taken to provide an $\mathcal{O}(\Delta^1)$ estimate of the post-quench dynamics. The time-dependent mean-field Hamiltonian takes the form

$$H_{\text{MFT}}(t) = -\sum_{s=0}^{\frac{L}{2}-1}\Big[\frac{J_0(t)}{2}c_{s,0}^\dagger c_{s,1} + \frac{J_1(t)}{2}c_{s,1}^\dagger c_{s+1,0} + \text{h.c.} + h_{\text{eff}}(t)\big(c_{s,0}^\dagger c_{s,0} - c_{s,1}^\dagger c_{s,1}\big)\Big] + E_0(t) \ , \tag{4.22}$$

where s now labels the unit cell and $a = 0, 1$ the sites within it such that the spin labelled (s, a) is at position $m = 2s + a$ in the chain. The constant term $E_0(t)$ does not have any effect on the equations of motion, but ensures that the expectation value of energy is conserved. The mean-field Hamiltonian contains the effective couplings

$$\begin{aligned} J_0(t) &= J(1+\alpha) + \Delta\langle c_{s,1}^\dagger c_{s,0}\rangle_t \ , \\ J_1(t) &= J(1-\alpha) + \Delta\langle c_{s+1,0}^\dagger c_{s,1}\rangle_t \ , \\ h_{\text{eff}}(t) &= h_s - \Delta\langle c_{s,0}^\dagger c_{s,0} - c_{s,1}^\dagger c_{s,1}\rangle_t \ . \end{aligned} \tag{4.23}$$

Note that $J_{0,1}(t)$ are generically complex at intermediate times and that h_{eff} is (up to a constant shift and rescaling) equal to the staggered magnetisation $m_s(t)$. The time evolution is simplest in momentum space, so we introduce the following Fourier transform, appropriate to a two site unit cell

$$c_{s,a} = \frac{1}{\sqrt{L}}\sum_s e^{ik(2s+a)}(c_+(k) + (-1)^a c_-(k)) \ . \tag{4.24}$$

Then the time evolution of the two-point functions $n_{\mu\nu}(k) = \langle c^\dagger_\mu(k) c_\nu(k)\rangle,\ \mu,\nu \in \{+,-\}$ is obtained from the Heisenberg equations of motion

$$\begin{aligned}
\frac{\mathrm{d}n_{++}(k,t)}{\mathrm{d}t} &= 2B' \,\mathrm{Re}(n_{+-}) - 2B\,\mathrm{Im}(n_{+-})\ , \\
\frac{\mathrm{d}n_{--}(k,t)}{\mathrm{d}t} &= -2B' \,\mathrm{Re}(n_{+-}) + 2B\,\mathrm{Im}(n_{+-})\ , \\
\frac{\mathrm{d}n_{+-}(k,t)}{\mathrm{d}t} &= (B' - iB)(n_{--} - n_{++}) - 2iA(k) n_{+-}\ .
\end{aligned} \tag{4.25}$$

Here $A(k,t), B(k,t)$ and $B'(k,t)$ are real functions that can be expressed in terms of $J_\pm(t) = J_0(t) \pm J_1(t)$ and $h_{\mathrm{eff}}(t)$ as

$$\begin{aligned}
A(k,t) &= \mathrm{Re}\left(J_+(t)\right)\cos k - \mathrm{Im}\left(J_+(t)\right)\sin k\ , \\
B(k,t) &= h_{\mathrm{eff}}(t)\ , \\
B'(k,t) &= \mathrm{Re}\left(J_-(t)\right)\sin k + \mathrm{Im}\left(J_-(t)\right)\cos k\ .
\end{aligned} \tag{4.26}$$

These equations can alternatively be derived by a first order truncation of the BBGKY hierarchy, *cf.* Ref. [54]

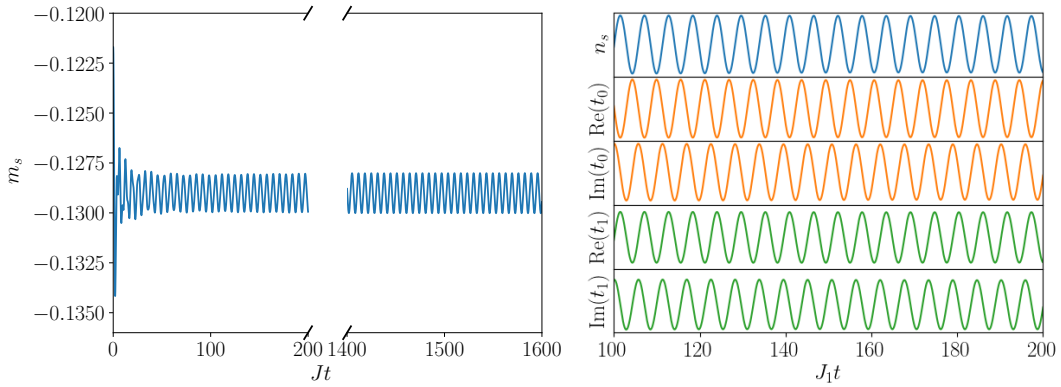

Figure 4.6: Left: Mean-field evolution of the staggered magnetisation after a quench with initial state $\rho(0, 0.4, 0.2, 4.0)$ and time evolved using the Hamiltonian $H(0.1, 0.4, 0.2)$. The oscillations are undamped at late times in this approximation up to the light-cone time set by the system size (here $L = 2000$). Right: Evolution of the mean-fields $t_0 = \langle c^\dagger_{s,0} c_{s,1}\rangle, t_1 = \langle c^\dagger_{s,1} c_{s+1,0}\rangle, n_s = \frac{1}{2}\langle c^\dagger_{s,0} c_{s,0} - c^\dagger_{s,1} c_{s,1}\rangle$ following a quench from the initial state $\rho(0, 0.4, 0.3, \infty)$ and evolved with the Hamiltonian $H(0.3, 0.4, 0.3)$.

We solve these equations of motion numerically, updating the mean-fields $J_\pm(t)$ and $h_{\mathrm{eff}}(t)$ every time step, and plot the resulting staggered magnetisation following a quench from an initial thermal state in Fig. 4.6, which shows clear oscillations that become highly monochromatic and undamped

at late times. The choice of thermal state is made to ensure that the system has an energy per site well above the ground state but still small compared to the gap. This ensures that there is a low density of quasiparticles in the system and that they can be treated as a dilute gas.

We now return to the physical origin of the oscillations and their frequency. To that end, we have considered ground state quenches at $\alpha = 0.4, h_s = 0.3$, i.e. initial density matrices $\rho(0, 0.4, 0.3, \infty)$, for several Δ. In this case we observe essentially a single oscillation frequency ω_B at intermediate and late times. Performing a fast Fourier transform using data from $t = 50$ up to $t = 2000$ gives a single sharp peak at the frequency ω_B. We compare this to the energy of the first excited state computed by exact diagonalisation on system sizes up to $L = 30$ in Fig. 4.7. We observe that the oscillation frequency observed in SCTDMFT is in very good agreement with the bound state gap at $q = 0$ for small interaction strengths $\Delta \lesssim 0.25J$. For small interactions strengths $\Delta \approx 0$ the ED results exhibit sizeable finite size effects that can be estimated using Eq. 4.21. These considerations motivate the following form of a fitting function

$$E_{\text{gap}}(L) = E_{\text{gap}}(\infty) + BL^{-2} + CL^{-4} \ . \tag{4.27}$$

This functional form indeed provides a good description of our numerical results for the gap deduced from ED on $L \in \{20, 22, 24, 26, 28, 30\}$ sites when Δ is small, whilst at larger Δ the ED is well converged already. This procedure provides the curve labelled 'ED (Extrapolated)' in Fig.4.7.

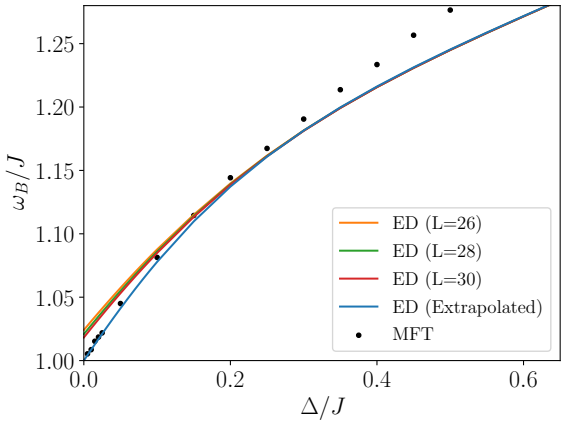

Figure 4.7: Estimation of the bound state mass using ED compared to the persistent frequency extracted from the mean-field evolution of the initial state $\rho(0, 0.4, 0.3, \infty)$ by the Hamiltonian $H(\Delta, 0.4, 0.3)$. The ED exhibits large finite size effects when $\Delta \to 0$ so we plot the result of extrapolating to $L = \infty$ by fitting the gap to a power series in $1/L^2$ up to L^{-4}.

The emergence of persistent oscillations of the expectation values of observables in the SCTDMFT can be understood as follows. The solutions to the self-consistency equations reported above exhibit periodic behaviour with a single frequency. As a result the SCTDMFT is equivalent to a periodically driven system with a Hamiltonian that is quadratic in fermions. It is well known that such systems typically synchronise at late times and physical observables then display persistent oscillations at the driving frequency [191].

4.3.3 Second Born approximation

The lack of damping in SCTDMFT is in fact not surprising as the method is perturbative to first order in Δ (at the level of the equations of motion). In thermal equilibrium we have to evaluate the self-energy to second order in Δ in order to obtain a non-vanishing imaginary part that signals a finite lifetime of the fermions. This suggests that finite lifetime effects in the nonequilibrium setting of interest here can be captured by the 'second Born approximation' [53, 54, 188]. We follow [53] in deriving the equations of motion for fermionic bilinears $\hat{n}_{\mu\nu}(k,t) = \hat{b}^\dagger_\mu(k,t)\hat{b}_\nu(k,t)$, where $\hat{b}^\dagger_\mu(k)$ are Bogoliubov fermions chosen to diagonalise the quadratic part of the Hamiltonian and given explicitly by (4.16)-(4.18). In these variables the Hamiltonian has the form

$$\hat{H}(\Delta,\alpha,h_s) = \sum_{k>0,\mu} \epsilon_\mu(k)\hat{b}^\dagger_\mu(k)\hat{b}_\mu(k) \ , + \Delta \sum_{\boldsymbol{\mu}} \sum_{k_1,\ldots k_4>0} V_{\boldsymbol{\mu}}(\boldsymbol{k})\hat{A}_{\boldsymbol{\mu}}(\boldsymbol{k}) \ , \tag{4.28}$$

where we have introduced shorthand notations $\boldsymbol{k} = (k_1,k_2,k_3,k_4)$, $\boldsymbol{\mu} = (\mu_1,\mu_2,\mu_3,\mu_4)$ and $\hat{A}_{\boldsymbol{\mu}}(\boldsymbol{k}) = b^\dagger_{\mu_1}(k_1)b^\dagger_{\mu_2}(k_2)b_{\mu_3}(k_3)b_{\mu_4}(k_4)$. The interaction coefficients $V_{\boldsymbol{\mu}}(\boldsymbol{k})$ can be chosen to be anti-symmetric

$$V_{\boldsymbol{\mu}}(\boldsymbol{k}) = -\frac{1}{4}\sum_{P\in\mathbb{Z}_2\times\mathbb{Z}_2} \mathrm{sign}(P) V'_{P(\boldsymbol{\mu})}(P(\boldsymbol{k})) \ . \tag{4.29}$$

Here P is an element of $\mathbb{Z}_2\times\mathbb{Z}_2$ where the first $\mathbb{Z}_2$ swaps $\mu_1 \leftrightarrow \mu_2, k_1 \leftrightarrow k_2$ and the second $\mathbb{Z}_2$ factor acts likewise on $3,4$. We define $\mathrm{sign}(P)$ as the product of the sign of each permutation. The unsymmetrised interaction components are equal to

$$\begin{aligned} V'_{\boldsymbol{\mu}}(\boldsymbol{k}) = &\frac{2e^{i(k_2-k_3)}}{L}\Big[g_{\mu_1}(k_1)f_{\mu_2}(k_2)f_{\mu_3}(k_3)g_{\mu_4}(k_4)e^{i(\varphi_{k_1}-\varphi_{k_4})}\big(\delta_{k_1+k_2,k_3+k_4} + \delta_{k_1+k_2-k_3-k_4,\pm\pi}\big) \\ &+ f_{\mu_1}(k_1)g_{\mu_2}(k_2)g_{\mu_3}(k_3)f_{\mu_4}(k_4)e^{i(\varphi_{k_2}-\varphi_{k_3})}\big(\delta_{k_1+k_2,k_3+k_4} - \delta_{k_1+k_2-k_3-k_4,\pm\pi}\big)\Big] \ , \end{aligned} \tag{4.30}$$

where we have defined

$$\begin{aligned} f_\mu(k) &= (1-\mu)\cos\frac{\theta_k}{2} + \mu\sin\frac{\theta_k}{2} \ , \\ g_\mu(k) &= \mu\cos\frac{\theta_k}{2} - (1-\mu)\sin\frac{\theta_k}{2} \ . \end{aligned} \tag{4.31}$$

The equations of motion to second order in Δ for $n_{\mu\nu} = \langle \hat{n}_{\mu\nu}(k,t)\rangle$ are obtained by truncating the BBGKY hierarchy as derived in [53, 54]. The result is

$$\begin{aligned}
\partial_t n_{\mu\nu}(k) &= i\epsilon_{\mu_\nu}(k) n_{\mu\nu}(k) + 4i\Delta \sum V_{\mu_1\mu_2\mu_3\mu}(k,q,q,k) e^{i(\epsilon_{\mu_1\nu}(k)+\epsilon_{\mu_2\mu_3}(q)t} n_{\mu_1\nu}(k,0) n_{\mu_2\mu_3}(q,0) \\
&\quad -4i\Delta \sum V_{\nu\mu_2\mu_3\mu_1}(k,q,q,k) e^{i(\epsilon_{\mu\mu_1}(k)+\epsilon_{\mu_2\mu_3}(q))t} n_{\mu\mu_1}(k,0) n_{\mu_2\mu_3}(q,0) \\
&\quad -\Delta^2 \int_0^t \mathrm{d}t' \sum K^{\gamma}_{\mu\nu}(k_1,k_2;k;t-t') n_{\gamma_1,\gamma_2}(k_1,t') n_{\gamma_3,\gamma_4}(k_2,t') \\
&\quad -\Delta^2 \int_0^t \mathrm{d}t' \sum L^{\{\alpha_i\}}_{\mu\nu}(k_1,k_2,k_3;k;t-t') n_{\alpha_1,\alpha_2}(k_1,t') n_{\alpha_3,\alpha_4}(k_2,t') n_{\alpha_5,\alpha_6}(k_3,t') \ ,
\end{aligned} \tag{4.32}$$

where the kernel functions $L_{\mu\nu}, K_{\mu\nu}$ are given by

$$\begin{aligned}
K^{\gamma}_{\mu\nu}(k_1,k_2;k;t) &= 4 \sum_{k_3,k_4>0} \sum_{\eta,\eta'} X^{\gamma_1\gamma_3\eta\eta';\eta\eta'\gamma_4\gamma_2}_{\boldsymbol{k};\boldsymbol{k}'}(\mu,\nu;k;t), \\
L^{\{\alpha_i\}}_{\mu\nu}(k_1,k_2,k_3;k;t) &= 8\sum_{\eta} \sum_{k_4>0} X^{\alpha_1\alpha_3\alpha_6\eta;\eta\alpha_5\alpha_4\alpha_2}_{\boldsymbol{k};\boldsymbol{k}'}(\mu,\nu;k;t) - 16 \sum_{\eta} X^{\alpha_1\alpha_3\eta\alpha_4;\alpha_5\eta\alpha_6\alpha_2}_{k_1k_2k_1k_2;k_3k_1k_3k_1}(\mu,\nu;k;t) \ , \\
X^{\gamma;\boldsymbol{\eta}}_{\boldsymbol{k};\boldsymbol{q}}(\mu,\nu;q;t) &= Y^{\gamma}_{\mu\nu}(\boldsymbol{k},q) V_{\boldsymbol{\eta}}(\boldsymbol{q}) e^{iE_{\gamma}(\boldsymbol{k})t} - (\boldsymbol{\gamma},\boldsymbol{k}) \leftrightarrow (\boldsymbol{\eta},\boldsymbol{q}) \ ,
\end{aligned} \tag{4.33}$$

and where $E_{\boldsymbol{\gamma}}(\boldsymbol{k}) = \epsilon_{\gamma_1}(k_1) + \epsilon_{\gamma_2}(k_2) - \epsilon_{\gamma_3}(k_3) - \epsilon_{\gamma_4}(k_4)$. The derivation of Eq. (4.32) is summarised in Appendix A.4. We note that $n_{\mu\nu}$ are different from the quantities $n_{\pm\pm}(k,t)$ considered in the SCTDMFT of the previous section. Taking this into account one sees that the SCTDMFT agrees with (4.32) up to order $\mathcal{O}(\Delta^1)$ and disagrees with the $\mathcal{O}(\Delta^2)$ terms as expected. Solving Eq. (4.32) requires a runtime of $\mathcal{O}(L^3 \times T)$ where T is the simulation time reached. Since simulating up to time T requires a system size at least $2v_{\mathrm{LR}}T$ where v_{LR} is the Lieb-Robinson velocity, investigating up to time T scales as $\mathcal{O}(T^4)$.

The second Born approximation is premised on the assumption that many-particle cumulants are small at intermediate times, whilst going beyond SCTDMFT by allowing for a non-Gaussian state. A priori, this is an uncontrolled approximation. However, we start in a Gaussian state in which all cumulants vanish and so the approximation must be accurate for early times, and becomes better as the interaction strength Δ becomes small. Furthermore, it gives rise to a Boltzmann equation at late times [53, 54] which is believed to become exact in the "Boltzmann scaling limit". This suggests that the approximation remains accurate on time scales $t \sim \Delta^{-2}$. At intermediate times one expects the second Born approximation to continue to provide useful physical insights even if it may not retain full quantitative accuracy. What I wish to establish in this chapter is that, whilst the SCTDMFT treatment agrees with the prediction of [157–160], the leading correction provided by the second Born approximation causes the oscillations to damp. Finally, we note that the second Born

approximation is complementary to TEBD in such cases, since the former can reproduce volume law entanglement but cannot fully capture strong interactions, whilst the latter method can only describe states with a finite amount of entanglement related to the bond dimension used but can describe strongly correlated states at sufficiently low entanglement.

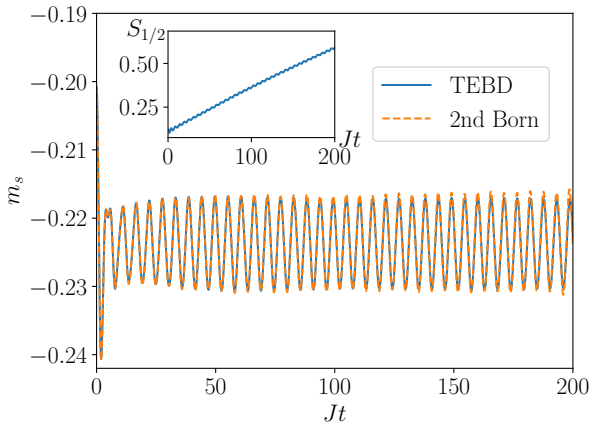

Figure 4.8: Staggered magnetisation for a quench from the ground state of $H(0, 0.4, 0.3)$ and time evolved with $H(0.2, 0.4, 0.3)$. This corresponds to a very small quench with quasiparticle density $\sim 1.6 \times 10^{-3}$. Accordingly very large system sizes and late times would be required to observe decay of oscillations. Inset: half chain entanglement entropy, which grows linearly for all times shown. TEBD calculation done with maximum bond dimension $\chi = 800$.

In order to clearly exhibit some of the issues associated with the damping of oscillations we first consider ground state quenches, in which we initialise the system in the ground state of $H(0, 0.4, 0.3)$ and time-evolve with $H(0.2, 0.4, 0.3)$ for a system size of $L = 300$. Fig. 4.8 shows the time evolution of the staggered magnetisation and observe long lived oscillations with no apparent damping on the long time scales considered.

This is however entirely expected as the quench produces a very small energy per site $\epsilon_{\text{quench}} \approx 0.0019J$ whilst the gap to create a quasiparticle is $\Delta_{\text{ex}} \approx 1.18J$. The resulting average inter-particle distance is therefore $\ell = \Delta_{\text{ex}}/\epsilon_{\text{Quench}} \approx 640$. That this exceeds the system size simulated means that finite size effects such as traversals will matter long before the many-body effects that would dampen the oscillations. The fact that we are effectively dealing with the linear response regime is also apparent from the fact that TEBD is able to access very large time scales $Jt \sim 100$, which means that the volume-law contribution to the entanglement entropy is still negligible.

These considerations show that the energy per site deposited by the quench should be small compared to the bound state energy, however it should not be so small that quasiparticle interactions

are negligible on accessible time scales. To overcome this problem we consider larger quenches of the interaction parameter as well as thermal initial states, which provide us with a simple parameter — the pre-quench temperature — to vary the post-quench energy density. For finite pre-quench temperatures we cannot easily use TEBD since the initial state has volume law entanglement, and so only show the second Born and SCTDMFT results. We compare the results obtained by the second Born approximation to SCTDMFT, which as discussed before exhibits persistent oscillations at a frequency that is very close to the bound state energy gap. In Fig. 4.9 we show results for

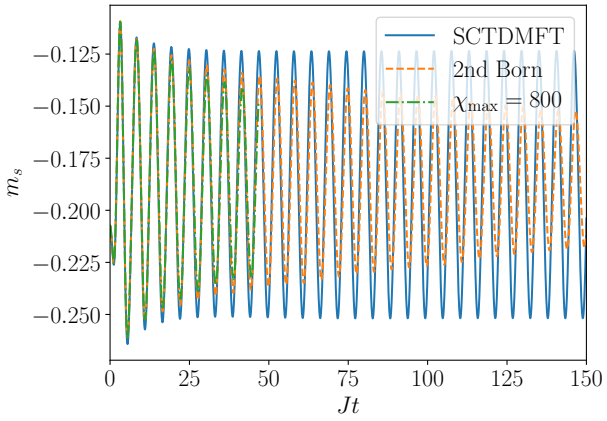

Figure 4.9: Staggered magnetisation for a quench from the ground state of $H(0, 0, 0.23)$ and time evolved with $H(0.2, 0.4, 0.3)$ using mean-field theory, the second Born approximation and a TEBD calculation with maximum bond dimension $\chi = 800$ and $L = 200$.

quench initialised in the ground state of $H(0, 0, 0.23)$ and time evolved with $H(0.2, 0.4, 0.3)$. Here the post-quench energy per site is $\epsilon_{\text{Quench}} \approx 0.040$ corresponding to a mean-free-path $\ell \approx 29$, which is much smaller than our system size of $L = 200$. We observe that the second Born approximation clearly shows the decay of the oscillatory behaviour of the staggered magnetisation. We plot the TEBD results only up to times $Jt = 40$, where our criterion is agreement of the numerical results for bond dimensions $\chi = 600$ and our maximal bond dimension $\chi_{\max} = 800$. The TEBD data show the beginning of a decay, consistent with the second Born results. In Figs 4.10 we show the behaviour of the staggered magnetisation after quenches from thermal initial states. In Fig. 4.10 we initialise the system in the thermal state of the non-interacting system at inverse temperature $J\beta_i = 4$, which corresponds to the same energy density as in Fig. 4.9. We again observe decaying oscillations. In the inset in that figure, we estimate the decay time by fitting a decaying exponential $A \exp(-t/\tau)$ to the successive peak to peak amplitudes, the resulting decay time for this particular quench is

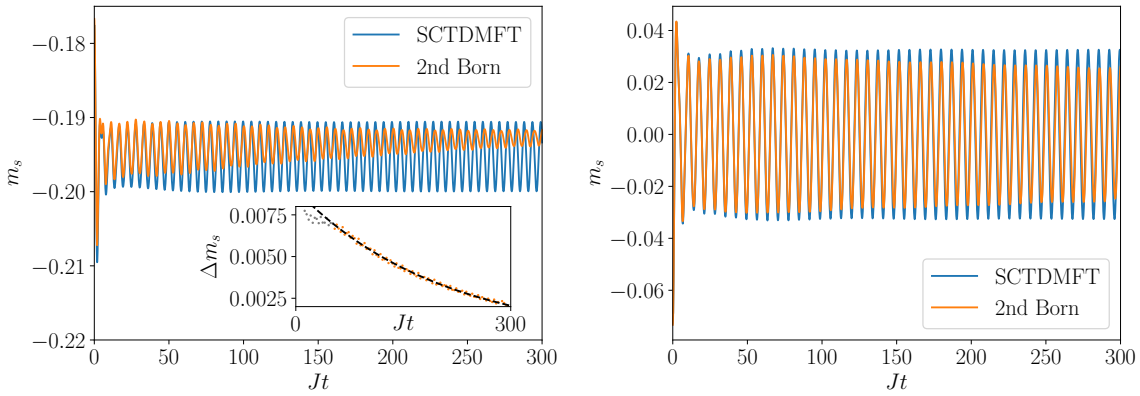

Figure 4.10: Left main: Staggered magnetisation for a quench from the thermal state $\rho(0, 0.4, 0.3, 4.0)$ of the non-interacting system and time evolved with $H(0.2, 0.4, 0.3)$. $L = 448$ used for the second Born approximation. The initial state is chosen such that the energy density is approximately the same as in Fig. 4.9. Left inset: successive peak to peak amplitudes of the oscillations in the second Born approximation, with an exponential fit (dashed black line). The grey scatter points are excluded from the fit. Right: Staggered magnetisation for a quench starting in the thermal state $\rho(0, 0.4, 0.10, 10.0)$ and time evolved with $H(0.2, 0.4, 0)$ on a ring with $L = 400$.

$J\tau \sim 200$. Finally, in Fig. 4.10, we also consider a lower temperature $J\beta_i = 10$, which corresponds to energy per site $\epsilon_{\text{Quench}} \approx 0.0037$ and mean-free-path $\ell \approx 250$. Here the oscillations are seen to decay very slowly.

4.4 Summary and conclusions

This chapter has carried out a detailed study of a mechanism that gives rise to long lived oscillations in the expectation values of local observables after quantum quenches. This mechanism is very different from quantum scars and occurs after small quenches in interacting many-particle systems with an excitation gap, which generate a regime that can be understood in terms of a low-density gas of (long lived) kinematically protected quasiparticles. Long lived oscillations can then occur in expectation values of observables that have matrix elements between the ground state and excited states that contain a single quasiparticle.

We have presented very strong evidence using a combination of matrix product state methods and perturbative approaches based on truncations of the BBGKY hierarchy that these oscillations decay at late times in all models we have considered. This is an important difference to models with exact quantum scars [68, 70].

Our results show that the linear response theory prediction is upheld only at the level of self-consistent mean-field theory. Going beyond mean-field theory to the second Born approximation provides evidence of damping. For small interaction strengths U the timescale of the decay is therefore generally expected to be $\mathcal{O}(U^{-2})$. Whilst it is not impossible that higher order corrections would cause the oscillations to remain at late times, this is highly unlikely as there is no reason to anticipate such an effect. Instead, truncating the BBGKY hierarchy at higher orders should merely modify the lifetime. We presented non-perturbative numerics using TEBD for the oscillations in both the spin-1 chain (Fig. 4.2) and dimerised XXZ chain (Fig. 4.9) which indicate our qualitative conclusions that the oscillations damp at intermediate times are robust to including higher orders.

These results differ from the prediction made in [159, 160] that the oscillations have infinite lifetime regardless of the quench strength λ. Whilst those papers are formulated in the continuum, the same arguments made therein lead to oscillations on the lattice that we have shown to decay.

The perturbative analysis of this chapter generalises straightforwardly to other interacting fermion and boson models with interactions that are local with regards to the elementary excitations of the unperturbed theory. We note that the much-studied Ising chain in a tilted field [142–144, 146, 150, 151, 153, 155] does not fall within this class of models. This is because when viewed as a perturbation of the transverse field Ising chain, which maps onto non-interacting fermions by the Jordan-Wigner transformation, the perturbing operator is not local in terms of these fermions, i.e. involves interaction vertices with arbitrarily large numbers of particles. This precludes employing approaches based on truncating the BBGKY hierarchy for the fermionic degrees of freedom.

A

A.1 Gaussian nature of Bogoliubov vacuum

In Sec. 2.1.1, I claimed that the Bogoliubov vacuum, $|\mathrm{B}\rangle$ was a Gaussian pure state, meaning that it could be written in the form

$$|\mathrm{B}\rangle = \exp(T_{ij}c_i^\dagger c_j^\dagger)|\mathrm{F}\rangle \ , \tag{A.1}$$

where $|\mathrm{F}\rangle$ is the vacuum of the original fermions. That is, $|\mathrm{F}\rangle$ and $|\mathrm{B}\rangle$ satisfy

$$\begin{aligned} \forall j : c_j|\mathrm{F}\rangle = 0 \ , \\ \forall j : \alpha_j|\mathrm{B}\rangle = 0 \ , \\ \alpha_j = U_{jm}c_m + V_{jm}c_m^\dagger \ . \end{aligned} \tag{A.2}$$

The first step in showing this is to notice that since $|\mathrm{B}\rangle$ has even fermion parity (with respect to the c fermions), then it can be written in the form

$$|\mathrm{B}\rangle = |\mathrm{F}\rangle + \sum_{n=1}^{\infty} T^{(2n)}_{m_1 m_2 \ldots m_{2n}} \prod_{r=1}^{2n} c^\dagger_{m_r}|\mathrm{F}\rangle \ . \tag{A.3}$$

Without loss of generality the $T^{(2n)}$ may be assumed to be antisymmetric under exchange of neighbouring indices. Considering the one fermion sector of $\alpha_j|\mathrm{B}\rangle = 0$ gives the equation

$$\begin{aligned} 0 =& \left(V_{jm}c_m^\dagger + U_{jm}c_m T^{(2)}_{ab}c_a^\dagger c_b^\dagger\right)|\mathrm{F}\rangle \ , \\ =& \left(V_{jm} + U_{ja}T^{(2)}_{ab}c_a c_b^\dagger + U_{ja}T^{(2)}_{ab}c_a c_b^\dagger c_a^\dagger\right)|\mathrm{F}\rangle \ , \\ =& (V_{jm} + 2U_{ja}T_{am})c_m^\dagger|\mathrm{F}\rangle \ . \end{aligned} \tag{A.4}$$

With the conclusion that

$$T^{(2)}_{am} = -\frac{1}{2}(U^{-1}V)_{am} \ . \tag{A.5}$$

We now wish to show by induction that

$$T^{(2n)}_{m_1 m_2 \ldots m_{2n-1} m_{2n}} = \left(-\frac{1}{2}\right)^n \frac{1}{n!}(U^{-1}V)_{m_1 m_2} \ldots (U^{-1}V)_{m_{2n-1} m_{2n}} \ . \tag{A.6}$$

To do so, assume this form holds for $T^{2(n-1)}$ and consider the $2n-1$ fermion sector of $\alpha_i|\mathrm{B}\rangle = 0$. This reads

$$0 = V_{ij} T^{2(n-1)}_{m_3 \ldots m_{2n}} c_j^\dagger \prod_{r=3}^{2n} c^\dagger_{m_r}|\mathrm{F}\rangle + U_{ij} T^{(2n)}_{m_1, \ldots m_{2n}} c_j \prod_{r=1}^{2n} c^\dagger_{m_r}|\mathrm{F}\rangle \ . \tag{A.7}$$

As before, in the term containing U_{ij}, the only values of j for which c_j does not annihilate the term are when it equals one of the m_r. Suppose $j = m_r$. Then we may commute c_j to be adjacent to $c^\dagger_{m_r}$ by incurring a sign $(-1)^{r-1}$. Because $T^{(2n)}$ is antisymmetric, we can absorb that sign by permuting the m_r index on $T^{(2n)}$ to the front for each of the $2n$ values of r. Relabelling the various summed over indices then yields

$$0 = \left(V_{i m_2} T^{2(n-1)}_{m_3 \ldots m_{2n}} + 2n U_{ir} T^{(2n)}_{r m_2 \ldots m_{2n}}\right) \prod_{r=2}^{2n} c^\dagger_{m_r}|\mathrm{F}\rangle \ , \tag{A.8}$$

with the result that

$$T^{(2n)}_{m_1 m_2 | m_3 \ldots m_4} = -\frac{1}{2n}(U^{-1}V)_{m_1 m_2} T^{2(n-1)}_{m_3 \ldots m_4} \ . \tag{A.9}$$

In conjunction with our induction hypothesis for $T^{2(n-1)}$, this proves that the Bogoliubov vacuum is obtained from the original fermion vacuum by Eq. (A.1).

A.2 Reality of certain mean-fields

When evaluating our self-consistent mean-fields, in both Chapter 3 and Chapter 4, we observe that some of them are real. In this appendix we explain why this is the case, beginning with a clarification of the site parity $\sigma^\alpha_j \mapsto \sigma^\alpha_{-j}$. This does not act on the fermions as $c_j \mapsto c_{-j}$ due to the presence of the Jordan-Wigner string. The simplest way to deduce the effect of site parity in the fermion basis is to look at the action of site parity on fermion bilinears, which can be simply related to spin operators without semi-infinite strings. In particular, we consider the following spin bilinears of definite parity

$$\begin{aligned} A =& \sigma^x_i \sigma^x_{i+1} \ , \\ B =& \sigma^y_i \sigma^y_{i+1} \ , \\ C^\pm =& \sigma^x_i \sigma^x_{i+1} \pm \sigma^y_i \sigma^y_{i+1} \ . \end{aligned} \tag{A.10}$$

We then note that the fermionic bilinears can be decomposed in terms of these via

$$\begin{aligned} c_i^\dagger c_j =& \frac{1}{4}(A + B - iC^-) \ , \\ c_j^\dagger c_i =& \frac{1}{4}(A + B + iC^-) \ , \\ c_i^\dagger c_j^\dagger =& \frac{1}{4}(A - B - iC^+) \ , \\ c_i c_j =& \frac{1}{4}(-A + B - iC^+) \ . \end{aligned} \tag{A.11}$$

We thus see that the action of site parity on the bilinears is to exchange $c_i^\dagger c_j$ with $c_j^\dagger c_i$ and therefore $t_{ij} = \langle c_i^\dagger c_j \rangle = t_{ji} \in \mathbb{R}$ as stated in the main text.

Additionally, the ANNNI Hamiltonian satisfies $H = H^* = H^T$ in both the spin and fermion bases. In particular, in the fermion basis $c_i c_j$ is also real. By the spectral theorem for real symmetric matrices we then know that the eigenvectors of H are real in the same basis and so

$$\langle c_i c_j \rangle_\beta = \frac{1}{Z(\beta)} \sum_n \langle E_n | c_i c_j | E_n \rangle e^{-\beta E_n} \in \mathbb{R} \tag{A.12}$$

is manifestly real in equilibrium. However, after the quench the corresponding time-evolved quantity becomes

$$\langle c_i c_j \rangle_t = \frac{1}{Z(\beta)} \sum_{n,n',m'} e^{-\beta E_n^0} \langle E_n | E_{m'} \rangle \langle E_{m'} | c_i c_j | E_{n'} \rangle \langle E_{n'} | E_n \rangle e^{-it(E_{m'} - E_{n'})} \ , \tag{A.13}$$

where E_n^0 are the pre-quench energies and $E_{m'}$ the post-quench energies. Even if the post-quench Hamiltonian is also real and thus the post-quench energy eigenstates $|E_{n'}\rangle$ real, the phase factors will cause it to be generically complex. However, at very late times we would expect that the system would come back to equilibrium via these factors dephasing and so the correlation function should become real again at late times. Since t_n are all real due to the site parity $\mathbb{Z}_2$ this implies that all effective couplings are real in equilibrium, and out of equilibrium the only complex one will be $\Delta_{\text{Eff}}^{(1)}(t)$.

A.3 Linear response

In this appendix we summarise how to derive Kubo linear response relations after a quantum quench that occurs at time $t = 0$, see e.g. Ref. [192]. The Hamiltonian is of the form

$$H(t) = \theta(-t) H_i + \theta(t) H_f + f(t) V \ , \tag{A.14}$$

where $\theta(t)$ is the Heaviside step function. If $f = 0$ this corresponds to a quench at $t = 0$. The linear response regime is when $f(t) \ll 1$ and for this to be genuinely nonequilibrium we require $f(t)$ to have support in the time period before the system thermalises after the quench.

We work in an interaction picture such that $H = H_0 + f(t)V$, where H_0 is generally not free. The interaction picture states $|\psi(t)\rangle_I$ are defined by

$$|\psi(t)\rangle_I = e^{iH_0 t} U(t, t_0) |\psi(t_0)\rangle \ , \tag{A.15}$$

where $U(t, t_0)$ is the full time-evolution operator associated with $H(t)$, $|\psi(t_0)\rangle$ is the Schrödinger picture state at t_0 and H_0 is considered time independent by requiring, according to (A.14), that $t_0 \geq 0$. Consistently, in the interaction picture the general operator $\mathcal{O}$ evolves in time as

$$\mathcal{O}_I(t) = e^{iH_0 t} \mathcal{O} e^{-iH_0 t} \ . \tag{A.16}$$

The time-evolution according to $H(t)$ of the expectation value of $\mathcal{O}$ in the state defined at t_0 by $\rho(t_0) = |\psi(t_0)\rangle\langle\psi(t_0)|$ can be expressed in the interaction picture as

$$\mathrm{Tr}\left(\rho(t)\,\mathcal{O}\right) = \mathrm{Tr}\left(\rho_I(t)\,\mathcal{O}_I(t)\right) \approx \mathrm{Tr}\left(\rho(t_0)\,\mathcal{O}_I(t)\right) - i\int_{t_0}^{t} f(t')\chi(t,t')\mathrm{d}t' \ , \tag{A.17}$$

where the susceptibility $\chi(t, t')$ is given by

$$\chi(t,t') \equiv \mathrm{Tr}\left(\rho(t_0)[\mathcal{O}_I(t), V_I(t')]\right) \ . \tag{A.18}$$

In the last step of (A.17) we have expressed $\rho_I(t) = |\psi(t)\rangle_{II}\langle\psi(t)|$ by the first two terms in its power series in the small function $f(t)$. Eq (A.17) is the usual linear response formula except that the time-translation invariance of the susceptibility is broken by the quench and hence $\chi(t, t')$ does not depend only on the time-difference $t - t'$.

A.4 Equations of motion in Second Born approximation

The method we use for deriving the equations of motion (4.32) is given in more detail in [53, 54], here we simply briefly recap the main points for completeness. The first step is to diagonalise the free part of the Hamiltonian using Eqs. (4.16)-(4.18) and rewrite the interaction in this basis, giving Eq. (4.30). This takes care of all system dependent properties and leaves us with the general problem of working out the BBGKY hierarchy of equations of motion generated by

$$\hat{H}(\Delta, \alpha, h_s) = \sum_{k>0,\mu} \epsilon_\mu(k)\hat{b}^\dagger_\mu(k)\hat{b}_\mu(k) \ , + \Delta \sum_{\boldsymbol{\mu}} \sum_{k_1,\ldots k_4>0} V_{\boldsymbol{\mu}}(\boldsymbol{k})\hat{A}_{\boldsymbol{\mu}}(\boldsymbol{k}) \ . \tag{A.19}$$

The Heisenberg equations of motion for the two-point operators $\hat{n}_{\mu\nu}(k,t) = b^\dagger_\mu(k,t)b_\nu(\mathrm{k,t})$ are

$$\frac{\partial \hat{n}_{\mu\nu}(k,t)}{\partial t} = i\epsilon_{\mu\nu}\hat{n}_{\mu\nu} + i\Delta \sum Y^{\boldsymbol{\mu}}_{\mu\nu}(k,\boldsymbol{q})\hat{A}_{\boldsymbol{\mu}}(\boldsymbol{q}) \ , \tag{A.20}$$

where $\epsilon_{\mu\nu}(k) = \epsilon_\mu(k) - \epsilon_\nu(k)$ and the coefficients of the quartic operators appearing are given explicitly in terms of the interaction potential $V_{\boldsymbol{\mu}}(\boldsymbol{k})$ by

$$\begin{aligned} Y^{\boldsymbol{\mu}}_{\alpha\beta}(k,\boldsymbol{q}) &= \delta_{\beta\mu_4}\delta_{k,q_4}V_{\mu_1\mu_2\mu_3\alpha}(\boldsymbol{q}) + \delta_{\beta\mu_3}\delta_{k,q_3}V_{\mu_1\mu_2\alpha\mu_4}(\boldsymbol{q}) \\ &- \delta_{\alpha\mu_2}\delta_{k,q_2}V_{\mu_1\beta\mu_3\mu_4}(\boldsymbol{q}) - \delta_{\alpha\mu_1}\delta_{k,q_1}V_{\beta\mu_2\mu_3\mu_4}(\boldsymbol{q}) \ . \end{aligned} \tag{A.21}$$

The quartic operators $\hat{A}_{\boldsymbol{\mu}}(\boldsymbol{k})$ likewise evolve according to the following Heisenberg equations of motion

$$\frac{\partial}{\partial t}\hat{A}_{\boldsymbol{\mu}}(\boldsymbol{k},t) = iE_{\boldsymbol{\mu}}(\boldsymbol{k})\hat{A}_{\boldsymbol{\mu}}(\boldsymbol{k},t) + i\Delta \sum_{\boldsymbol{\gamma}} \sum_{\boldsymbol{q}>0} V_{\boldsymbol{\gamma}}(\boldsymbol{q}) \left[\hat{A}_{\boldsymbol{\gamma}}(\boldsymbol{q},t), \hat{A}_{\boldsymbol{\mu}}(\boldsymbol{k},t)\right] \ , \tag{A.22}$$

where $E_{\boldsymbol{\mu}}(\boldsymbol{k}) = \epsilon_{\mu_1}(k_1) + \epsilon_{\mu_2}(k_2) - \epsilon_{\mu_3}(k_3) - \epsilon_{\mu_4}(k_4)$. This equation contains products of up to six fermionic operators on the right hand side, and carrying on in this way generates the BBGKY hierarchy of equations of motion. The second Born approximation consists of truncating at this level which we do by formally integrating Eq. (A.22) to obtain an integral expression for $\hat{A}_{\boldsymbol{\mu}}(\boldsymbol{k},t)$ in terms of its value at $t = 0$ which can be substituted into the Heisenberg equations of motion (A.20), which gives

$$\begin{aligned} \frac{\partial}{\partial t} n_{\mu\nu}(k,t) =& i\epsilon_{\mu\nu}(k)n_{\mu\nu}(k,t) + i\Delta \sum_{\boldsymbol{\eta}} \sum_{\boldsymbol{q}>0} Y^{\boldsymbol{\eta}}_{\mu\nu}(k,\boldsymbol{q}) \left\langle \hat{A}_{\boldsymbol{\eta}}(\boldsymbol{q},0)\right\rangle e^{itE_{\boldsymbol{\eta}}(\boldsymbol{q})} \\ &+\Delta^2 \sum_{\boldsymbol{\eta},\boldsymbol{\gamma}} \sum_{\boldsymbol{q},\boldsymbol{p}>0} \int_0^t \mathrm{d}s \ \left\langle \hat{A}_{\boldsymbol{\gamma}}(\boldsymbol{p},s)\hat{A}_{\boldsymbol{\eta}}(\boldsymbol{q},s)\right\rangle \times \left(Y^{\boldsymbol{\gamma}}_{\mu\nu}(k,\boldsymbol{p})e^{i(t-s)E_{\boldsymbol{\gamma}}(\boldsymbol{p})}V_{\boldsymbol{\eta}}(\boldsymbol{q}) - (\boldsymbol{p},\boldsymbol{\gamma}) \leftrightarrow (\boldsymbol{q},\boldsymbol{\gamma})\right) \ . \end{aligned} \tag{A.23}$$

Neglecting the 4- and 6-particle cumulants in (A.23) then leads to Eq. (4.32).

Part B

Open Systems

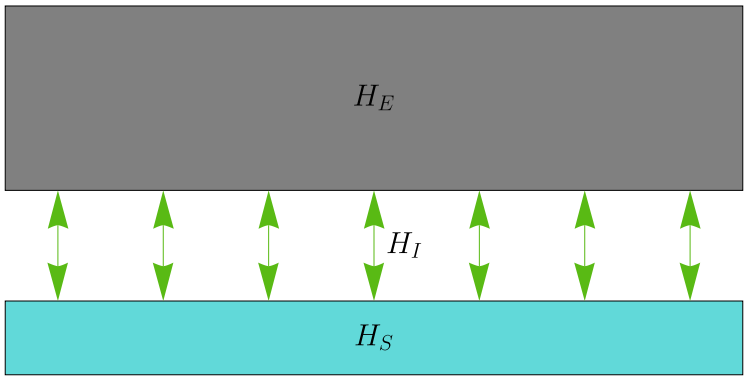

Do I dare
Disturb the universe?

The Love Song of J. Alfred Prufrock
T.S. Eliot

5

Introduction to dynamics in open quantum systems

The first part of this thesis was concerned with quantum quenches in closed quantum systems — that is, systems that do not interact with their surroundings. In the remaining half of this thesis, I wish to discuss open quantum systems. Every real system is coupled (potentially very weakly) to some environment (unless your system of study is the entire universe!), so the question of how to incorporate dissipation due to this environment is an important fundamental question. It is also a much harder question, in general, than the corresponding question for closed systems and requires new tools. This chapter is intended to be a short overview of open quantum systems and some exactly solvable many body examples present in the literature. This is to prepare the reader for Chapter 6, which analyses a particular toy model with unusual algebraic features, which can be exploited to provide a rare exact solution to the nonequilibrium dynamics.

5.1 Why study open systems?

Whilst most standard tools for many body quantum mechanics only apply to closed systems, real systems are invariably influenced by their environment. We are now entering an era of 'noisy intermediate scale quantum' (NISQ) devices [20], capable of genuinely useful computation but lacking full error correction. A good understanding of the effects of noise in both digital quantum computers [193, 194] and analog quantum simulators [195] is clearly desirable. I am particularly interested, in

this and the following chapter, in theoretical insights that can be gained through analytic solutions to solvable models of quantum matter coupled to noisy environments. Such solutions are even rarer in the open case than the closed one and a variety of numerical [196–200] and perturbative [201, 202] approaches have also been developed.

Another motivation to study open quantum systems is to discover quantum generalisations of the comparatively better understood theory of nonequilibrium classical dynamics. In the classical case one such piece of understanding is provided by the 'macroscopic fluctuation theory' [203–205] which improves upon traditional linear expansions about equilibrium and allows for descriptions of nonequilibrium stationary states arbitrarily far from equilibrium that satisfy nonlinear evolution equations. A important role in the development of macroscopic fluctuation theory was played by exactly solvable models of stochastic lattice gases, such as exclusion processes, making these a natural starting point for investigations into open quantum systems [206–209].

Finally, there may be interesting new physics to be observed in nonequilibrium systems with noise. Proposals exist for engineering specific types of noise to yield target quantum states [210–212] including topologically ordered states [213,214] and simulations of lattice gauge theories [215]. Whilst these works aim to use noise to make experimental realisations of already theoretically predicted phenomena simpler, one might also hope that in studying the dynamics of open systems qualitatively new phenomena may be discovered and utilised.

5.2 The Markov assumption - Lindblad formalism

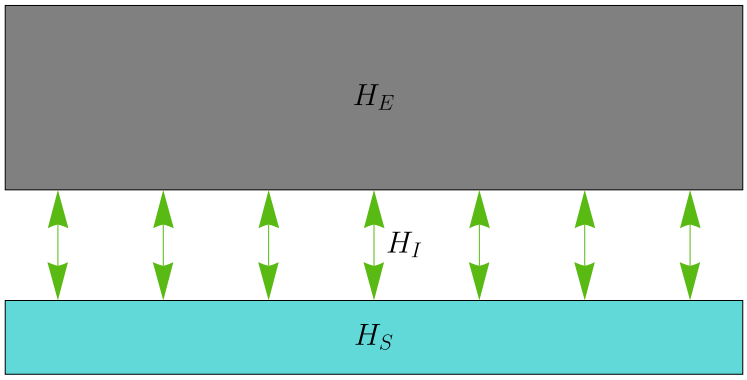

Figure 5.1: Pictorial representation of an open system weakly coupled to an environment. The combined system evolves under $H_S + H_E + H_I$.

An important ingredient moving forwards will be to make an assumption that the open system we are interested in is *Markovian*. That is, that the time evolution of a subsystem depends on that subsystem's current state only, and not on its history. To see why this is a drastic simplification, consider for a moment what it means for a system to be open to an environment. Taken together, the system and the environment must still be described by quantum mechanics, and therefore the Schrödinger equation. The Hamiltonian may be written as

$$H = H_{\mathrm{S}} + H_{\mathrm{E}} + H_{\mathrm{I}} \ , \tag{5.1}$$

with $H_{\mathrm{S}}, H_{\mathrm{E}}, H_{\mathrm{I}}$ being Hamiltonians for the system, environment and the interaction between them respectively. Even if the initial state of the system is not entangled with the environment (that is, $|\psi(0)\rangle = |\psi(0)\rangle_S |\psi(0)\rangle_E$ factorises as a product of an initial state of the system and an initial state of the environment), H_I will cause them to become entangled at later times. The reduced density matrix at time t therefore will be

$$\begin{aligned} \rho_{\mathrm{S}}(t) =& \mathrm{Tr}_{\mathrm{E}} |\psi(t)\rangle\langle\psi(t)| \ , \\ |\psi(t)\rangle =& \exp\left[-i(H_S + H_E + H_I)\right] |\psi(0)\rangle_S |\psi(0)\rangle_E \ . \end{aligned} \tag{5.2}$$

In general therefore, one might have to model the entire system to answer questions only about a subsystem. This is clearly counter to the idea of considering a subsystem evolving under its own dynamics, plus a small amount of noise.

Part of the difficulty is that as the system of study evolves, so does the environment. Even worse, the system evolution influences the environment, which in turn influences the system again in a form of 'back action'. To get around these problems we make the assumption that the environment relaxes much faster than the dynamical time of the system and can therefore always be assumed to be in equilibrium. Specifically, suppose that the environment is described by operators $B_\alpha(t)$ and consider the reservoir correlation functions

$$F_{\alpha\beta}(t,s) = \langle B_\alpha(t) B_\beta(t-s) \rangle \ . \tag{5.3}$$

If the bath correlations decay in time as $F(t,s) \sim \exp(-s/\tau_B)$ then we want $\tau_B \ll \tau_S$, where τ_S is the timescale of dynamics in the subsystem S of interest. One also generally requires a weak coupling approximation to ensure that the state of the reservoir does not change appreciably during the evolution and the back action can be ignored. These assumptions allow us to justify a *Markovian* approximation, that the dynamics of the reduced density matrix $\rho_{\mathrm{S}}(t)$ depends only on the current

state of the system $\rho_{\rm S}(t)$. That is, the time evolution is given by some quantum channel Λ_t satisfying the semigroup conditions

$$\begin{aligned}\rho_{\rm S}(t) =&\Lambda_t(\rho_{\rm S}(0)) \ ,\\ \Lambda_0 =&\mathbb{1} \ ,\\ \Lambda_{t+s} =&\Lambda_t\Lambda_s \ ,\end{aligned} \tag{5.4}$$

Assuming continuity and the semigroup conditions, the channel Λ_t can be written in exponential form as

$$\Lambda_t = \exp(t\mathcal{L}) \ , \tag{5.5}$$

where the generator $\mathcal{L}$ is often called the 'Lindbladian'. If $\mathcal{L}$ is bounded then any valid continuous time evolution (the meaning of 'valid' to be explained below) can be given in terms of the Lindblad equation [216–218] for the evolution of the density matrix:

$$\frac{\mathrm{d}\rho}{\mathrm{d}t} = -i[H,\rho] + \sum_a J_a\left(L_a\rho L_a^\dagger - \frac{1}{2}\{L_a^\dagger L_a,\rho\}\right) \ , \tag{5.6}$$

with all $J_a > 0$. The operators L_a are termed 'jump operators' and depend on the exact nature of the noise. The derivation of the Lindblad equation requires that, in addition to the semigroup conditions (5.4), the channel Λ_t is completely positive and trace preserving. Preserving the trace is a natural requirement, since the trace of a valid density matrix must be 1. A positive channel is one that maps positive operators to positive operators, which again is a natural restriction. Complete positivity is the stronger requirement that if we append some number of ancillary qubits to our quantum system, and act with the same quantum channel Λ_t (with the ancilla bits untouched), then this channel must also preserve positivity. Complete positivity implies positivity but not vice versa. It is known that all completely positive, trace preserving maps can be obtained as a result of unitary evolution on a larger quantum system followed by tracing out the ancillary degrees of freedom, a result known as the Stinespring dilation theorem [219].

5.3 The superoperator formalism and some previous results

The key observation about the Lindblad equation (5.6) is that the density matrix enters linearly in every term. The density matrix is a member of the vector space of linear operators on $\mathcal{H}$, denoted

as $\mathrm{End}(\mathcal{H}) \equiv \mathcal{H}' \otimes \mathcal{H}$ where $\mathcal{H}'$ is the dual Hilbert space. This identification allows us to recast the Lindblad equation in the form of a Schrödinger equation

$$\frac{\mathrm{d}}{\mathrm{d}t}|\rho\rangle\rangle = \mathcal{L}|\rho\rangle\rangle \ . \tag{5.7}$$

From here on, vectors in the underlying Hilbert space are denoted using single angle brackets $|\psi\rangle$, whilst members of $\mathrm{End}(\mathcal{H})$ are given double angle brackets when treated in this manner. The advantage of the superoperator formalism is it allows us to convert Lindblad equations into (non-Hermitian) Schrödinger equations on an enlarged Hilbert space with local dimension d^2 where d is the local dimension of the original model. For instance, for a spin chain, the vector $|\rho\rangle\rangle$ lives in a Hilbert space describing a two leg ladder geometry, see Fig. 5.2. The object $\mathcal{L} : \mathrm{End}(\mathcal{H}) \to \mathrm{End}(\mathcal{H})$ is a

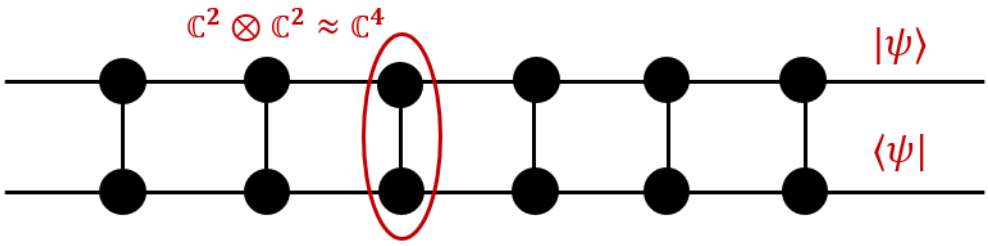

Figure 5.2: Two leg ladder structure of the doubled Hilbert space $\mathcal{H}' \otimes \mathcal{H}$ for an open spin chain.

'superoperator' because it acts on operators, and is called the *Lindbladian* or *Lindblad superoperator*. It is given explicitly, for bosonic jump operators, by

$$\mathcal{L} = -iH_L + iH_R + \sum_a J_a \left(L_{a,L} L^\dagger_{a,R} - \frac{1}{2}\left[(L^\dagger_a L_a)_L + (L^\dagger_a L_a)_R \right] \right) \ , \tag{5.8}$$

where the subscripts L/R refer to left and right multiplication. That is, the *super*operator O_L is defined as left multiplication by the (regular) operator O. The following few remarks hopefully clarify the idea of the construction:

1. The superoperators O_L and O'_R commute. This is a restatement of the associativity of matrix multiplication $(O\rho)O' = O(\rho O')$.
2. $(OO')_L = O_L O'_L$.
3. $(OO')_R = O'_R O_R$. Note that the order has swapped compared to the previous remark.

It is straightforwards to obtain a concrete representation of the superoperators $O_{L/R}$. First, note that by rewriting ρ as a vector $|\rho\rangle\!\rangle$ we are performing an 'index-raising' map

$$\rho = \sum_{\alpha,\beta} \rho^{\alpha}_{\ \beta} |\alpha\rangle\langle\beta| \mapsto |\rho\rangle\!\rangle = \sum_{\alpha\beta} \rho^{\alpha\beta} |\alpha\rangle \otimes |\beta\rangle. \tag{5.9}$$

Additionally, right multiplication by an operator O must turn into left multiplication by some superoperator O_R such that

$$O_R |\rho\rangle\!\rangle = |\rho O\rangle\!\rangle \ . \tag{5.10}$$

Now, consider right multiplication by an operator O under the index-raising map

$$\rho O = \sum_{\alpha\beta} \left(\sum_{\gamma} \rho^{\alpha}_{\ \gamma} O^{\gamma}_{\ \beta} \right) |\alpha\rangle\langle\beta| \mapsto |\rho O\rangle\!\rangle = \sum_{\alpha\beta} \left(\sum_{\gamma} \rho^{\alpha\gamma} O^{\ \beta}_{\gamma} \right) |\alpha\rangle \otimes |\beta\rangle \ , \tag{5.11}$$

which therefore implies that $O_R = \mathbb{1} \otimes \left(O^{\ \beta}_{\gamma} |\beta\rangle\langle\gamma| \right)$. Note that the indices are swapped compared to Eq. (5.9), indicating that the right multiplication action is implemented via the transpose of the original operator, along with acting on bras instead of kets. Left multiplication is simply implemented via the operator acting on kets. This can be summarised as $O_L = O \otimes \mathbb{1}$ and $O_R = \mathbb{1} \otimes O^T$.

5.3.1 Integrability

As discussed above, exactly solvable models of Lindblad time evolution are desirable in order to gain insight into the behaviour of noisy quantum systems and the effects of decoherence. The simplest example of such solvable Lindblad systems was introduced in [220] and utilises the superoperator formalism. In this work, the author noted that if the jump operators L_a are linear in fermionic creation/annihilation operators, then the Lindblad superoperator is a quadratic form and standard free fermion techniques can be applied. This insight has been applied to gain numerous insights into such free but dissipative models [221–228]. A characteristic feature of free theories is the fundamental boson or fermion operators fulfil linear equations of motion and concomitantly so do the Green's functions of interest.

More recently, several solvable many particle Lindblad equations have been identified through the discovery of Lindblad equations that can be related to *interacting* Yang-Baxter integrable models [229–239]. In contrast to free theories, the equations of motion for correlation functions do not generally close in these models, but instead form an infinite hierarchy of coupled nonlinear equations. If $\mathcal{H}$ is the Hilbert space of a spin chain, then $\mathrm{End}(\mathcal{H}) \sim \mathcal{H}' \otimes \mathcal{H}$ is the Hilbert space of a two leg ladder. Ref. [233], therefore, took an approach based on identifying Lindblad dynamics which in the

superoperator formalism can be related to Hamiltonians for two leg ladders which are known to be Yang-Baxter integrable. Systematic searches for Yang-Baxter integrable Lindblad dynamics have also been done by searching for R matrix solutions to the Yang-Baxter equation which are of the form implied by the Lindblad equation [239]. Another class of Lindblad equations which can exploit integrability are "triangular" models which add particle loss (but not gain) and dephasing terms to otherwise number conserving integrable models [234,235,240]. In a basis ordered by particle number these Lindblad superoperators will be triangular, and the spectrum can be found by analysing the spectrum of the integrable model in each particle number sector, despite the model as a whole being non-integrable.

It is not necessary for there to be a direct link to integrable Hamiltonian systems for some exact solutions to be obtainable. In fact, there exist classes of models which are not quadratic in which some or all local correlation functions satisfy closed hierarchies of equations of motion [241–247]. This permits one to obtain some exact results on the dynamics, although full solutions typically remain out of reach.

5.3.2 Operator space fragmentation: the ASEP

A related but different route of constructing Yang-Baxter integrable Lindblad equations was discovered in Ref. [248] and will be the basis of the study in Chapter 6. It is based on a "fragmentation" of the space of operators into an exponential (in system size) number of subspaces that are left invariant under the dissipative evolution. Importantly, this mechanism applies to a quantum version of the asymmetric simple exclusion process (ASEP) [249–252].

The *classical* ASEP is one of the stochastic lattice gases that, as mentioned earlier, were important to the development of macroscopic fluctuation theory. In the classical ASEP one considers L lattice sites, each of which can be occupied or unoccupied by a particle. Particles may then hop to the left with rate J_1 and to the right with rate J_2. Importantly, these rates are set to 0 if the site a particle would otherwise hop to is occupied. Particles therefore interact with each other by means of hard-core repulsion. The ASEP is exactly solvable by mapping the transition matrix for the corresponding master equation to the Hamiltonian of an XXZ chain whose solution can be found using the Bethe ansatz [253–261].

The quantum ASEP is given by setting the Hamiltonian $H = 0$ and adopting the following jump operators

$$L_j^{(1)} = \sigma_j^+ \sigma_{j+1}^- \ , \quad L_j^{(2)} = \sigma_j^- \sigma_{j+1}^+, \tag{5.12}$$

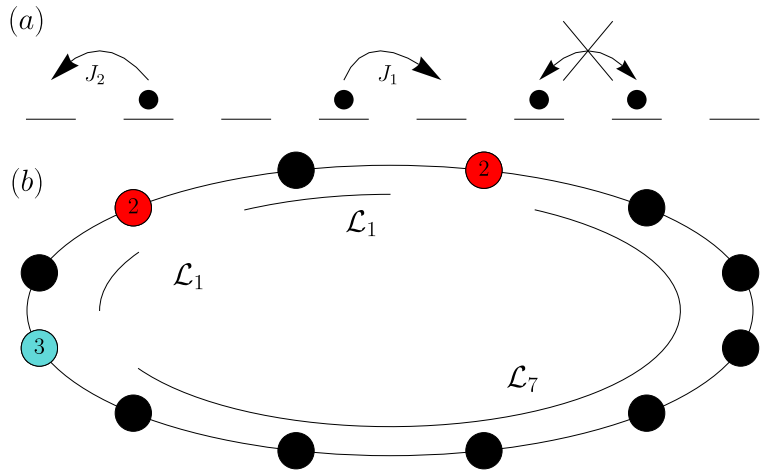

Figure 5.3: (a) Diagram of the classical ASEP, showing allowed transitions and their rates. Excluded transitions to occupied sites are shown with the crossed out arrows. (b) Schematic picture of the fragmentation in the quantum ASEP, showing a fixed distribution of defects. The projection of the total Lindblad superoperator on this subspace can be written as a sum of Lindbladians for each of the disjoint chains obtained by removing the defect sites.

with rates $J_1, J_2 > 0$, respectively describing hopping to the left and right. This Lindblad equation can be obtained [208] as the averaged dynamics of a stochastic quantum model of particles hopping with random amplitudes, first introduced in its symmetric form in Ref. [206] and further analysed in Refs. [207, 262–264]. In order to study the fluctuations of system degrees of freedom that are induced by coupling to the bath — a question that has been extensively studied for classical systems (see e.g. [265–271]) — it is necessary to go beyond this description, see e.g. [206, 208, 263], but these fluctuations can still be described in terms of a quantum master equation of Lindblad form [209].

In order to obtain an explicit expression for the Lindblad superoperator $\mathcal{L}$ we pick the following basis of the local Hilbert space of operators acting on site j:

$$|1\rangle\!\rangle_j = |\uparrow\rangle_j\ {}_j\langle\uparrow|, \quad |2\rangle\!\rangle_j = |\uparrow\rangle_j\ {}_j\langle\downarrow|, \quad |3\rangle\!\rangle_j = |\downarrow\rangle_j\ {}_j\langle\uparrow|, \quad |4\rangle\!\rangle_j = |\downarrow\rangle_j\ {}_j\langle\downarrow|. \tag{5.13}$$

A basis of local superoperators acting on these states in then given by

$$E_j^{ab} = |a\rangle\!\rangle_j\ {}_j\langle\!\langle b| \ . \tag{5.14}$$

The Lindbladian in this basis has the form [248]

$$\begin{aligned}\mathcal{L}_{\text{ASEP}} =&\mathcal{L}_{\text{Diag}} + \mathcal{L}_{\text{Defect}}\\ \mathcal{L}_{\text{Diag}} =&\sum_j J_1 E_j^{14}E_{j+1}^{41} + J_2 E_j^{41}E_{j+1}^{14} - J_1 E_j^{44}E_{j+1}^{11} - J_2 E_j^{11}E_{j+1}^{44}\ ,\\ \mathcal{L}_{\text{Defect}} =&-\frac{1}{2}\sum_j (E_j^{22}+E_j^{33})(J_1 E_{j+1}^{11} + J_2 E_{j+1}^{44}) + (E_{j+1}^{22}+E_{j+1}^{33})(J_2 E_j^{11} + J_1 E_j^{44})\\ &-\frac{1}{2}\sum_j (J_1+J_2)(E_j^{22}E_{j+1}^{33} + E_j^{33}E_{j+1}^{22})\ ,\end{aligned} \tag{5.15}$$

where $\mathcal{L}_{\text{Diag}}$ leaves invariant the subspace of diagonal density matrices

$$|\rho\rangle\!\rangle_{\text{Diag}} = \sum_{\boldsymbol{\sigma}} \rho^{\boldsymbol{\sigma}\boldsymbol{\sigma}} |\boldsymbol{\sigma}\rangle \otimes |\boldsymbol{\sigma}\rangle\ , \quad |\boldsymbol{\sigma}\rangle = \otimes_{j=1}^{L} |\sigma_j\rangle_j\ , \sigma_j \in \{\uparrow,\downarrow\}. \tag{5.16}$$

These diagonal density matrices correspond to probability distributions over 'classical' states of a chain of spins that can only be up or down, where the probability to be in the state $|\boldsymbol{\sigma}\rangle$ is given by $P(\boldsymbol{\sigma}) = \rho^{\boldsymbol{\sigma}\boldsymbol{\sigma}}$. Conversely, an off-diagonal density matrix would represent a probabilistic mixture of quantum superpositions of these classical states.

There were two key insights made in [248] into this Lindbladian: firstly, that the the states $|1\rangle\!\rangle$ and $|4\rangle\!\rangle$ enter in a very different way to the states $|2\rangle\!\rangle$ and $|3\rangle\!\rangle$, which is emphasised by the split into $\mathcal{L}_{\text{Diag}} + \mathcal{L}_{\text{Defect}}$. In particular, the states $|2\rangle\!\rangle$ and $|3\rangle\!\rangle$ appear only via E_j^{22} and E_j^{33}, so there are no terms that enable these to hop. A state of the quantum ASEP is therefore given first by specifying some distribution of 'type 2' and 'type 3' particles, which are to be viewed as frozen defects. This defines an exponentially large number of invariant subspaces under the Lindblad dynamics, in much the same way as occurs in Hilbert space fragmentation and hence the authors dubbed this phenomenon 'operator space fragmentation'. The fragmentation in this model is simpler than the examples of Hilbert space fragmentation considered in [64–66, 272] because the local integrals of motion are not emergent and are simply the operators E_j^{22} and E_j^{33} themselves.

The second key insight of [248] was that the projection of the Lindbladian on each invariant subspace is equivalent to a direct sum of integrable XXZ Hamiltonians governing the regions between defects. This enables the spectrum of the Lindblad superoperator to be computed exactly. Nonetheless, a computation of how observables time evolve following a quench is highly non-trivial and the integrability by itself is not sufficient. The aim of Chapter 6 will be to revisit this model by viewing it as a two-dimensional subspace of a larger four parameter model that maintains the operator space fragmentation. We will show that this larger model contains a three parameter family,

such that the projection of the Lindblad superoperator to each invariant subspace can be mapped to free fermions.

5.3.3 Free Lindblad systems

A key piece of machinery I will use in Chapter 6 is the diagonalisation procedure for 'free Lindbladians' originally used in [273]. This is a procedure for dealing with Lindblad superoperators quadratic in some set of Majorana fermion modes a_i satisfying

$$\{a_i, a_j\} = 2\delta_{ij} \ , \ i,j = 1,2,\dots 2M \ . \tag{5.17}$$

The key result of Chapter 6 will be a Lindbladian exhibiting operator space fragmentation such that on each invariant subspace the Lindblad superoperator projects to some quadratic linear operator of the form

$$\mathcal{L} = \frac{1}{4}\boldsymbol{a}\cdot A\cdot \boldsymbol{a}. \tag{5.18}$$

Here and elsewhere $(\cdot)$ represents the dot product with no complex conjugation, that is $v\cdot w = \sum_i v_i w_i$ and not $\sum_i v_i^* w_i$. A is a $2M\times 2M$ matrix whose symmetric part contributes only a multiple of the identity to $\mathcal{L}$ and can be therefore ignored in the following whilst $\boldsymbol{a}$ is the length $2M$ vector containing each a_i. Assuming A to be diagonalisable, antisymmetry ensures its eigenvalues come in pairs $\pm\beta_j$ which we order as $\beta_1, -\beta_1 \dots$. We then normalise the eigenvectors according to

$$\boldsymbol{v}_r \cdot \boldsymbol{v}_s = (\sigma^x \otimes \mathbb{1})_{rs} \ . \tag{5.19}$$

Finally we define new fermion operators by

$$b_j = \boldsymbol{v}_{2j-1}\cdot \mathbf{a}/\sqrt{2} \ , \quad b'_j = \boldsymbol{v}_{2j}\cdot \mathbf{a}/\sqrt{2}. \tag{5.20}$$

These fulfil simple 'almost-canonical' anticommutation relations due to (5.19)

$$\{b_j, b_k\} = 0 = \{b'_j, b'_k\} \ , \quad \{b_j, b'_k\} = \delta_{j,k} \ , \tag{5.21}$$

and put the Lindbladian into the form

$$\mathcal{L} = \frac{1}{2}\sum_k \beta_k - \sum_k \beta_k b'_k b_k \ . \tag{5.22}$$

Note that b' and b are not Hermitian conjugates and so $\mathcal{L}$ is not Hermitian either. The left and right eigenstates of this L are therefore not obtained from each other simply by conjugation. They are instead constructed by introducing separate left and right vacua annihilated by b' and b respectively:

$$\forall k: \quad \langle\langle L|b'_k = 0, \quad b_k|R\rangle\rangle = 0 \ , \tag{5.23}$$

acting on these with the b'_k (b_k) gives an occupation number representation for the right (left) eigenstates:

$$|k_1, k_2, \ldots\rangle\!\rangle = b'_{k_1} b'_{k_2} \ldots |R\rangle\!\rangle \ ,$$
$$\langle\!\langle k_1, k_2, \ldots| = \langle\!\langle L| \ldots b_{k_2} b_{k_1} \ldots \ . \tag{5.24}$$

These are the right (left) eigenvectors of $\mathcal{L}$. In terms of the occupation numbers $n_k = 0, 1$ of each fermion mode these have eigenvalues

$$\mathcal{L} \prod_k (b'_k)^{n_k} |R\rangle\!\rangle = \lambda \prod_k (b'_k)^{n_k} |R\rangle\!\rangle \ ,$$
$$\lambda = \frac{1}{2} \sum \beta_k - \sum n_k \beta_k \ . \tag{5.25}$$

I'm being quoted to introduce something, but I have no idea what it is and certainly don't endorse it.

xkcd.com/1942/
Randall Munroe

6 An Exact Quench in an Open System

This chapter is based on [1], which considers a Lindblad equation that, for particular initial conditions, reduces to an asymmetric simple exclusion process with additional loss and gain terms. The resulting Lindbladian exhibits operator-space fragmentation and each block is Yang-Baxter integrable. For particular loss/gain rates the model can be mapped to free fermions. The chapter ends by computing the full quantum dynamics for an initial product state when the model is tuned to the free fermion subspace.

6.1 Introduction

In order to show how the operator-space fragmentation can be exploited in practice to obtain a full solution of the dissipative dynamics, this chapter will now consider a generalisation of the quantum ASEP. As we will show, the Lindbladian of this model exhibits operator-space fragmentation and in each sector can be mapped onto a Lindbladian that is quadratic in fermions. The resulting dynamics can then be solved exactly.

This chapter is organised as follows: Section 6.2 introduces the model of interest, which can be viewed as an ASEP with additional loss/gain terms. Subsection 6.2.1 then shows that the operator space fragmentation is retained when generalising the ASEP in this way and recaps on how this may be used to find correlation functions.

Section 6.3 then analyses the Lindbladian's projection on to each of these subspaces, focusing on a particular subset of parameters, for which the Lindbladian in each sector can be mapped onto a bilinear form in auxiliary fermions. We show that the subspace of diagonal density matrices is invariant under time evolution and reduces to a classical stochastic process similar to ones that have been previously studied in the literature [274–277]. We employ Jordan-Wigner and Bogoliubov transforms to solve the dynamics in this sector and show that it has an infinite temperature steady state. In Section 6.5 we consider the defect problem and outline how to efficiently find the spectrum of the Lindbladian. In Section 6.6 we consider evolution out of an initial product state and compute the transverse spin-spin correlation function. Lastly, we relegate some technical calculations necessary for the conclusions in the main text to two appendices.

6.2 The model

We wish to generalise the quantum ASEP model defined by taking a spin-1/2 chain with periodic boundary conditions and no coherent dynamics ($H = 0$) along with the jump operators (5.12). To this end consider two additional jump operators such that the dynamics is governed by the Lindblad equation (5.6) with jump operators [278]

$$\begin{aligned} L_j^{(1)} &= \sigma_j^+ \sigma_{j+1}^- \ , \quad L_j^{(2)} = \sigma_j^- \sigma_{j+1}^+, \\ L_j^{(3)} &= \sigma_j^+ \sigma_{j+1}^+ \ , \quad L_j^{(4)} = \sigma_j^- \sigma_{j+1}^-. \end{aligned} \tag{6.1}$$

In terms of Jordan-Wigner fermions the first two of these correspond to hopping left and right and constitute the quantum ASEP. The two new operators represent pair creation and annihilation on neighbouring sites, respectively. In general, the rates of these may all be different and one obtains a four parameter family of models [278]. In contrast to the quantum ASEP, the additional jump operators describe processes that violate spin rotational invariance around the z-direction (or equivalently particle number conservation at the level of Jordan-Wigner fermions) so that the magnetisation is no longer conserved. As we will see, this leads to interesting new effects compared to the ASEP. Our choice of model is not motivated by any particular experimental setup, but aims to address a problem in mathematical physics, namely to obtain a many-particle Lindblad equation exhibiting operator-space fragmentation that can be solved exactly in practice. Having said this, in a particular parameter regime and for diagonal initial density matrices our model reduces to a classical master equation that has been argued to describe the kinetics of excitons in certain polymers [274] and it would be interesting to investigate whether quantum effects could be relevant to this system.

Working in the same basis (5.13) as for the ASEP we again find it convenient to split the Lindbladian up as

$$\mathcal{L} = \mathcal{L}_{\text{Diag}} + \mathcal{L}_{\text{Defect}} \ , \tag{6.2}$$

where

$$\begin{aligned}
\mathcal{L}_{\text{Diag}} = &\sum_j J_1 E_j^{14} E_{j+1}^{41} + J_2 E_j^{41} E_{j+1}^{14} + J_3 E_j^{14} E_{j+1}^{14} + J_4 E_j^{41} E_{j+1}^{41} \\
&- \sum_j J_1 E_j^{44} E_{j+1}^{11} + J_2 E_j^{11} E_{j+1}^{44} + J_3 E_j^{44} E_{j+1}^{44} + J_4 E_j^{11} E_{j+1}^{11} \ , \qquad (6.3) \\
\mathcal{L}_{\text{Defect}} = &-\frac{1}{2}\sum_j (E_j^{22} + E_j^{33})([J_1 + J_4]E_{j+1}^{11} + [J_2 + J_3]E_{j+1}^{44}) \\
&- \frac{1}{2}\sum_j (E_{j+1}^{22} + E_{j+1}^{33})([J_2 + J_4]E_j^{11} + [J_1 + J_3]E_j^{44}) \\
&- \frac{J_1 + J_2 + J_3 + J_4}{2}(E_j^{22} E_{j+1}^{33} + E_j^{33} E_{j+1}^{22}). \qquad (6.4)
\end{aligned}$$

If we initialise the system in a purely diagonal density matrix, the Lindblad equation (5.6) reduces to a classical master equation with transition matrix $\mathcal{L}_{\text{Diag}}$. This describes generalisations of the asymmetric simple exclusion process [249–252] similar to the diffusion-annihilation models studied in [274–277]. If we set $J_3 = J_4 = 0$, we recover the ASEP with periodic boundary conditions.

6.2.1 Operator-space fragmentation

The origin of operator-space fragmentation in the model (6.2), (6.3), (6.4) is the presence of strictly local conservation laws

$$[\mathcal{L}, E_j^{22}] = 0 = [\mathcal{L}, E_j^{33}]. \tag{6.5}$$

These conservation laws imply that particles of species $2, 3$ are left invariant by the dynamics and we therefore refer to these as "defects". The Hilbert space of operators thus breaks up into exponentially many invariant subspaces with fixed occupancies of defects. The fragmentation of operator-space does not rely on the fact our model is one dimensional. Indeed, operator-space fragmentation occurs if we consider a square lattice and jump operators defined on all nearest neighbour bonds

$$\begin{aligned}
L_{(i,j)}^{(l)} &= \sigma_{(i,j)}^{+}\sigma_{(i+1,j)}^{-} \ , \quad L_{(i,j)}^{(r)} = \sigma_{(i,j)}^{-}\sigma_{(i+1,j)}^{+} \ , \\
L_{(i,j)}^{(u)} &= \sigma_{(i,j)}^{+}\sigma_{(i,j+1)}^{-} \ , \quad L_{(i,j)}^{(d)} = \sigma_{(i,j)}^{-}\sigma_{(i,j+1)}^{+} \ . \qquad (6.6)
\end{aligned}$$

In this case the $2L^2$ operators $E_{(i,j)}^{22}, E_{(i,j)}^{33}$ are then strictly conserved. By focusing on one dimensional models, however, we allow for the possibility that the Lindbladian's action on each subspace

can be mapped to an integrable model. However, the occurrence of fragmentation will have implications for the dynamics in higher dimensions as well.

This operator-space fragmentation then allows observables to be computed by analysing each sector separately. As discussed earlier, for the ASEP ($J_3 = J_4 = 0$) the key result was that restricted to each defect-subspace the Lindbladian becomes integrable (as it is can be mapped to disjoint XXZ chains with diagonal boundary fields). Integrability techniques can be similarly applied to the projections of (6.2), (6.3), (6.4) to the relevant invariant subspaces [277, 278] but we do not pursue this line of enquiry here and instead impose a particular constraint on the rates J_1, J_2, J_3, J_4 which will allow us to construct a mapping to free fermions.

It should be stressed that for a particular observable, it may not be necessary to deal with very many invariant subspaces. This is illustrated by the transverse spin-spin correlation function

$$S^{+-}_{0,\ell+1} = \mathrm{Tr}\left[\sigma^+_0 \sigma^-_{\ell+1} \rho(t)\right] . \tag{6.7}$$

This depends only on the subspace with a type 3 defect at site 0 (equivalently site L) and a type 2 defect at site $\ell + 1$. To see this, note that in the superoperator formalism traces are replaced by inner products with the state

$$\langle\langle \mathbb{1}_{\mathrm{cl}}| = \otimes_{j=1}^{L} \left[{}_j\langle\langle 1| + {}_j\langle\langle 4|\right] . \tag{6.8}$$

An immediate consequence of the fact that the time evolution operator $e^{\mathcal{L}t}$ preserves traces is that $\langle\langle \mathbb{1}_{\mathrm{cl}}|$ is a left eigenvector of the time evolution operator with eigenvalue 1. If there is a unique steady state of the system then it is also the only left eigenvector with this property, a fact that we will use later. The spin operators act by left multiplication so in the superoperator formalism they are mapped to

$$\begin{aligned} \sigma^+_0 &\mapsto \sigma^+_0 \otimes \mathbb{1}_0 = (E^{13}_0 + E^{24}_0) , \\ \sigma^-_{\ell+1} &\mapsto \sigma^-_{\ell+1} \otimes \mathbb{1}_{\ell+1} = (E^{42}_{\ell+1} + E^{31}_{\ell+1}) . \end{aligned} \tag{6.9}$$

Since $\langle\langle \mathbb{1}_{\mathrm{cl}}|$ only contains states $\langle\langle 1|, \langle\langle 4|$ the only terms that survive in the trace are then

$$S^{+-}_{0,\ell+1} = \left[{}_0\langle\langle 3| \otimes \langle\langle \mathbb{1}_{[1,\ell]}| \otimes {}_{\ell+1}\langle\langle 2| \otimes \langle\langle \mathbb{1}_{[\ell+2,L-1]}|\right] |\rho(t)\rangle\rangle , \tag{6.10}$$

where we have introduced

$$\langle\langle \mathbb{1}_{[a,b]}| = \otimes_{j=a}^{b} \left[{}_j\langle\langle 1| + {}_j\langle\langle 4|\right] . \tag{6.11}$$

Eq. (6.10) shows that the correlation function depends only on the projection of $|\rho(t)\rangle$ on the two defect subspace described above. This means the correlation function can be written in terms of propagators defined on open chain segments:

$$G_{[a,b]} = \langle\langle \mathbb{1}_{[a,b]} | e^{\mathcal{L}_{[a,b]} t} | \rho_{[a,b]} \rangle\rangle. \tag{6.12}$$

In the ASEP case these propagators involve computing the overlap of a time evolved state in the finite length XXZ model (with diagonal boundary fields) with the state $\langle \mathbb{1}_{\rm cl}|$. The rest of this chapter will consider a different subspace of the full four-parameter model which reduces to free fermions, thus allowing the calculation of $G_{[a,b]}$ for some initial states, although its calculation for general states is still difficult .

6.3 Free fermions

6.3.1 "Classical" sector

As we noted earlier, the subspace of diagonal density matrices (5.16) is invariant under the dynamics. The "classical" part $\mathcal{L}_{\rm Diag}$ of the Lindbladian acts on this 2^L dimensional subspace of diagonal density matrices and can be expressed in terms of Pauli matrices τ_j defined by

$$\tau_j^z = E_j^{11} - E_j^{44} \ , \quad \tau_j^+ = E_j^{14} \ . \tag{6.13}$$

We find

$$\begin{aligned}
\mathcal{L}_{\rm Diag} = &\sum_j J_1 \tau_j^+ \tau_{j+1}^- + J_2 \tau_j^- \tau_{j+1}^+ + J_3 \tau_j^+ \tau_{j+1}^+ + J_4 \tau_j^- \tau_{j+1}^- \\
&- \frac{1}{4} \sum_j (J_1 - J_2 - J_3 + J_4) \mathbb{1}_j \tau_{j+1}^z + (-J_1 + J_2 - J_3 + J_4) \tau_j^z \mathbb{1}_{j+1} \\
&- \frac{1}{4} \sum_j (J_1 + J_2 - J_3 - J_4) \tau_j^z \tau_{j+1}^z + (J_1 + J_2 + J_3 + J_4) \mathbb{1}_j \mathbb{1}_{j+1}.
\end{aligned} \tag{6.14}$$

We now observe that under the constraint

$$J_1 + J_2 = J_3 + J_4, \tag{6.15}$$

the model (6.14) can be mapped to a free fermionic theory by means of a Jordan-Wigner transformation. In the periodic case we use that $\sum_j^L \mathbb{1}_j \tau_{j+1}^z - \tau_j^z \mathbb{1}_{j+1} = 0$ to obtain

$$\begin{aligned}
\mathcal{L}_{\rm Diag} = &\sum_{j=1}^{L-1} \left\{ J_1 c_{j+1}^\dagger c_j + J_2 c_j^\dagger c_{j+1} - J_3 c_j c_{j+1} - J_4 c_{j+1}^\dagger c_j^\dagger + (J_4 - J_3) c_j^\dagger c_j \right\} \\
&+ (-1)^{\hat{N}} \left(J_1 c_1^\dagger c_L + J_2 c_L^\dagger c_1 - J_3 c_1^\dagger c_L^\dagger - J_4 c_L c_1 \right) - J_4 L,
\end{aligned} \tag{6.16}$$

where $\hat{N}$ is the total fermion number operator. Since each term in the Lindbladian preserves fermion parity, the operator $(-1)^{\hat{N}}$ is conserved and we can work in definite parity sectors where it equals $+1$ (periodic, or Ramond, boundary conditions) or -1 (anti-periodic, or Neveu-Schwarz, boundary conditions). It will furthermore be convenient in the following to define

$$\begin{aligned} 2J_+ &= J_1 + J_2 = J_3 + J_4 \ , \\ 2J_- &= J_1 - J_2 \ , \\ 2\mu &= J_4 - J_3 \ , \end{aligned} \tag{6.17}$$

in terms of which the Lindbladian can be written (defining $c_{L+1} = (-1)^{\hat{N}} c_1$) as

$$\begin{aligned} \mathcal{L}_{\text{Diag}} = (J_+ + \mu)L + \sum_{j=1}^{L} \Big\{ &(J_+ + J_-) c_j^\dagger c_{j+1} + (J_+ - J_-) c_{j+1}^\dagger c_j \\ &- \left[(J_+ + \mu) c_j c_{j+1} + (J_+ - \mu) c_{j+1}^\dagger c_j^\dagger \right] + 2\mu c_j^\dagger c_j \Big\}. \end{aligned} \tag{6.18}$$

We largely focus on the special case $\mu = 0$ in the following but do discuss the steady state in the imbalanced case in Section 6.4.1. Crucially the constraints (6.17) enforce that $J_3 + J_4 \neq 0$, which takes us away from the ASEP limit $J_3 = J_4 = 0$, see Fig. 6.1. Hence the exact solutions presented below cannot be related to known results for the ASEP.

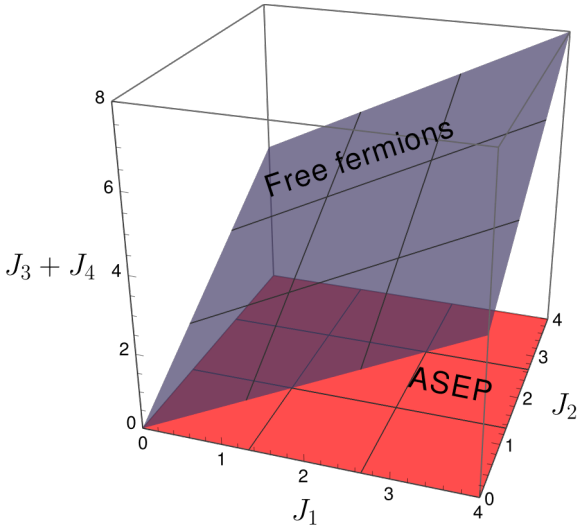

Figure 6.1: 3 dimensional cut of the four parameter space of the model, projecting out the μ direction. At fixed μ the space of free fermions is the plane denoted in blue, whilst the original ASEP model occupies the plane shown in red.

6.3.2 Two defect sector

We now consider the case where there are two defects that without loss of generality can be taken to be located at positions $\ell+1$ and L. Inspection of (6.2), (6.3), (6.4) shows that on the corresponding subspace the Lindbladian takes the form

$$\mathcal{L} = \begin{cases} \mathcal{L}_{[1,\ell]} + \mathcal{L}_{[\ell+2,L-1]} & \text{if } 0 < \ell < L-1 \ , \\ \mathcal{L}_{[2,L-1]} + c & \text{if } \ell = 0 \ , \\ \mathcal{L}_{[1,L-2]} + c & \text{if } \ell = L-2 \ , \end{cases} \tag{6.19}$$

where

$$\begin{aligned} \mathcal{L}_{[1,\ell]} = &\sum_{j=1}^{\ell-1} J_1 E_j^{14} E_{j+1}^{41} + J_2 E_j^{41} E_{j+1}^{14} + J_3 E_j^{14} E_{j+1}^{14} + J_4 E_j^{41} E_{j+1}^{41} \\ &- \sum_{j=1}^{\ell-1} J_1 E_j^{44} E_{j+1}^{11} + J_2 E_j^{11} E_{j+1}^{44} + J_3 E_j^{44} E_{j+1}^{44} + J_4 E_j^{11} E_{j+1}^{11} \\ &- \frac{1}{2}\Big([J_1+J_4] E_1^{11} + [J_2+J_3] E_1^{44} + [J_2+J_4] E_\ell^{11} + [J_1+J_3] E_\ell^{44} \Big), \end{aligned} \tag{6.20}$$

and the constant c is given by $c = -(J_1+J_2+J_3+J_4)/2 = -2J_+$ if one of the defects is of type 2 and one of type 3 and zero if the two defects are of the same type. Imposing the constraint (6.15) and carrying out a Jordan-Wigner transformation to spinless fermions we arrive at a free fermion chain with open boundary conditions

$$\begin{aligned} \mathcal{L}_{[1,\ell]} = &-J_+(\ell+1) - \mu \sum_{j=1}^{\ell} (2 c_j^\dagger c_j - 1) \\ &+ \sum_{j=1}^{\ell-1} \Big\{ J_1 c_{j+1}^\dagger c_j + J_2 c_j^\dagger c_{j+1} - J_3 c_j c_{j+1} - J_4 c_{j+1}^\dagger c_j^\dagger) \Big\}. \end{aligned} \tag{6.21}$$

6.3.3 q defect sector

The Lindbladian for the entire chain restricted to the invariant subspace with q defects at locations $\ell_1, \dots \ell_q$ is simply a sum of Lindbladians for the q disjoint finite chains obtained by removing the sites ℓ_j from the original chain

$$\mathcal{L} = \sum_{j=0}^{q} \mathcal{L}_{[\ell_j+1, \ell_{j+1}-1]} \tag{6.22}$$

Here $\ell_0 = \ell_q$ so that for instance in the 1 defect sector the corresponding Lindbladian $\mathcal{L}_{[\ell+1,\ell-1]}$ corresponds to the original ring with a single site removed. If the defects ℓ_j, ℓ_{j+1} are not immediate

neighbours then these are exactly as given in Eq (6.21). If there are two neighbouring defects then the only term in the full Lindbladian that acts on them is

$$\mathcal{L}_{[\ell,\ell+1]} = -2J_+(E^{22}_\ell E^{33}_{\ell+1} + E^{33}_\ell E^{22}_{\ell+1}) \tag{6.23}$$

which contributes $c = -2J_+$ if the neighbouring defects are different species and 0 if they are the same.

6.4 Dynamics in the classical subspace

As a first step to understanding this model, we solve it exactly in the diagonal subspace. We focus initially on the balanced ($\mu = 0$) case. Our system has periodic boundary conditions in terms of the original spins and (anti)-periodic boundary conditions for Jordan-Wigner fermions in sectors of (even) odd fermion parity. We therefore go to Fourier space

$$c(k_n) = \frac{1}{\sqrt{L}} \sum_j e^{ik_n j} c_j \ , \quad k_n = \frac{2\pi(n+\delta)}{L}. \tag{6.24}$$

where $\delta = 0, 1/2$ for states with odd or even fermion parity respectively. We then carry out a Bogoliubov transformation to diagonalise the Lindbladian

$$\begin{aligned} c^\dagger(k) &= \cos(k/2) b_{-k} - i \sin(k/2) b^\dagger_k \ , \\ c(k) &= i \sin(k/2) b_k + \cos(k/2) b^\dagger_{-k} \ . \end{aligned} \tag{6.25}$$

Despite the fact that $\mathcal{L}$ is non-Hermitian, this transformation is still unitary. We have

$$\mathcal{L}^{\text{Diag}} = \sum_k \epsilon(k) b^\dagger_k b_k \ , \tag{6.26}$$

where the non-Hermitian nature of the Lindbladian presents through the complex eigenvalues

$$\epsilon(k) = -2J_+ + 2iJ_- |\sin k| \ . \tag{6.27}$$

The time evolved operators are

$$b_k(t) = e^{-\mathcal{L}^{\text{Diag}} t} b_k e^{\mathcal{L}^{\text{Diag}} t} = e^{\epsilon(k) t} b_k \ . \tag{6.28}$$

We can now immediately conclude that the stationary state is unique and given simply by the Bogoliubov vacuum

$$b_k |0\rangle\rangle = 0. \tag{6.29}$$

This implies that $\langle\langle 0|\mathcal{L} = 0$ and ,exploiting uniqueness, we therefore have

$$\langle\langle \mathbb{1}_{\rm cl}| = \langle\langle 0| \ . \tag{6.30}$$

This is turn shows that the stationary state $|0\rangle\rangle$ is the completely mixed (infinite temperature) state, which we now demonstrate in more detail.

An important question is what operators of the original spin-chain problem can have finite expectation values within the defect-free subspace. To answer this we project the original Pauli matrices σ_j on to the diagonal subspace and write the result in terms of the τ_j operators. Defining projection operators by

$$P_j = E_j^{11} + E_j^{44}, \tag{6.31}$$

we have

$$\begin{aligned} &P_j \left[\sigma_j^z \otimes \mathbb{1}_j\right] P_j = P_j \left[E^{11} - E^{44} + E^{22} - E^{33}\right] P_j = \tau_j^z = 1 - 2n_j \ , \\ &P_j \left[\sigma_j^\alpha \otimes \mathbb{1}_j\right] P_j = 0 \ , \quad \alpha = x, y. \end{aligned} \tag{6.32}$$

This shows that the only physical operators with non-zero expectation in the stationary state are

$$\mathcal{O}_{j_1,\ldots,j_n} = n_{j_1} \ldots n_{j_n} \ . \tag{6.33}$$

The expectation value of $\mathcal{O}_{j_1,\ldots,j_n}$ can be obtained using Wick's theorem with the help of the elementary two-point functions

$$\begin{aligned} \langle\langle 0|c_j^\dagger c_{j+\ell}|0\rangle\rangle &= \frac{\delta_{\ell,0}}{2} + \frac{\delta_{\ell,1} + \delta_{\ell,-1}}{4}, \\ \langle\langle 0|c_j c_{j+\ell}|0\rangle\rangle &= \frac{\delta_{\ell,-1} - \delta_{\ell,1}}{4}, \\ \langle\langle 0|c_j^\dagger c_{j+\ell}^\dagger|0\rangle\rangle &= \frac{\delta_{\ell,1} - \delta_{\ell,-1}}{4}. \end{aligned} \tag{6.34}$$

Here we have replaced the state $\langle\langle \mathbb{1}_{\rm cl}|$ used to compute traces with the left Bogoliubov vacuum $\langle\langle 0|$ following the discussion above. As a result, we find that all such expectations factorise

$$\langle\langle 0|\mathcal{O}_{j_1,\ldots,j_n}|0\rangle\rangle = \langle\langle 0|n_{j_1}|0\rangle\rangle \ldots \langle\langle 0|n_{j_n}|0\rangle\rangle = \frac{1}{2^n} \ . \tag{6.35}$$

We now make use of the fact that a density operator is fully determined by the expectation values of a complete set of operators to conclude that in terms of the original problem the stationary state is the infinite temperature state

$$\rho_{\rm stat} = \frac{1}{2^L} \sum_{\sigma_1,\ldots,\sigma_L} |\sigma_1, \ldots, \sigma_L\rangle\langle\sigma_1, \ldots, \sigma_L|. \tag{6.36}$$

6.4.1 Imbalanced loss and gain

We now briefly discuss the nature of the steady state with imbalanced loss and gain. When $\mu \neq 0$ the Lindbladian in the defect-free sector is given by

$$\mathcal{L} = -(J_+ + \mu)L + \sum_{j=1}^{L} \left\{ J_1 c_{j+1}^\dagger c_j + J_2 c_j^\dagger c_{j+1} - J_3 c_j c_{j+1} - J_4 c_{j+1}^\dagger c_j^\dagger + 2\mu c_j^\dagger c_j \right\} \ , \tag{6.37}$$

where the appropriate Ramond or Neveu-Schwarz boundary conditions are assumed. We make use of the translational symmetry in the defect-free problem to Fourier transform this to give

$$\mathcal{L} = \text{const} + \sum_{k>0} \boldsymbol{c}_k^\dagger A_k(\mu) \boldsymbol{c}_k \ , \tag{6.38}$$

where $\boldsymbol{c}_k = \begin{pmatrix} c_k & c_{-k}^\dagger \end{pmatrix}^T$ the matrix $A_k(\mu)$ is 2×2 and non-Hermitian

$$A_k(\mu) = 2J_+ \begin{pmatrix} i\Delta \sin k + \cos k + \nu & -i(1+\nu)\sin k \\ +i(1-\nu)\sin k & i\Delta \sin k - \cos k - \nu \end{pmatrix} \ . \tag{6.39}$$

Here we have introduced the dimensionless parameters

$$\nu = \frac{\mu}{J_+} = \frac{J_4 - J_3}{J_4 + J_3} \quad \Delta = \frac{J_-}{J_+} = \frac{J_1 - J_2}{J_1 + J_2} \ , \tag{6.40}$$

The parameter ν satisfies $-1 \leq \nu \leq 1$ where the extreme case of $\nu = -1$ corresponds to only particle loss and $\nu = 1$ to only gain. The eigenvalues of $A_k(\mu)$ are

$$\epsilon_k^\pm(\mu) = 2J_+(i\Delta \sin k \pm (1 + \nu \cos k)) \ . \tag{6.41}$$

For $\nu \neq \pm 1$ these are always distinct. Degerate eigenvalues only occur for $\nu = 1, k = \pi$ and $\nu = -1, k = 0$ which both yield $A_k(\mu) = 0$. $A_k(\mu)$ is thus always diagonalisable, however it is not unitarily diagonalisable if $\mu \neq 0$. In this case we cannot perform a canonical transformation as for the balanced case.

We can however perform an almost canonical transformation by defining the matrix

$$S_k = \frac{1}{\sqrt{1 + \nu \cos k}} \begin{pmatrix} \sin \frac{k}{2} & -i(1+\nu)\cos \frac{k}{2} \\ -i \cos \frac{k}{2} & (1-\nu)\sin \frac{k}{2} \end{pmatrix}, \tag{6.42}$$

chosen such that $S^{-1}AS$ is diagonal and $\det(S) = 1$. We then define

$$\begin{pmatrix} b'_{+,k} & b_{-,k} \end{pmatrix} = \begin{pmatrix} c_k^\dagger & c_{-k} \end{pmatrix} S_k \ , \tag{6.43}$$

$$\begin{pmatrix} b_{+,k} \\ b'_{-,k} \end{pmatrix} = S_k^{-1} \begin{pmatrix} c_k \\ c_{-k}^\dagger \end{pmatrix} \ . \tag{6.44}$$

These are almost canonical fermions in that they satisfy the relations

$$\begin{aligned}\{b_{\sigma,k}, b_{\tau,q}\} &= \quad 0 = \{b'_{\sigma,k}, b'_{\tau,q}\} \ , \\ \{b'_{\sigma,k}, b_{\tau,q}\} &= \qquad \delta_{\sigma,\tau}\delta_{k,q} \ . \end{aligned} \tag{6.45}$$

We note that $b_{+,-k} = -b_{-,k}$ due to the choice of normalisation in the definition of S_k, which allows us to consistently define

$$\begin{aligned} b_k = \theta(k)b_{+,k} + \theta(-k)b_{-,k} &= \frac{\text{sgn } k}{\sqrt{1+\nu\cos k}}\Big((1-\nu)\sin\frac{k}{2}c_k + i(1+\nu)\cos\frac{k}{2}c^\dagger_{-k}\Big) \ , \\ b'_k = \theta(k)b'_{+,k} + \theta(-k)b'_{-,k} &= \frac{\text{sgn } k}{\sqrt{1+\nu\cos k}}\Big(-i\cos\frac{k}{2}c_{-k} + \sin\frac{k}{2}c^\dagger_k\Big) \ . \end{aligned} \tag{6.46}$$

This then allows us to write the Lindbladian in terms of the almost canonical fermion operators as

$$\mathcal{L} = \text{const} + \sum_k \epsilon^-_k b'_k b_k \ , \tag{6.47}$$

where we have used that $\epsilon^+_k = -\epsilon^-_{-k}$. The constant can be seen to be 0 by carefully keeping track of the constants discarded throughout this argument. We can now define left and right vacua by

$$\forall k: \quad \langle\langle L|b'_k = 0, \quad b_k|R\rangle\rangle = 0. \tag{6.48}$$

Since $\langle\langle L|\mathcal{L} = 0$ has only one solution, we conclude that

$$\langle\langle L| = \langle\langle \mathbb{1}_{\text{cl}}| = {}_0\langle\langle 0|\prod_{k>0}\Big(1 + i\cot\frac{k}{2}c_{-k}c_k\Big) \ , \tag{6.49}$$

where $|0\rangle\rangle_0$ is the fermionic vacuum state

$$c_j|0\rangle\rangle_0 = 0 \ . \tag{6.50}$$

The expression for $\langle\langle L|$ in terms of the original fermions in (6.49) is easily verified by acting with b'_k and using (6.46). The right eigenstate can be expressed as a squeezed state via

$$|R\rangle\rangle \quad = \tfrac{1}{\mathcal{N}}\textstyle\prod_{k>0}\Big(1 - i\frac{1+\nu}{1-\nu}\cot\frac{k}{2}c^\dagger_k c^\dagger_{-k}\Big)|0\rangle\rangle_0, \tag{6.51}$$

where $\mathcal{N}$ is chosen such that $\langle\langle L|R\rangle\rangle = 1$. This can be verified by acting with b_k and using (6.46).

As before we may consider the expectation values of all operators in the classical subspace - the operators σ^x, σ^y project to zero and all physical operators are given in terms of fermions by products of densities

$$\mathcal{O}_{j_1\ldots j_r} = n_{j_1}\ldots n_{j_r} \ . \tag{6.52}$$

The simplest such expectation value is

$$\langle\langle n_j \rangle\rangle_\infty = \lim_{t\to\infty} \mathrm{Tr}\big[n_j\ \rho(t)\big] = \langle\langle L|n_j|R\rangle\rangle. \tag{6.53}$$

As we have seen above, for $\mu = 0$ the steady state corresponds to a completely mixed state and we have $\langle\langle n_j \rangle\rangle_\infty = 1/2$. When $\mu \neq 0$ and assuming that the steady state is uncorrelated we have the following relation expressing the balance between particle gain and loss

$$J_3 \langle\langle n_j \rangle\rangle_\infty^2 = J_4[1 - \langle\langle n_j \rangle\rangle_\infty]^2. \tag{6.54}$$

If this relation holds we may solve for the particle density

$$\langle\langle n_j \rangle\rangle_\infty = \frac{1+\nu-\sqrt{1-\nu^2}}{2\nu}\ , \tag{6.55}$$

where we have used (6.40). We now verify (6.55) by direct calculation. Due to translation invariance $\langle\langle n_j \rangle\rangle_\infty$ is the same on each site and we can instead calculate the average occupation of the k modes

$$\frac{1}{L}\sum_k \langle\langle n_k \rangle\rangle = \frac{1}{L}\sum_k \frac{1+\nu}{1+\nu\cos k}\cos^2\frac{k}{2}\langle\langle L|b_{-k}b'_{-k}|R\rangle\rangle\ . \tag{6.56}$$

In the thermodynamic limit this turns into an integral

$$\begin{aligned}\langle\langle n_m \rangle\rangle_\infty &= \frac{(1+\nu)}{4\pi}\oint \frac{1+\cos k}{1+\nu\cos k}\,\mathrm{d}k \\ &= \frac{1+\nu-\sqrt{1-\nu^2}}{2\nu}\ .\end{aligned} \tag{6.57}$$

This indeed agrees with (6.55). We note that the stationary state (6.51) has a simple product form in terms of the spin states $|1\rangle\rangle$, $|4\rangle\rangle$ on which the spin operators τ_j^α act, *cf.* (6.13).

$$\begin{aligned}\langle\langle L| &= \otimes_{j=1}^L \left[{}_j\langle\langle 1| + {}_j\langle\langle 4|\right]\ , \\ |R\rangle\rangle &= \frac{1}{(1+\alpha)^L}\otimes_{j=1}^L \left[|1\rangle\rangle_j + \alpha|4\rangle\rangle_j\right]\ ,\end{aligned} \tag{6.58}$$

where

$$\alpha = \sqrt{\frac{1+\nu}{1-\nu}}\ . \tag{6.59}$$

6.4.2 Time dependence

We return to considering only the balanced case of $\mu = 0$ and now consider the time dependent problem. As we have seen above, on the diagonal subspace we have

$$P_j\left[\sigma_j^z \otimes \mathbb{1}\right] P_j = 1 - 2c_j^\dagger c_j = P_j\left[\mathbb{1}\otimes\tilde{\sigma}_j^z\right] P_j \tag{6.60}$$

This allows us to identify

$$|\sigma_1,\ldots,\sigma_L\rangle\langle\sigma_1,\ldots,\sigma_L| = c^\dagger_{j_1}\ldots c^\dagger_{j_n}|0\rangle\!\rangle_0 \ , \tag{6.61}$$

where j_k are the positions of down spins ordered such that $j_1 < j_2 \cdots < j_n$ and $|0\rangle_0$ is the fermionic vacuum, which is related to the Bogoliubov vacuum state by

$$|0\rangle\!\rangle_0 = 2^{-L}\prod_{k>0}\left[1 + i\cot(k/2)b^\dagger_k b^\dagger_{-k}\right]|0\rangle\!\rangle. \tag{6.62}$$

Using this and an initial density matrix in our subspace we can calculate

$$\langle\!\langle \mathbb{1}_{\rm cl}|n_{j_1}(t)\ldots n_{j_n}(t)|\rho(0)\rangle\!\rangle. \tag{6.63}$$

We can thus compute the expectations of any observables in this subspace at arbitrary times using free-fermion techniques. As an example we now compute $\langle\!\langle n_j(t)\rangle\!\rangle$ for a system initially in the classical Néel state

$$\rho(0) = |\uparrow\downarrow\uparrow\downarrow\ldots\rangle\langle\uparrow\downarrow\uparrow\downarrow\ldots|. \tag{6.64}$$

In terms of fermions this can be written as

$$|\rho_{\rm Néel}\rangle\!\rangle = \prod_{j=1}^{N/2} c^\dagger_{2j}|0\rangle\!\rangle_0. \tag{6.65}$$

In practice it will be more useful to work with the original fermion operators than the Bogoliubov ones. Solving their equations of motion gives

$$\begin{aligned} c^\dagger(k,t) &= f(k,t)c^\dagger(k) + g(k,t)c(-k) \ , \\ c(-k,t) &= -g(k,t)c^\dagger(k) + h(k,t)c(-k) \ , \end{aligned} \tag{6.66}$$

where

$$\begin{aligned} f(k,t) &= \cos^2(k/2)e^{\epsilon(-k)t} + \sin^2(k/2)e^{-\epsilon(k)t} \ , \\ g(k,t) &= \tfrac{i}{2}\sin(k)\left[e^{\epsilon(-k)t} - e^{-\epsilon(k)t}\right], \\ h(k,t) &= \cos^2(k/2)e^{-\epsilon(k)t} + \sin^2(k/2)e^{\epsilon(-k)t} \ . \end{aligned} \tag{6.67}$$

This then allows us to write

$$\begin{aligned} n_j(t) &= \frac{1}{L}\sum_{p,q} e^{ij(p-q)}c^\dagger(p,t)c(q,t) \\ &= \sum_m \left[\tilde{f}_{m-j}(t)c^\dagger_m + \tilde{g}_{m-j}(t)c_m\right]\sum_n\left[\tilde{h}_{n-j}(t)c_n - \tilde{g}_{n-j}(t)c^\dagger_n\right], \end{aligned} \tag{6.68}$$

where we have defined

$$\tilde{f}_n(t) = \frac{1}{L}\sum_p e^{-ipn} f(p,t) \ . \tag{6.69}$$

To calculate $\langle \mathbb{1}_{\rm cl}|n_j(t)|\rho_{\rm Néel}\rangle$ it is helpful to split the double sum in $n_j(t)$'s Fourier series into

$$\sum_{m,n} = \sum_{n \text{ even}} \delta_{mn} + \sum_{n \text{ odd}} \delta_{mn} + \sum_{\substack{n \text{ even} \\ m\neq n}} + \sum_{\substack{n \text{ odd} \\ m\neq n}} \ . \tag{6.70}$$

A straightforward calculation then gives

$$\begin{aligned}
\langle n_j(t)\rangle = & \sum_{n \text{ even}} \tilde{h}_{n-j}(t)\tilde{f}_{n-j}(t) - \sum_{n \text{ odd}} \tilde{g}^2_{n-j}(t) \\
& + \sum_{\substack{n<m \\ \text{even}}} \left[\tilde{g}_{n-j}(t)\tilde{h}_{m-j}(t) - \tilde{g}_{m-j}(t)\tilde{h}_{n-j}(t)\right](-1)^{\frac{n+m}{2}} \\
& - \sum_{\substack{n<m \\ \text{odd}}} \left[\tilde{g}_{n-j}(t)\tilde{f}_{m-j}(t) - \tilde{g}_{m-j}(t)\tilde{f}_{n-j}(t)\right](-1)^{\frac{n+m}{2}} \\
& + \sum_{\substack{m \text{ odd} \\ n \text{ even}}} \mathrm{sgn}(n-m)\tilde{h}_{n-j}(t)\tilde{f}_{m-j}(t)(-1)^{\frac{n+m+1}{2}} \\
& - \sum_{\substack{m \text{ even} \\ n \text{ odd}}} \mathrm{sgn}(n-m)(-1)^{\frac{n+m}{2}}\tilde{g}_{n-j}(t)\tilde{g}_{m-j}(t)(-1)^{\frac{n+m}{2}} \ .
\end{aligned} \tag{6.71}$$

The time evolution of the particle density (6.71) is shown in Fig. 6.2. As we are working at balanced particle creation and annihilation ($J_3 = J_4$), $\langle\langle n_j(t)\rangle\rangle$ relaxes to 1/2 at late times for all values of j.

Figure 6.2: Relaxation of $n_j(t)$ for odd/even sites towards the steady state value from an initial Néel state. Calculated for $J_+ = 1.0, J_- = 0.9$.

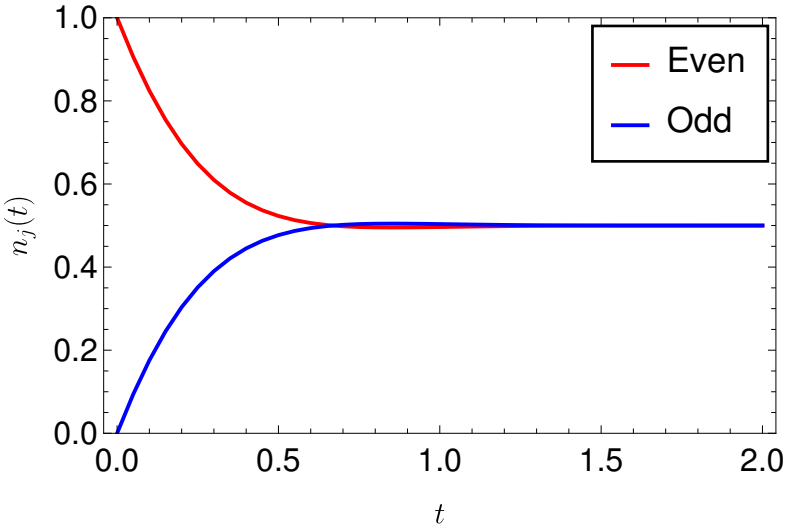

6.5 Two defect sector

We now turn to the defect sector problem. The Lindbladian in the sector with q defects can be written as a sum over quadratic open chain Lindbladians of the form

$$\mathcal{L}_M = -J_+(M+1) + \sum_{j=1}^{M-1} \Big\{ J_2 c_j^\dagger c_{j+1} + J_1 c_{j+1}^\dagger c_j - J_+ \Big(c_{j+1}^\dagger c_j^\dagger + c_j c_{j+1} \Big) \Big\}. \tag{6.72}$$

As these are not Hermitian, the standard analysis of Lieb, Schultz and Mattis [81] for diagonalising Hamiltonians quadratic in fermionic creation/annihilation operators does not apply. Instead, we switch to Majorana fermions [220]

$$a_{2j-1} = c_j + c_j^\dagger \ , \quad a_{2j} = i(c_j - c_j^\dagger). \tag{6.73}$$

and apply the analysis of [220] outlined in subsection 5.3.3. In terms of the Majorana operators, $\mathcal{L}_M$ is expressed as

$$\mathcal{L}_M = -(M+1)J_+ + \frac{1}{4}\boldsymbol{a}\cdot A \cdot \boldsymbol{a}, \tag{6.74}$$

In our case the $2M \times 2M$ anti-symmetric matrix A is block tridiagonal and given by

$$A = \begin{pmatrix} 0 & -C^{\mathrm{T}} & 0 & \dots & 0 \\ C & 0 & -C^{\mathrm{T}} & 0 & \vdots \\ 0 & C & 0 & \ddots & 0 \\ \vdots & 0 & \ddots & 0 & -C^{\mathrm{T}} \\ 0 & \dots & 0 & C & 0 \end{pmatrix} \ , \quad C = \begin{pmatrix} J_- & -2iJ_+ \\ 0 & J_- \end{pmatrix}. \tag{6.75}$$

We note, in addition to antisymmetry ensuring the eigenvalues of A occur in $\pm\beta_j$ pairs, that the complex eigenvalues also in complex conjugate pairs. This can be seen by noting that one obtains A^* from A by conjugating C by σ^z. In particular this means that if $A\boldsymbol{v} = \beta\boldsymbol{v}$ then also

$$A(\mathbb{1}_n \otimes \sigma^z)\boldsymbol{v}^* = \beta^*(\mathbb{1}_n \otimes \sigma^z)\boldsymbol{v}^* \ . \tag{6.76}$$

The eigenvalues of A are plotted in the complex plane for a small system size ($L = 12$) in Fig. 6.3. For the matrix A in our problem it is not a simple matter to find a closed form analytic expression for the spectrum, but we can gain insight into what the solutions look like by deforming our Lindbladian by adding a boundary term $J_-(n_1 - n_L)$. We stress that the resulting Lindbladian is unphysical.

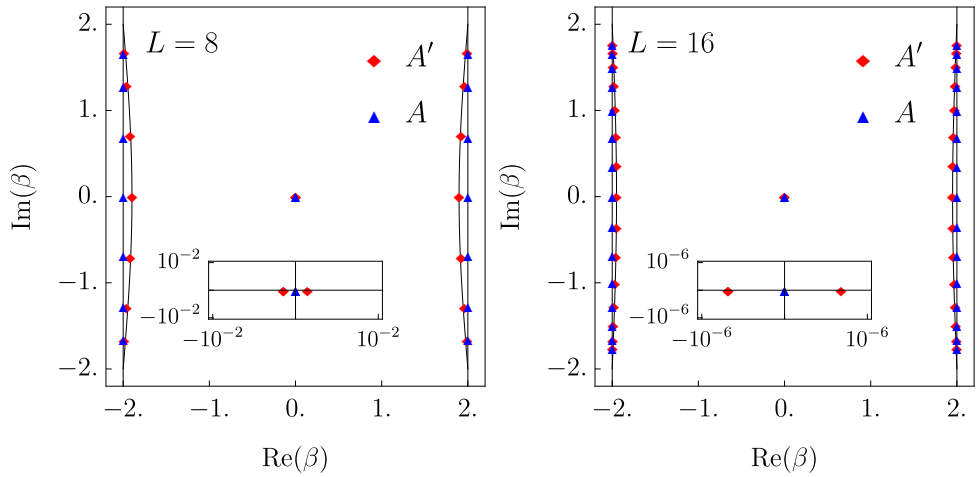

Figure 6.3: Eigenvalues of A' (red diamonds), A (blue triangles) for $L = 8$ (left) and $L = 16$ (right), $J_+ = 1.0, J_- = 0.9$. Inset shows a zoomed in view around the near-zero eigenvalues. Black curves through the red diamonds are guides to the eyes.

Then the matrix A is modified to A'

$$A' = \begin{pmatrix} B & -C^{\mathrm{T}} & 0 & \dots & 0 \\ C & 0 & -C^{\mathrm{T}} & 0 & \vdots \\ 0 & C & 0 & \ddots & 0 \\ \vdots & 0 & \ddots & 0 & -C^{\mathrm{T}} \\ 0 & \dots & 0 & C & -B \end{pmatrix}, \quad B = -iJ_- \begin{pmatrix} 0 & 1 \\ -1 & 0 \end{pmatrix}. \tag{6.77}$$

It is now straightforward to obtain the eigenvectors of the matrix A'. We make an ansatz $\boldsymbol{v} = (v_1, v_2, \dots)^{\mathrm{T}}$ where

$$v_n = z^n \begin{pmatrix} 1 \\ iz \end{pmatrix} + A_z (-1)^n z^{-n} \begin{pmatrix} 1 \\ -iz^{-1} \end{pmatrix}. \tag{6.78}$$

For this to be an eigenvector we require $A_z = z^2$ and z to satisfy

$$0 = (z^{2M} - (-1)^M)(\Delta z^2 - 2z - \Delta). \tag{6.79}$$

The associated eigenvalues are then given by

$$\beta_z = 2J_+ + J_-(z^{-1} - z). \tag{6.80}$$

This only gives rise to M linearly independent eigenvectors, all with non-negative eigenvalues. We however get the full spectrum using this ansatz by reflecting in the imaginary axis. Thus in this case we find that the positive real part eigenvalues consist of $M - 1$ values of z that are roots of unity

$z = e^{-ik}$ which recovers the periodic boundary condition result. There are also two eigenvalues that are exactly 0 — for our actual boundary conditions these become two small real eigenvalues $\pm\beta_0$ (they cannot be complex as the requirement that β^* is an eigenvalue would then give four nearly zero eigenvalues which is too many). We plot the eigenvalues in the complex plane in Figure 6.3 for both A and A' to highlight the impact of removing the boundary potential.

6.6 Transverse correlation function

We now turn to observables that involve defects. We focus on the particular example of an initial product state with ferromagnetic order along some direction in spin space

$$|\psi(0)\rangle = \left(1+|\alpha|^2\right)^{-L/2} \bigotimes_{m=1}^{L} \left[|\uparrow\rangle + \alpha|\downarrow\rangle\right]_m. \tag{6.81}$$

Our aim is to determine

$$S^{+-}_{0,\ell+1} = \mathrm{Tr}\left[\rho(t)\sigma^+_L\sigma^-_{\ell+1}\right]. \tag{6.82}$$

As we showed above in (6.10) this involves only the projection of $|\rho(t)\rangle\rangle$ onto the subspace with two defects

$$S^{+-}_{0,\ell+1} = \langle\langle \mathbb{1}_{\mathrm{cl}}|\sigma^+_0\sigma^-_{\ell+1}\Pi_{0,\ell+1}|\rho(t)\rangle\rangle = \langle\langle \mathbb{1}_{\mathrm{cl}}|\sigma^+_0\sigma^-_{\ell+1}e^{\mathcal{L}t}\Pi_{0,\ell+1}|\rho(0)\rangle\rangle, \tag{6.83}$$

where

$$\Pi_{0,\ell+1} = E^{33}_0 \otimes_{j=1}^{\ell} P_j E^{22}_{\ell+1} \otimes_{k=\ell+2}^{L-1} P_k\ . \tag{6.84}$$

Applying $\Pi_{0,\ell+1}$ to the initial density matrix $|\rho(0)\rangle\rangle = |\psi(0)\rangle\langle\psi(0)|$ gives

$$\Pi_{0,\ell+1}|\rho(0)\rangle\rangle = (1+|\alpha|^2)^{-L}|\alpha|^2|3\rangle\rangle_L \otimes |\rho_{[1,\ell]}\rangle\rangle \otimes |2\rangle\rangle_{\ell+1} \otimes |\rho_{[\ell+2,L-1]}\rangle\rangle, \tag{6.85}$$

where

$$|\rho_{[a,b]}\rangle\rangle \equiv \otimes_{m=a}^{m=b}\left[|1\rangle\rangle + |\alpha|^2|4\rangle\rangle\right]_m. \tag{6.86}$$

We now see that the transverse spin-spin correlation function reduces in this initial state to

$$\begin{aligned}\mathrm{Tr}\left[\rho(t)\sigma^+_1\sigma^-_\ell\right] &= \gamma(1+\gamma)^{-L}\tilde{G}_\ell(t)\tilde{G}_{L-\ell-2}(t)\\ \tilde{G}_N(t) &= \langle\langle \mathbb{1}_{[1,N]}|e^{\mathcal{L}_N t}|\rho_{[1,N]}\rangle\rangle.\end{aligned} \tag{6.87}$$

Here we have defined $\gamma = |\alpha|^2$ since all quantities depend only on γ and have separated out an overall factor $\gamma(1+\gamma)^N$ for convenience.

The propagators $\tilde{G}$ are defined on the finite chains discussed in Section 6.5 and can be expressed in terms of fermions as

$$\tilde{G}_N(t) = \quad {}_0\Big\langle\Big\langle 0\Big| \prod_{j=0}^{N-1} (1 + c_{N-j}) e^{\mathcal{L}_N t} \prod_{k=1}^{N} (1 + \gamma c_k^\dagger) \Big|0\Big\rangle\Big\rangle_0 \ . \tag{6.88}$$

As shown in B.1 we can rewrite this as

$$\tilde{G}_N(t) = {}_0\langle\langle 0|(1+X)e^Y e^{\mathcal{L}_N t} e^{\gamma^2 Y^\dagger}(1+\gamma X^\dagger)|0\rangle\rangle_0 \ , \tag{6.89}$$

where

$$X = \sum_{j=1}^{N} c_j \ , \quad Y = \sum_{n<m} c_m c_n \ . \tag{6.90}$$

Using fermion parity conservation this simplifies to

$$\tilde{G}_N(t) = {}_0\langle\langle 0|e^Y e^{\mathcal{L}_N t} e^{\gamma^2 Y^\dagger}|0\rangle\rangle_0 + \gamma \ {}_0\langle\langle 0|X e^Y e^{\mathcal{L}_N t} e^{\gamma^2 Y^\dagger} X^\dagger|0\rangle\rangle_0 \ . \tag{6.91}$$

The two terms above can be written in the form

$$\tilde{G}_N^{(\alpha)} = \mathrm{Tr}\left[\tilde{\rho}^{(\alpha)} e^Y e^{\mathcal{L}_N t} e^{\gamma^2 Y^\dagger}\right], \quad \alpha = 1, 2 \ , \tag{6.92}$$

where e^Y,$e^{\mathcal{L}_N t}$, $e^{\gamma^2 Y^\dagger}$ are all manifestly Gaussian as are the $\tilde{\rho}^{(\alpha)}$ since they are the ground states of the quadratic Hamiltonians

$$H_1 = \sum_{j=1}^{N} n_j \ , \quad H_2 = -n(p=0) + \sum_{p\neq 0} n(p) \ . \tag{6.93}$$

Thus (6.92) is now in the form of the trace of a product of Gaussian operators and can be evaluated. The procedure for this is given in detail in B.1. Here we outline the two key steps to the evaluation. The first step is to realise that since a product of Gaussian operators is Gaussian, we have

$$\rho^{(\alpha)} = \frac{e^{\gamma^2 Y^\dagger} \tilde{\rho}^{(\alpha)} e^Y}{Z^{(\alpha)}} = \frac{1}{\mathcal{Z}(W^{(\alpha)})} e^{a \cdot W^{(\alpha)} \cdot a/4}. \tag{6.94}$$

Here, $Z^{(\alpha)}$ and $\mathcal{Z}(W^{(\alpha)})$ are two different normalisation factors defined each defined such that $\mathrm{Tr}\rho^{(a)} = 1$. The $Z^{(a)}$ are calculated in B.2 and given by B.18. Writing the time evolution operator in the form

$$e^{\mathcal{L}_N t} = e^{\frac{1}{4} a \cdot A_N \cdot a} \ , \tag{6.95}$$

we then obtain the following expression for the propagators (*cf.* B.1)

$$\mathrm{Tr}\left[\rho^{(\alpha)} e^{\frac{1}{4} a \cdot A_N \cdot a}\right] = Z^{(\alpha)} \left(\frac{\det(e^{W^{(\alpha)}} e^{A_N} + e^{-A_N} e^{-W^{(\alpha)}} + 2)}{\det(e^{W^{(\alpha)}} + e^{-W^{(\alpha)}} + 2)} \right)^{1/4} \ . \tag{6.96}$$

The second step is to use the fact that a Gaussian is determined by its second moments to change from working with the density matrix $e^{a\cdot W\cdot a/4}$ itself to instead working with its correlation matrix $\Gamma_{mn} = \mathrm{Tr}[\rho a_n a_m] - \delta_{mn}$. We calculate the latter in B.2 by rewriting the trace as an inner product which can be evaluated in terms of Jordan-Wigner spins. Once Γ is found, W is obtained through $\Gamma = \tanh\frac{W}{2}$, or equivalently

$$e^W = (1-\Gamma)^{-1}(1+\Gamma). \tag{6.97}$$

This then leads to an apparent difficulty since the correlation matrices corresponding to $\rho^{(\alpha)}$ (which are fixed through our choice of initial condition) satisfy $(\Gamma^{(\alpha)})^2 = 1$, implying that they have only eigenvalues equal to ± 1 and the method set out above appears to break down. This issue can be dealt with by noting that

$$\Gamma^{(\alpha)} = \Pi_+^{(\alpha)} - \Pi_-^{(\alpha)} \ , \tag{6.98}$$

where $\Pi_\pm^{(\alpha)}$ are projectors onto the two N dimensional subspaces corresponding to eigenvalues 1 and -1 of $\Gamma^{(\alpha)}$ respectively. These would correspond to eigenvalues $\pm\infty$ in W, which we regulate by setting them equal to $\pm\Lambda$ and taking the limit $\Lambda \to \infty$ in the end of the calculation. That is, we put:

$$e^{W^{(\alpha)}/2} = e^{\Lambda/2}\Pi_+^{(\alpha)} + e^{-\Lambda/2}\Pi_-^{(\alpha)} \ , \tag{6.99}$$

which simplifies (6.96) to read

$$\mathrm{Tr}\left[\rho^{(\alpha)} e^{\frac{1}{4}a\cdot A_N t\cdot a}\right] = \left(\det(\Pi_+^{(\alpha)} e^{A_N t} + \Pi_-^{(\alpha)} e^{-A_N t})\right)^{1/4} \equiv d_N^{(\alpha)} \ . \tag{6.100}$$

This yields a simple expression for the propagator

$$\tilde{G}_N(t) = \quad e^{-J_+(N+1)t}\left[Z^{(1)} d_N^{(1)} + \gamma Z^{(2)} d_N^{(2)}\right]. \tag{6.101}$$

Substituting this into (6.87) then gives the transverse correlation function

$$\begin{aligned} S^{+-}_{0,\ell+1}(t) = \frac{\gamma}{(1+\gamma)^L} \quad & e^{-J_+ L t}\left(Z^{(1)} d_\ell^{(1)} + \gamma Z^{(2)} d_\ell^{(2)}\right) \\ & \times \left(Z^{(1)} d_{L-\ell-2}^{(1)} + \gamma Z^{(2)} d_{L-\ell-2}^{(2)}\right). \end{aligned} \tag{6.102}$$

The determinants $d_N^{(\alpha)}$ can now be straightforwardly computed numerically. In Fig. 6.4 we plot the transverse correlator at separation 2, $S^{+-}_{0,2}(t)$, as a function of time. We observe that the correlator decays quite quickly, and monotonically, from its initial value. We note however that this is the full correlation function and that more physically interesting is the connected correlator

$$S^{+-}_{\ell+1,C} = \mathrm{Tr}[S_0^+ S^-_{\ell+1}\rho(t)] - \mathrm{Tr}[S_0^+\rho(t)]\mathrm{Tr}[S^-_{\ell+1}\rho(t)]. \tag{6.103}$$

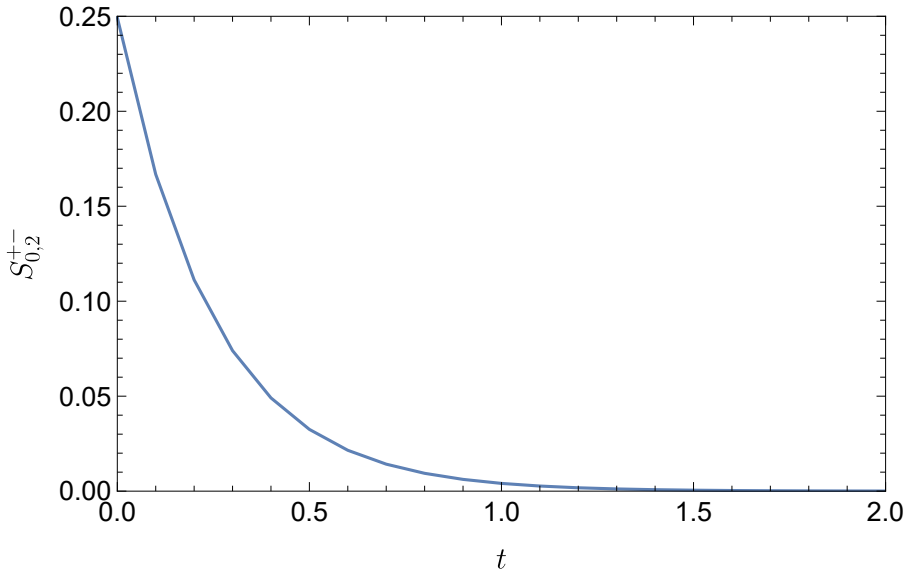

Figure 6.4: Full correlation function $S^{+-}_{0,2}(t)$ for $L = 30$ sites, $J_- = 0.9, J_+ = 1.0$ and $\gamma = 0.9$.

Here we have used the translation invariance of our initial condition to express the correlation function in terms of only the distance between the defects (note that this is $\ell + 1$ and not ℓ). The one point functions depend on the same propagators as the 2-point functions since

$$\mathrm{Tr}[S^+_0 \rho(t)] = \langle\langle \mathbb{1}_{\mathrm{cl}} | E^{13}_0 E^{24}_0 | \rho(t) \rangle\rangle = \frac{\alpha}{1+\gamma} G_{L-1}, \tag{6.104}$$

which gives

$$S^{+-}_{\ell+1,C} = \frac{\gamma}{(1+\gamma)^2} \left[G_\ell G_{L-\ell-2} - G^2_{L-1} \right]. \tag{6.105}$$

Where we have expressed this in terms of $G_N = (1+\gamma)^{-N} \tilde{G}_N$ as this is more natural. In particular, since our initial state was a product state we have $G_N(0) = 1$ for all N and so the connected correlation function is initially 0, indicating no correlations. We then expect that the Lindblad evolution will correlate neighbouring sites. This is countered by the fact that the steady state values of observables are all governed by the diagonal subspace values and so the connected correlations must go to zero at long times. In Figure 6.5(a), we plot the corresponding values for varying site separations and note an approximately exponential decrease with distance. In Figure 6.5(b), we plot the connected correlation between sites 1 and 3. We are able to observe that the dissipative dynamics does produce some correlations although they are small. Given that they also exponentially decay, the correlation generation would most likely not be visible had we started in an initially correlated

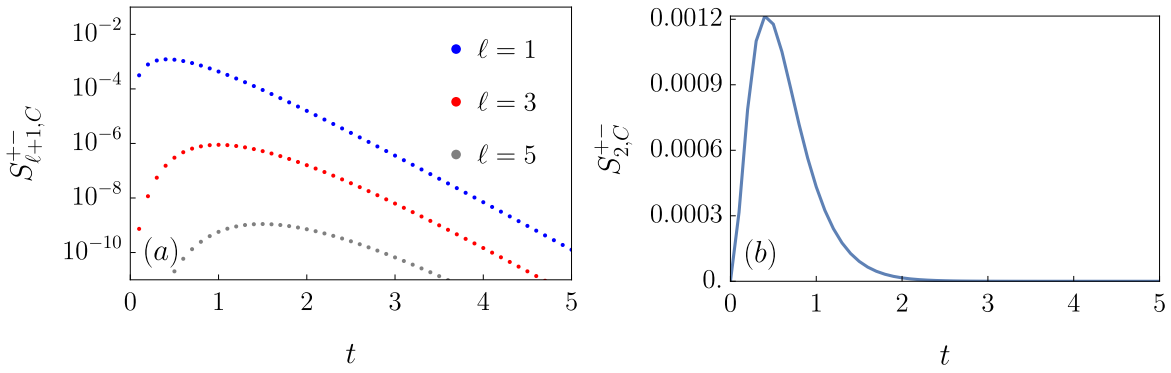

Figure 6.5: Connected correlation function for chain length $L = 30$ and $J_- = 0.9, J_+ - 1.0, \gamma = 0.9$. (a) Connected correlations decay exponentially with separation $d = \ell + 1$. (b) Connected correlation function for $\ell = 1$, showing correlation generation.

state. We perform these calculations for total chain lengths of $L = 30$, one might wonder if this is large enough to be essentially in the thermodynamic limit (in the sense that finite size effects are small enough to neglect). In fact, we find that the numerical values of the connected correlator vary very little as we increase L so long as it is larger than twice the separation $\ell + 1$. To show this we plot the connected correlator for $\ell = 3$ for $L = 8, 9, 10$ in Figure 6.6(a). Since the difference between the result for $9, 10$ is too small to be visible, we plot the residual (along with the corresponding residual for $L = 10, 11$) in Figure 6.6(b).

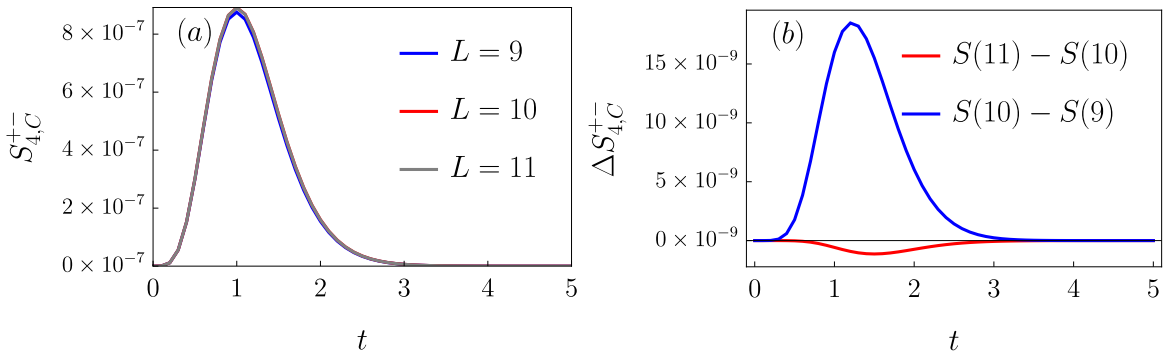

Figure 6.6: Finite size effects for $\ell = 3$. $J_- = 0.9, J_+ - 1.0, \gamma = 0.9$: (a) Correlation function for three different chain lengths $L = 8, 9, 10$. (b) Residuals between correlation function at $L = 9, 10$ and $L = 10, 11$.

6.7 Conclusions

We have considered a dissipative many particle quantum system described by a Lindblad equation that for particular initial conditions reduces to an asymmetric simple exclusion process with additional pair creation and annihilation terms. The Lindbladian exhibits operator-space fragmentation and for particular pair creation/annihilation rates the model can be mapped to free fermions. The model thus extends the class of solvable Lindblad systems and in particular provides a concrete example of a setting where operator-space fragmentation can be used to compute correlation functions exactly. We have restricted attention to initial product states in order to make calculations simpler as well as to allow us to see the generation of correlations through dissipation in our model. Even though the initial states we have considered here are quite simple the analysis is not straightforward. It would be interesting to attempt to generalise our analysis to the case of entangled initial states. It would also be interesting to study the time evolution of entanglement measures such as entanglement negativity within this model.

B

B.1 Fermion identities

B.1.1 Mixed parity fermion products

To arrive at Eq. (6.89) the key identity is that for any collection of mutually anti-commuting variables $\{\zeta_i\}_{i=1}^N$ the following holds

$$\prod_{i=1}^{N}(1+\zeta_i) = \left(1+\sum_{i=1}^{N}\zeta_i\right)\prod_{1\leq j<k\leq N}(1+\zeta_j\zeta_k). \tag{B.1}$$

This identity immediately provides a convenient decomposition into even and odd fermion parity parts. It can be proven by focusing on the odd and even components and using induction. To do so note that the even terms have the form

$$\mathbf{E}\left[\prod_{i=1}^{N}(1+\zeta_i)\right] = \sum_{\substack{k \text{ even}\\ k\leq N}}\left(\sum_{1\leq i_1<\cdots<i_k\leq N}\zeta_{i_1}\ldots\zeta_{i_k}\right). \tag{B.2}$$

The counterpart for the odd terms is completely analogous. When multiplying this by $\sum_{j=1}^{N}\zeta_j$ the result will be a sum of $(N-k)\binom{N}{k}$ non-zero terms, each of which contain $k+1$ distinct ζ's. Moreover, in each term k of the ζ's will be in ascending order by construction, with the final one appearing in each possible position. Thus $k/2$ pairs will cancel and the remaining $\frac{(N-k)}{k+1}\binom{N}{k} = (N-k-1)\binom{N}{k+1}$ terms are precisely those in the corresponding expansion of the odd part. We thus need only prove

by induction the statement about the even terms

$$\sum_{k=2m}\left(\sum_{1\le i_1<\cdots<i_k\le N}\zeta_{i_1}\dots\zeta_{i_k}\right)=\prod_{1\le j<k\le N}(1+\zeta_j\zeta_k)\ . \tag{B.3}$$

To this end we assume the induction hypothesis up to $N-1$ and notice that for N sites we can rewrite the product of quadratic terms as

$$\prod_{i<j}^{N-1}(1+\zeta_i\zeta_j)\prod_{\omega=1}^{N-1}(1+\zeta_\omega\zeta_N)=\prod_{i<j}^{N-1}(1+\zeta_i\zeta_j)(1+\sum_{\omega=1}^{N-1}\zeta_\omega\zeta_N). \tag{B.4}$$

We then use the induction hypothesis on the first factor on the right hand side. When multiplied by the second factor two things can happen: (i) it gets multiplied by 1, thus generating all possible even terms not including ζ_N, (ii) it gets multiplied by $(\sum_{\omega=1}^{N-1}\zeta_\omega)\zeta_N$. For the latter note that multiplying by $\sum\zeta_\omega$ generates all possible odd expressions without ζ_N and multiplying by ζ_N at the end then gives the desired result. Along with the observation that the base case of $N=0$ is trivial this completes the proof of (B.1).

In the context of Eq. (6.89) we set $\zeta_i=\gamma c_i^\dagger$ so that we have

$$\prod_{k=1}^{N}(1+\gamma c_k^\dagger)=\prod_{1\le m<n\le N}(1+\gamma^2c_m^\dagger c_n^\dagger)(1+\gamma\sum_{k=1}^{N}c_k^\dagger)\ . \tag{B.5}$$

This is the desired simplification upon defining X,Y in the main text and applying the standard result that $e^{Y^\dagger}=\prod_{m<n}(1+c_m^\dagger c_n^\dagger)$ where $Y^\dagger=\sum_{m<n}c_m^\dagger c_n^\dagger$.

B.1.2 Trace of Gaussian operators

The main result required in the derivation of (6.96) is the identity [279]

$$\mathrm{Tr}[e^{a\cdot W\cdot a/4}]=\sqrt{\det(e^{W/2}+e^{-W/2})}. \tag{B.6}$$

Here a_j are Majorana fermions and W an antisymmetric matrix. We note that (B.6) is easy to establish if W is diagonalisable. In that case its eigenvalues come in pairs $\pm\beta_k$ and the left hand side becomes

$$\mathrm{Tr}[e^{\sum_k\beta_k(\frac{1}{2}-n_k)}]=\prod_{\mathrm{Re}\beta_k>0}\left[e^{\beta_k/2}+e^{-\beta_k/2}\right]. \tag{B.7}$$

Because W is anti-symmetric, its eigenvalues come in $\pm$ pairs and so the determinant contains exactly two copies of each factor on the right hand side of (B.7). This then establishes (B.6). If W is not diagonalisable then we define

$$f[W]=\mathrm{Tr}[e^{a\cdot W\cdot a/4}]-\sqrt{\det(e^{W/2}+e^{-W/2})}. \tag{B.8}$$

Since $f[W] = 0$ for all diagonalisable matrices (which is a dense subset of all matrices) and f is a continuous function, we have $f = 0$ identically.

We also make heavy use of a result following from the Baker-Campbell-Hausdorff formula, namely that for Majorana fermions a_j normalised such that $\{a_i, a_j\} = 2\delta_{ij}$

$$e^{\frac{1}{4}a\cdot W_1\cdot a}e^{\frac{1}{4}a\cdot W_2\cdot a} = e^{\frac{1}{4}a\cdot W_3\cdot a} \ , \tag{B.9}$$

where $e^{W_3} = e^{W_1}e^{W_2}$. Along with (B.6) this allows us to write

$$\begin{aligned} \mathrm{Tr}[e^{\frac{1}{4}a\cdot W_1\cdot a}e^{\frac{1}{4}a\cdot W_2\cdot a}] \quad &= \sqrt{\det(e^{W_3/2} + e^{-W_3/2})} \\ &= \left[\det(e^{W_3} + e^{-W_3} + 2)\right]^{1/4} \ . \end{aligned} \tag{B.10}$$

B.2 Correlation matrices

The two correlation matrices we need are given by the inner products

$$\Gamma^{(1)}_{mn} + \delta_{mn} = \frac{\langle\langle 0|e^Y a_n a_m e^{\gamma^2 Y^\dagger}|0\rangle\rangle}{\langle\langle 0|e^Y e^{\gamma^2 Y^\dagger}|0\rangle\rangle} \ , \tag{B.11}$$

$$\Gamma^{(2)}_{mn} + \delta_{mn} = \frac{\langle\langle 0|Xe^Y a_n a_m e^{\gamma^2 Y^\dagger}X^\dagger|0\rangle\rangle}{\langle\langle 0|Xe^Y e^{\gamma^2 Y^\dagger}X^\dagger|0\rangle\rangle}. \tag{B.12}$$

The denominators are equal to the normalisation factors $Z^{(1)}, Z^{(2)}$ that appear in the final result (6.102). Both numerators and denominators can be found by making use of (B.1) in the form

$$\prod_{j=1}^{N}\left(1+\gamma c_k^\dagger\right) + \prod_{j=1}^{N}\left(1-\gamma c_k^\dagger\right) = 2e^{\gamma^2 Y^\dagger} \ , \tag{B.13}$$

$$\prod_{j=1}^{N}\left(1+\gamma c_k^\dagger\right) - \prod_{j=1}^{N}\left(1-\gamma c_k^\dagger\right) = 2\gamma X e^{\gamma^2 Y^\dagger} \ . \tag{B.14}$$

Using (B.14) we can express the correlation matrices as

$$\Gamma^{(1)}_{mn} + \delta_{mn} = \tfrac{g^{++}_{mn}+g^{+-}_{mn}}{Z^{++}+Z^{+-}} \ , \quad \Gamma^{(2)}_{mn} + \delta_{mn} = \tfrac{g^{++}_{mn}-g^{+-}_{mn}}{Z^{++}-Z^{+-}} \ , \tag{B.15}$$

where we have defined

$$g^{\sigma\sigma'}_{mn} = \langle\langle 0|\textstyle\prod_{j=0}^{N-1}(1+\sigma c_{N-j})a_n a_m \prod_{k=1}^{N}(1+\sigma'\gamma c_k^\dagger)|0\rangle\rangle \ , \tag{B.16}$$

$$Z^{\sigma\sigma'} = \langle\langle 0|\textstyle\prod_{j=0}^{N-1}(1+\sigma c_{N-j}) \prod_{k=1}^{N}(1+\sigma'\gamma c_k^\dagger)|0\rangle\rangle \ . \tag{B.17}$$

A simple calculation then gives that $g^{++}_{mn} = g^{--}_{mn}$ and $g^{+-}_{mn} = g^{-+}_{mn}$ and likewise for $Z^{\sigma\sigma'}$. Explicit expressions for $g^{\sigma\sigma'}_{mn}$ and $Z^{\sigma\sigma'}$ are readily obtained by reverting to their respective representations in terms of spins (i.e. undoing the Jordan-Wigner transformation). We find

$$\begin{aligned} Z^{(1)} &= \frac{1}{2}\left[(1+\gamma)^N + (1-\gamma)^N\right] \ , \\ Z^{(2)} &= \frac{1}{2}\left[(1+\gamma)^N - (1-\gamma)^N\right] , \end{aligned} \tag{B.18}$$

and $\Gamma^{(\alpha)}$ are anti-symmetric $2N \times 2N$ block matrices of the form

$$\Gamma^{(\alpha)} = \frac{1}{x^N - (-1)^\alpha y^N} \begin{pmatrix} \Gamma^{(\alpha)}_0 & -(\Gamma^{(\alpha)}_1)^{\mathrm{T}} & \dots & -(\Gamma^{(\alpha)}_{N-1})^{\mathrm{T}} \\ \Gamma^{(\alpha)}_1 & \Gamma^{(\alpha)}_0 & \dots & \vdots \\ \vdots & \dots & \dots & \vdots \\ \Gamma^{(\alpha)}_{N-1} & \dots & \dots & \Gamma^{(\alpha)}_0 \end{pmatrix} , \quad \alpha = 1, 2. \tag{B.19}$$

The 2×2 blocks are given by

$$\begin{aligned} \Gamma^{(\alpha)}_0 &= \begin{pmatrix} 0 & i(f_{N-1} \pm f_1) \\ -i(f_{N-1} - (-1)^\alpha f_1) & 0 \end{pmatrix} , \\ \Gamma^{(\alpha)}_a &= \begin{pmatrix} f_{N-a} - (-1)^\alpha f_a & -i(f_{a-1} - (-1)^\alpha f_{N-a+1}) \\ -i(f_{a+1} - (-1)^\alpha f_{N-a-1}) & -(f_{N-a} - (-1)^\alpha f_a) \end{pmatrix} , \end{aligned} \tag{B.20}$$

where we have defined

$$x = 1 + \gamma \ , \quad y = 1 - \gamma \ , \quad f_a = x^a y^{N-a} \ . \tag{B.21}$$

One can verify that $(\Gamma^{(\alpha)})^2 = \mathbb{1}$. Since $\Gamma^{(\alpha)}$ is anti-symmetric it therefore has equal numbers of eigenvalues ± 1, which we used in the main text. The eigenvectors depend on x, y and we find these numerically to determine the correct projectors to use.

Forgive these wild and wandering cries,
Confusions of a wasted youth;
Forgive them where they fail in truth,
And in thy wisdom make me wise.

In Memoriam A.H.H.
Alfred, Lord Tennyson

7 Conclusions

In this thesis, I have tried to present a coherent picture of what happens following a quantum quench in one dimensional systems. In Part A I have focused on systems that are well isolated from their environments and whose time evolution is therefore described by the Schrödinger equation. Part B then concentrated on the interaction with the environment and presented an exact solution for the dynamics of a toy model of nonequilibrium open dynamics described by a particular Lindblad equation.

Beginning with Part A, I have presented experimental motivation to consider nonequilibrium dynamics of closed quantum systems, which are directly measurable in a range of experimental platforms including ultracold neutral atoms, trapped ions and superconducting quantum circuits. I then offered a brief overview of some theoretical background needed to make sense of Chapters 3 and 4. In particular, Chapter 2 gave a detailed discussion of the solution of the transverse field Ising model using the Jordan-Wigner transformation, since it serves as a point of departure for the analysis in both chapters.

The research content of Part A began with constructing a mean-field approximation for quenches in the anisotropic next-nearest neighbour Ising model, an extension of the solution to the TFIM. This approximation is sufficiently accurate to answer the important physical question of how (equilibrium) quantum critical points impact the nonequilibrium dynamics. By building on earlier numerical studies, Chapter 3 established that such a mean-field approximation can capture signatures of quantum

criticality and give insights into the underlying physics. In particular, the mean-field theory allows a convenient tool to calculate long-ranged correlation functions and thereby show that the strong response of the system to quenching near the critical point to be a result of the large growth of the correlation length following such a quench. Moreover, the mean-field theory provides a simple criterion for analysing whether a quench is able to access the ground state properties of the quantum critical point by suggesting a cutoff for the post-quench temperature. An unexpected outcome of this analysis was the discovery of long lived oscillations in local observables following quenches in the ferromagnetic phase of the ANNNI. These are a result of interactions, being absent in the TFIM and caused by the presence of a bound state in the low-energy spectrum of the ANNNI not present in the TFIM. Despite the fact that mean-field theory is a quadratic approximation, this interaction effect is captured in the equal time correlation functions. However, when investigating non-equal time correlation functions there was no evidence that the mean-field theory was able to reproduce the expected poles in the linear response functions, for which a higher order theory is needed.

The peculiar oscillations in the ANNNI raised a question that Chapter 4 then attempts to answer: do the oscillations decay at late times? The conventional wisdom is that chaotic systems such as the ANNNI model should have all local observables relax to stationary values at late times as a result of the eigenstate thermalisation hypothesis. However, at the mean-field level there was no indication of the oscillations damping in the ANNNI up to a time much longer than a simplistic quasiparticle scattering argument suggests. The appropriate tool for going beyond mean-field theory in these short ranged lattice fermion models is the second Born approximation. This has currently only been formulated for theories with a $\mathsf{U}(1)$ particle number conservation. Chapter 4, therefore, primarily considers a simpler model with $\mathsf{U}(1)$ symmetry, that possesses such oscillations. At mean-field level this model has persistent oscillations which may be used to perform 'quench spectroscopy' to determine the bound state mass. At the next order beyond mean-field (provided by the Second Born approximation) there is an exponential decay; higher orders likely provide a small modification of the lifetime. Still, it would be worthwhile to formulate a $\mathsf{U}(1)$ violating second Born theory and apply it to the ANNNI. Moreover, a topic of much interest has been similar oscillations for quenches in the ferromagnetic phase of the tilted field Ising model; in that case the interaction involves large numbers of particles so BBGKY hierarchy based methods are inappropriate. Nonetheless, the results of Chapter 4 should be treated as proof of principle that such oscillations need not be infinitely long lived and in the absence of a compelling reason to believe the interaction in the tilted field Ising

model would produce differing physics it may be considered as evidence that the oscillations in that case likely also decay at late times.

Part B continued the discussion of quantum quenches by introducing open quantum systems and advocating for the study of exactly solvable examples as tools to build our understanding of this relatively less explored arena. In Chapter 5 I introduced the Lindblad formalism, which applies to Markovian systems and explained how the superoperator formalism allows the Lindblad equation to be recast as a non-Hermitian Schrödinger equation. This mapping allows several exact solutions to be obtained by comparing the result to known exactly solvable Hermitian systems. In particular, the Lindblad superoperator for the quantum asymmetric simple exclusion process is known to take the form of a direct sum of a large number of superoperators which can be related to the transition matrix of the classical ASEP, and are therefore integrable. Having reviewed this construction in Chapter 5, Chapter 6 considered a generalisation of the model which admits a free fermion description on a subset of parameters. Using the appropriate generalisation of the free fermion techniques outlined in Chapter 2 to the non-Hermitian case, Chapter 6 found an exact solution for the dynamics following a quench from an initial product state. It would be of interest to extend the range of initial states which can be handled, and equation of motion methods might be useful for this, whilst allowing the generalisation to weakly interacting quenches through means of methods such as the self-consistent time-dependant mean-field theory and second Born approximations used in Part A.

Bibliography

[1] J. H. Robertson and F. H. L. Essler, Exact solution of a quantum asymmetric exclusion process with particle creation and annihilation *J. Stat. Mech.* **2021** no. 10, (Oct, 2021) 103102.

[2] J. H. Robertson, R. Senese, and F. H. L. Essler, A simple theory for quantum quenches in the ANNNI model *SciPost Phys.* **15** (2023) 032.

[3] J. H. Robertson, R. Senese, and F. H. L. Essler, Decay of long-lived oscillations after quantum quenches in gapped interacting quantum systems *Phys. Rev. A* **109** (Mar, 2024) 032208.

[4] J. Berges, S. Borsányi, and C. Wetterich, Prethermalization *Phys. Rev. Lett.* **93** (Sep, 2004) 142002.

[5] M. Moeckel and S. Kehrein, Interaction Quench in the Hubbard Model *Phys. Rev. Lett.* **100** (May, 2008) 175702.

[6] M. Kollar, F. A. Wolf, and M. Eckstein, Generalized Gibbs ensemble prediction of prethermalization plateaus and their relation to nonthermal steady states in integrable systems *Phys. Rev. B* **84** (Aug, 2011) 054304.

[7] T. Langen, R. Geiger, and J. Schmiedmayer, Ultracold atoms out of equilibrium *Annual Review of Condensed Matter Physics* **6** no. 1, (2015) 201–217.

[8] F. Schäfer, T. Fukuhara, S. Sugawa, Y. Takasu, and Y. Takahashi, Tools for quantum simulation with ultracold atoms in optical lattices *Nature Reviews Physics* **2** no. 8, (Aug, 2020) 411–425.

[9] W. S. Bakr, J. I. Gillen, A. Peng, S. Fölling, and M. Greiner, A quantum gas microscope for detecting single atoms in a Hubbard-regime optical lattice *Nature* **462** no. 7269, (Nov, 2009) 74–77.

[10] L. W. Cheuk, M. A. Nichols, M. Okan, T. Gersdorf, V. V. Ramasesh, W. S. Bakr, T. Lompe, and M. W. Zwierlein, Quantum-gas microscope for fermionic atoms *Phys. Rev. Lett.* **114** (May, 2015) 193001.

[11] S. Inouye, M. R. Andrews, J. Stenger, H.-J. Miesner, D. M. Stamper-Kurn, and W. Ketterle, Observation of Feshbach resonances in a Bose–Einstein condensate *Nature* **392** no. 6672, (Mar, 1998) 151–154.

[12] C. Chin, R. Grimm, P. Julienne, and E. Tiesinga, Feshbach resonances in ultracold gases *Rev. Mod. Phys.* **82** (Apr, 2010) 1225–1286.

[13] Y.-J. Lin, R. L. Compton, K. Jiménez-García, J. V. Porto, and I. B. Spielman, Synthetic magnetic fields for ultracold neutral atoms *Nature* **462** no. 7273, (Dec, 2009) 628–632.

[14] R. Onofrio, Physics of our Days: Cooling and thermometry of atomic Fermi gases *Physics-Uspekhi* **59** no. 11, (Nov, 2016) 1129.

[15] E. Altman, *et al.*, Quantum simulators: architectures and opportunities *PRX Quantum* **2** (Feb, 2021) 017003.

[16] H. Bernien, *et al.*, Probing many-body dynamics on a 51-atom quantum simulator *Nature* **551** no. 7682, (Nov, 2017) 579–584.

[17] A. Houck, H. Tureci, and J. Koch, On-chip quantum simulation with superconducting circuits *Nature Physics* **8** (04, 2012) 292–299.

[18] F. Arute, *et al.*, Quantum supremacy using a programmable superconducting processor *Nature* **574** no. 7779, (Oct, 2019) 505–510.

[19] J. Zhang, G. Pagano, P. W. Hess, A. Kyprianidis, P. Becker, H. Kaplan, A. V. Gorshkov, Z.-X. Gong, and C. Monroe, Observation of a many-body dynamical phase transition with a 53-qubit quantum simulator *Nature* **551** no. 7682, (Nov, 2017) 601–604.

[20] J. Preskill, Quantum computing in the NISQ era and beyond *Quantum* **2** (Aug., 2018) 79.

[21] J. M. Deutsch, Quantum statistical mechanics in a closed system *Phys. Rev. A* **43** (Feb, 1991) 2046–2049.

[22] M. Srednicki, Chaos and quantum thermalization *Phys. Rev. E* **50** (Aug, 1994) 888–901.

[23] L. D'Alessio, Y. Kafri, A. Polkovnikov, and M. Rigol, From quantum chaos and eigenstate thermalization to statistical mechanics and thermodynamics *Advances in Physics* **65** no. 3, (May, 2016) 239–362.

[24] M. Rigol, V. Dunjko, and M. Olshanii, Thermalization and its mechanism for generic isolated quantum systems *Nature* **452** no. 7189, (Apr, 2008) 854–858.

[25] H. Kim, T. N. Ikeda, and D. A. Huse, Testing whether all eigenstates obey the eigenstate thermalization hypothesis *Phys. Rev. E* **90** (Nov, 2014) 052105.

[26] R. Steinigeweg, A. Khodja, H. Niemeyer, C. Gogolin, and J. Gemmer, Pushing the limits of the eigenstate thermalization hypothesis towards mesoscopic quantum systems *Phys. Rev. Lett.* **112** (Apr, 2014) 130403.

[27] K. R. Fratus and M. Srednicki, Eigenstate thermalization in systems with spontaneously broken symmetry *Phys. Rev. E* **92** (Oct, 2015) 040103.

[28] F. H. L. Essler and A. J. J. M. de Klerk, Statistics of matrix elements of local operators in integrable models 2023.

[29] E. H. Lieb and D. W. Robinson, The finite group velocity of quantum spin systems *Communications in Mathematical Physics* **28** (Sep, 1972) "251–257".

[30] S. Bravyi, M. B. Hastings, and F. Verstraete, Lieb-Robinson bounds and the generation of correlations and topological quantum order *Phys. Rev. Lett.* **97** (Jul, 2006) 050401.

[31] H. Rieger and F. Iglói, Semiclassical theory for quantum quenches in finite transverse Ising chains *Phys. Rev. B* **84** (Oct, 2011) 165117.

[32] B. Blass, H. Rieger, and F. Iglói, Quantum relaxation and finite-size effects in the XY chain in a transverse field after global quenches *Europhysics Letters* **99** no. 3, (Aug, 2012) 30004.

[33] P. Calabrese and J. Cardy, Evolution of entanglement entropy in one-dimensional systems *Journal of Statistical Mechanics: Theory and Experiment* **2005** no. 04, (Apr, 2005) P04010.

[34] P. Calabrese and J. Cardy, Time dependence of correlation functions following a quantum quench *Phys. Rev. Lett.* **96** (Apr, 2006) 136801.

[35] P. Calabrese and J. Cardy, Quantum quenches in extended systems *Journal of Statistical Mechanics: Theory and Experiment* **2007** no. 06, (Jun, 2007) P06008.

[36] P. Calabrese and J. Cardy, Quantum quenches in 1+ 1 dimensional conformal field theories *Journal of Statistical Mechanics: Theory and Experiment* **2016** no. 6, (2016) 064003.

[37] L. Bonnes, F. H. L. Essler, and A. M. Läuchli, "Light-cone" dynamics after quantum quenches in spin chains *Phys. Rev. Lett.* **113** (Oct, 2014) 187203.

[38] M. B. Hastings, An area law for one-dimensional quantum systems *Journal of Statistical Mechanics: Theory and Experiment* **2007** no. 08, (Aug., 2007) P08024–P08024.

[39] J. Eisert, M. Cramer, and M. B. Plenio, Colloquium: Area laws for the entanglement entropy *Rev. Mod. Phys.* **82** (Feb, 2010) 277–306.

[40] F. G. S. L. Brandão and M. Cramer, Entanglement area law from specific heat capacity *Phys. Rev. B* **92** (Sep, 2015) 115134.

[41] A. Anshu, I. Arad, and D. Gosset, An area law for 2d frustration-free spin systems in *Proceedings of the 54th Annual ACM SIGACT Symposium on Theory of Computing*, STOC '22. ACM, June, 2022.

[42] A. Anshu, A. W. Harrow, and M. Soleimanifar, Entanglement spread area law in gapped ground states *Nature Physics* **18** no. 11, (Nov, 2022) 1362–1366.

[43] A. Nahum, J. Ruhman, S. Vijay, and J. Haah, Quantum entanglement growth under random unitary dynamics *Phys. Rev. X* **7** (Jul, 2017) 031016.

[44] T. Zhou and A. Nahum, Entanglement membrane in chaotic many-body systems *Phys. Rev. X* **10** (Sep, 2020) 031066.

[45] M. Rigol, A. Muramatsu, and M. Olshanii, Hard-core bosons on optical superlattices: Dynamics and relaxation in the superfluid and insulating regimes *Phys. Rev. A* **74** (Nov, 2006) 053616.

[46] M. Rigol, V. Dunjko, V. Yurovsky, and M. Olshanii, Relaxation in a completely integrable many-body quantum system: an ab initio study of the dynamics of the highly excited states of 1D lattice hard-core bosons *Phys. Rev. Lett.* **98** (Feb, 2007) 050405.

[47] M. Fagotti and F. H. L. Essler, Reduced density matrix after a quantum quench *Phys. Rev. B* **87** (Jun, 2013) 245107.

[48] E. Ilievski, J. De Nardis, B. Wouters, J.-S. Caux, F. H. L. Essler, and T. Prosen, Complete generalized Gibbs ensembles in an interacting theory *Phys. Rev. Lett.* **115** (Oct, 2015) 157201.

[49] B. Wouters, J. De Nardis, M. Brockmann, D. Fioretto, M. Rigol, and J.-S. Caux, Quenching the anisotropic Heisenberg chain: exact solution and generalized Gibbs ensemble predictions *Phys. Rev. Lett.* **113** (Sep, 2014) 117202.

[50] G. Goldstein and N. Andrei, Failure of the local generalized Gibbs ensemble for integrable models with bound states *Phys. Rev. A* **90** (Oct, 2014) 043625.

[51] F. H. L. Essler and M. Fagotti, Quench dynamics and relaxation in isolated integrable quantum spin chains *J. Stat. Mech.* **2016** no. 6, (2016) 064002.

[52] T. Kinoshita, T. Wenger, and D. S. Weiss, A quantum Newton's cradle *Nature* **440** (Apr, 2006) 900–903.

[53] B. Bertini, F. H. L. Essler, S. Groha, and N. J. Robinson, Prethermalization and thermalization in models with weak integrability breaking *Phys. Rev. Lett.* **115** (Oct, 2015) 180601.

[54] B. Bertini, F. H. L. Essler, S. Groha, and N. J. Robinson, Thermalization and light cones in a model with weak integrability breaking *Phys. Rev. B* **94** (Dec, 2016) 245117.

[55] P. W. Anderson, Absence of diffusion in certain random lattices *Phys. Rev.* **109** (Mar, 1958) 1492–1505.

[56] D. Basko, I. Aleiner, and B. Altshuler, Metal–insulator transition in a weakly interacting many-electron system with localized single-particle states *Annals of Physics* **321** no. 5, (2006) 1126–1205.

[57] R. Nandkishore and D. A. Huse, Many-body localization and thermalization in quantum statistical mechanics *Annual Review of Condensed Matter Physics* **6** no. 1, (Mar., 2015) 15–38.

[58] M. Serbyn, Z. Papić, and D. A. Abanin, Universal Slow Growth of Entanglement in Interacting Strongly Disordered Systems *Phys. Rev. Lett.* **110** (Jun, 2013) 260601.

[59] J. Šuntajs, J. Bonča, T. Prosen, and L. Vidmar, Quantum chaos challenges many-body localization *Phys. Rev. E* **102** (Dec, 2020) 062144.

[60] J. Šuntajs, J. Bonča, T. Prosen, and L. Vidmar, Ergodicity breaking transition in finite disordered spin chains *Phys. Rev. B* **102** (Aug, 2020) 064207.

[61] D. Sels and A. Polkovnikov, Dynamical obstruction to localization in a disordered spin chain *Phys. Rev. E* **104** (Nov, 2021) 054105.

[62] M. Kiefer-Emmanouilidis, R. Unanyan, M. Fleischhauer, and J. Sirker, Evidence for unbounded growth of the number entropy in many-body localized phases *Phys. Rev. Lett.* **124** (Jun, 2020) 243601.

[63] D. Abanin, J. Bardarson, G. De Tomasi, S. Gopalakrishnan, V. Khemani, S. Parameswaran, F. Pollmann, A. Potter, M. Serbyn, and R. Vasseur, Distinguishing localization from chaos: challenges in finite-size systems *Annals of Physics* **427** (Apr., 2021) 168415.

[64] P. Sala, T. Rakovszky, R. Verresen, M. Knap, and F. Pollmann, Ergodicity breaking arising from Hilbert space fragmentation in dipole-conserving Hamiltonians *Phys. Rev. X* **10** (Feb, 2020) 011047.

[65] V. Khemani, M. Hermele, and R. Nandkishore, Localization from Hilbert space shattering: From theory to physical realizations *Phys. Rev. B* **101** (May, 2020) 174204.

[66] T. Rakovszky, P. Sala, R. Verresen, M. Knap, and F. Pollmann, Statistical localization: From strong fragmentation to strong edge modes *Phys. Rev. B* **101** (Mar, 2020) 125126.

[67] C. J. Turner, A. A. Michailidis, D. A. Abanin, M. Serbyn, and Z. Papić, Weak ergodicity breaking from quantum many-body scars *Nature Physics* **14** no. 7, (Jul, 2018) 745–749.

[68] S. Moudgalya, N. Regnault, and B. A. Bernevig, Entanglement of exact excited states of Affleck-Kennedy-Lieb-Tasaki models: Exact results, many-body scars, and violation of the strong eigenstate thermalization hypothesis *Phys. Rev. B* **98** (Dec, 2018) 235156.

[69] M. Serbyn, D. A. Abanin, and Z. Papić, Quantum many-body scars and weak breaking of ergodicity *Nature Physics* **17** no. 6, (Jun, 2021) 675–685.

[70] S. Moudgalya, B. A. Bernevig, and N. Regnault, Quantum many-body scars and Hilbert space fragmentation: a review of exact results *Reports on Progress in Physics* **85** no. 8, (Jul, 2022) 086501.

[71] A. Chandran, T. Iadecola, V. Khemani, and R. Moessner, Quantum many-body scars: A quasiparticle perspective *Annual Review of Condensed Matter Physics* **14** no. Volume 14, 2023, (2023) 443–469.

[72] M. Olshanii, Atomic scattering in the presence of an external confinement and a gas of impenetrable bosons *Phys. Rev. Lett.* **81** (Aug, 1998) 938–941.

[73] E. H. Lieb, R. Seiringer, and J. Yngvason, One-dimensional bosons in three-dimensional traps *Phys. Rev. Lett.* **91** (Oct, 2003) 150401.

[74] J. Yngvason, E. H. Lieb, and R. Seiringer, One-Dimensional Behavior of Dilute, Trapped Bose Gases *Communications in Mathematical Physics* **244** no. 2, (Jan, 2004) 347–393.

[75] R. Coldea, D. A. Tennant, E. M. Wheeler, E. Wawrzynska, D. Prabhakaran, M. Telling, K. Habicht, P. Smeibidl, and K. Kiefer, Quantum criticality in an Ising chain: Experimental evidence for emergent E_8 symmetry *Science* **327** no. 5962, (2010) 177–180.

[76] T. Giamarchi, *Quantum Physics in One Dimension*. Oxford University Press, 12, 2003.

[77] N. D. Mermin and H. Wagner, Absence of ferromagnetism or antiferromagnetism in one- or two-dimensional isotropic Heisenberg models *Phys. Rev. Lett.* **17** (Dec, 1966) 1307–1307.

[78] M. Collura and F. H. L. Essler, How order melts after quantum quenches *Phys. Rev. B* **101** (Jan, 2020) 041110.

[79] J. Cardy, *Scaling and Renormalization in Statistical Physics*. Cambridge Lecture Notes in Physics. Cambridge University Press, 1996.

[80] A. Stern, Anyons and the quantum Hall effect—A pedagogical review *Annals of Physics* **323** no. 1, (2008) 204–249. January Special Issue 2008.

[81] E. Lieb, T. Schultz, and D. Mattis, Two soluble models of an antiferromagnetic chain *Annals of Physics* **16** no. 3, (1961) 407–466.

[82] S. Sachdev, *Quantum Phase Transitions*. Cambridge University Press, 2000.

[83] U. Schollwöck, The density-matrix renormalization group in the age of matrix product states *Annals of Physics* **326** no. 1, (Jan, 2011) 96–192.

[84] S. R. White, Density matrix formulation for quantum renormalization groups *Phys. Rev. Lett.* **69** (Nov, 1992) 2863–2866.

[85] S. R. White, Density-matrix algorithms for quantum renormalization groups *Phys. Rev. B* **48** (Oct, 1993) 10345–10356.

[86] G. Vidal, Efficient classical simulation of slightly entangled quantum computations *Phys. Rev. Lett.* **91** (Oct, 2003) 147902.

[87] G. Vidal, Efficient simulation of one-dimensional quantum many-body systems *Phys. Rev. Lett.* **93** (Jul, 2004) 040502.

[88] P. Silvi, F. Tschirsich, M. Gerster, J. Jünemann, D. Jaschke, M. Rizzi, and S. Montangero, The Tensor Networks Anthology: Simulation techniques for many-body quantum lattice systems *SciPost Phys. Lect. Notes* (2019) 8.

[89] J. Eisert, Entanglement and tensor network states 2013. https://doi.org/10.48550/arXiv.1308.3318.

[90] N. Schuch, M. M. Wolf, F. Verstraete, and J. I. Cirac, Computational complexity of projected entangled pair states *Phys. Rev. Lett.* **98** (Apr, 2007) 140506.

[91] M. Suzuki, Fractal decomposition of exponential operators with applications to many-body theories and Monte Carlo simulations *Physics Letters A* **146** no. 6, (1990) 319–323.

[92] J. Haegeman, J. I. Cirac, T. J. Osborne, I. Pižorn, H. Verschelde, and F. Verstraete, Time-dependent variational principle for quantum lattices *Phys. Rev. Lett.* **107** (Aug, 2011) 070601.

[93] J. Haegeman, C. Lubich, I. Oseledets, B. Vandereycken, and F. Verstraete, Unifying time evolution and optimization with matrix product states *Phys. Rev. B* **94** (Oct, 2016) 165116.

[94] P. Weinberg and M. Bukov, QuSpin: a Python package for dynamics and exact diagonalisation of quantum many body systems part I: spin chains *SciPost Physics* **2** no. 1, (Feb, 2017) 003.

[95] P. Weinberg and M. Bukov, QuSpin: a Python package for dynamics and exact diagonalisation of quantum many body systems. Part II: bosons, fermions and higher spins *SciPost Phys.* **7** (2019) 020.

[96] M. Gaudin, Une démonstration simplifiée du théorème de wick en mécanique statistique *Nuclear Physics* **15** (1960) 89–91.

[97] E. R. Caianiello and S. Fubini, On the algorithm of Dirac spurs *Il Nuovo Cimento (1943-1954)* **9** no. 12, (Dec, 1952) 1218–1226.

[98] G. Del Vecchio Del Vecchio and B. Doyon, The hydrodynamic theory of dynamical correlation functions in the XX chain *Journal of Statistical Mechanics: Theory and Experiment* **2022** no. 5, (May, 2022) 053102.

[99] M. Wimmer, Algorithm 923: efficient numerical computation of the Pfaffian for dense and banded skew-symmetric matrices *ACM Trans. Math. Softw.* **38** no. 4, (Aug, 2012) 1–17.

[100] P. Calabrese, F. H. L. Essler, and M. Fagotti, Quantum quench in the transverse-field Ising chain *Phys. Rev. Lett.* **106** (Jun, 2011) 227203.

[101] P. Calabrese, F. H. L. Essler, and M. Fagotti, Quantum quench in the transverse field Ising chain: I. Time evolution of order parameter correlators *Journal of Statistical Mechanics: Theory and Experiment* **2012** no. 07, (July, 2012) P07016.

[102] F. H. L. Essler, S. Evangelisti, and M. Fagotti, Dynamical correlations after a quantum quench *Physical Review Letters* **109** no. 24, (2012) 247206.

[103] H. Dreyer, M. Bejan, and E. Granet, Quantum computing critical exponents *Phys. Rev. A* **104** (Dec, 2021) 062614.

[104] E. Granet, H. Dreyer, and F. Essler, Out-of-equilibrium dynamics of the XY spin chain from form factor expansion *SciPost Physics* **12** no. 1, (2022) 019.

[105] S. Bhattacharyya, S. Dasgupta, and A. Das, Signature of a continuous quantum phase transition in non-equilibrium energy absorption: Footprints of criticality on higher excited states *Scientific Reports* **5** no. 1, (Nov, 2015) 16490.

[106] A. Haldar, K. Mallayya, M. Heyl, F. Pollmann, M. Rigol, and A. Das, Signatures of quantum phase transitions after quenches in quantum chaotic one-dimensional systems *Phys. Rev. X* **11** (Sep, 2021) 031062.

[107] F. H. L. Essler and M. Fagotti, Quench dynamics and relaxation in isolated integrable quantum spin chains *Journal of Statistical Mechanics: Theory and Experiment* **2016** no. 6, (Jun, 2016) 064002.

[108] M. Cazalilla and M.-C. Chung, Quantum quenches in the Luttinger model and its close relatives *Journal of Statistical Mechanics: Theory and Experiment* **2016** no. 6, (2016) 064004.

[109] W. S. Bakr, A. Peng, M. E. Tai, R. Ma, J. Simon, J. I. Gillen, S. Fölling, L. Pollet, and M. Greiner, Probing the superfluid–to–Mott insulator transition at the single-atom level *Science* **329** no. 5991, (2010) 547–550.

[110] F. Meinert, M. J. Mark, E. Kirilov, K. Lauber, P. Weinmann, A. J. Daley, and H.-C. Nägerl, Quantum quench in an atomic one-dimensional Ising chain *Phys. Rev. Lett.* **111** (Jul, 2013) 053003.

[111] Y. Takasu, T. Yagami, H. Asaka, Y. Fukushima, K. Nagao, S. Goto, I. Danshita, and Y. Takahashi, Energy redistribution and spatiotemporal evolution of correlations after a sudden quench of the Bose-Hubbard model *Science Advances* **6** no. 40, (2020) eaba9255.

[112] M. Heyl, F. Pollmann, and B. Dóra, Detecting equilibrium and dynamical quantum phase transitions in Ising chains via out-of-time-ordered correlators *Phys. Rev. Lett.* **121** (Jul, 2018) 016801.

[113] P. Titum, J. T. Iosue, J. R. Garrison, A. V. Gorshkov, and Z.-X. Gong, Probing ground-state phase transitions through quench dynamics *Phys. Rev. Lett.* **123** (Sep, 2019) 115701.

[114] C. B. Dağ, P. Uhrich, Y. Wang, I. P. McCulloch, and J. C. Halimeh, Detecting quantum phase transitions in the quasi-stationary regime of Ising chains 2021. https://arxiv.org/abs/2110.02995.

[115] S. Paul, P. Titum, and M. F. Maghrebi, Hidden Quantum Criticality and Entanglement in Quench Dynamics 2022. https://arxiv.org/abs/2202.04654.

[116] I. Peschel and V. J. Emery, Calculation of spin correlations in two-dimensional Ising systems from one-dimensional kinetic models *Zeitschrift für Physik B Condensed Matter* **43** (Sep, 1981) 241–249.

[117] W. Selke, The ANNNI model — Theoretical analysis and experimental application *Physics Reports* **170** no. 4, (1988) 213–264.

[118] A. K. Chandra and S. Dasgupta, Floating phase in the one-dimensional transverse axial next-nearest-neighbor Ising model *Phys. Rev. E* **75** (Feb, 2007) 021105.

[119] C. Karrasch and D. Schuricht, Dynamical phase transitions after quenches in nonintegrable models *Phys. Rev. B* **87** (May, 2013) 195104.

[120] D. Allen, P. Azaria, and P. Lecheminant, A two-leg quantum Ising ladder: a bosonization study of the ANNNI model *Journal of Physics A: Mathematical and General* **34** no. 21, (2001) L305.

[121] M. Beccaria, M. Campostrini, and A. Feo, Evidence for a floating phase of the transverse ANNNI model at high frustration *Phys. Rev. B* **76** (Sep, 2007) 094410.

[122] S. Suzuki, J.-i. Inoue, and B. K. Chakrabarti, *Quantum Ising phases and transitions in transverse Ising models*, vol. 862. Springer, 2012.

[123] A. Y. Kitaev, Unpaired Majorana fermions in quantum wires *Physics-Uspekhi* **44** no. 10S, (Oct, 2001) 131.

[124] C. Itzykson and J.-M. Drouffe, *Statistical Field Theory*, vol. 1 of *Cambridge Monographs on Mathematical Physics*. Cambridge University Press, 1989.

[125] A. Polkovnikov, K. Sengupta, A. Silva, and M. Vengalattore, Colloquium: Nonequilibrium dynamics of closed interacting quantum systems *Rev. Mod. Phys.* **83** (Aug, 2011) 863–883.

[126] M. Rigol, Quantum quenches in the thermodynamic limit *Phys. Rev. Lett.* **112** (Apr, 2014) 170601.

[127] M. Rigol, Fundamental asymmetry in quenches between integrable and nonintegrable systems *Phys. Rev. Lett.* **116** (Mar, 2016) 100601.

[128] D. Boyanovsky, F. Cooper, H. J. de Vega, and P. Sodano, Evolution of inhomogeneous condensates: Self-consistent variational approach *Phys. Rev. D* **58** (Jun, 1998) 025007.

[129] S. Sotiriadis and J. Cardy, Quantum quench in interacting field theory: A self-consistent approximation *Phys. Rev. B* **81** (Apr, 2010) 134305.

[130] Y. D. van Nieuwkerk and F. H. L. Essler, Self-consistent time-dependent harmonic approximation for the sine-Gordon model out of equilibrium *Journal of Statistical Mechanics: Theory and Experiment* **2019** no. 8, (Aug, 2019) 084012.

[131] A. Lerose, B. Žunkovič, J. Marino, A. Gambassi, and A. Silva, Impact of nonequilibrium fluctuations on prethermal dynamical phase transitions in long-range interacting spin chains *Physical Review B* **99** no. 4, (2019) 045128.

[132] M. Collura and F. H. L. Essler, How order melts after quantum quenches *Phys. Rev. B* **101** (Jan, 2020) 041110.

[133] Y. D. van Nieuwkerk and F. H. L. Essler, On the low-energy description for tunnel-coupled one-dimensional Bose gases *SciPost Physics* **9** no. 2, (Aug, 2020) 025.

[134] Y. D. van Nieuwkerk, J. Schmiedmayer, and F. H. L. Essler, Josephson oscillations in split one-dimensional Bose gases *SciPost Physics* **10** no. 4, (Apr, 2021) 090.

[135] M. Moeckel and S. Kehrein, Real-time evolution for weak interaction quenches in quantum systems *Annals of Physics* **324** no. 10, (2009) 2146–2178.

[136] M. Moeckel and S. Kehrein, Crossover from adiabatic to sudden interaction quenches in the Hubbard model: prethermalization and non-equilibrium dynamics *New Journal of Physics* **12** no. 5, (2010) 055016.

[137] F. H. L. Essler, S. Kehrein, S. R. Manmana, and N. J. Robinson, Quench dynamics in a model with tuneable integrability breaking *Phys. Rev. B* **89** (Apr, 2014) 165104.

[138] N. Nessi and A. Iucci, Equations of motion for the out-of-equilibrium dynamics of isolated quantum systems from the projection operator technique *Journal of Physics: Conference Series* **568** no. 1, (Dec, 2014) 012013.

[139] N. Nessi and A. Iucci, Glass-like behavior in a system of one dimensional fermions after a quantum quench 2015. https://arxiv.org/abs/1503.02507.

[140] S. Bravyi, M. B. Hastings, and F. Verstraete, Lieb-Robinson bounds and the generation of correlations and topological quantum order *Physical review letters* **97** no. 5, (2006) 050401.

[141] E. Barouch and B. M. McCoy, Statistical mechanics of the XY model. II. Spin-correlation functions *Physical Review A* **3** no. 2, (1971) 786.

[142] C.-J. Lin and O. I. Motrunich, Quasiparticle explanation of the weak-thermalization regime under quench in a nonintegrable quantum spin chain *Phys. Rev. A* **95** (Feb, 2017) 023621.

[143] M. Kormos, M. Collura, G. Takács, and P. Calabrese, Real-time confinement following a quantum quench to a non-integrable model *Nature Physics* **13** no. 3, (Nov, 2016) 246–249.

[144] M. Collura, M. Kormos, and G. Takács, Dynamical manifestation of the Gibbs paradox after a quantum quench *Phys. Rev. A* **98** (Nov, 2018) 053610.

[145] O. Pomponio, L. Pristyák, and G. Takács, Quasi-particle spectrum and entanglement generation after a quench in the quantum Potts spin chain *Journal of Statistical Mechanics: Theory and Experiment* **2019** no. 1, (Jan, 2019) 013104.

[146] N. J. Robinson, A. J. A. James, and R. M. Konik, Signatures of rare states and thermalization in a theory with confinement *Phys. Rev. B* **99** (May, 2019) 195108.

[147] B. Blaß and H. Rieger, Test of quantum thermalization in the two-dimensional transverse-field Ising model *Scientific Reports* **6** no. 1, (Dec, 2016) 38185.

[148] L. Villa, J. Despres, and L. Sanchez-Palencia, Unraveling the excitation spectrum of many-body systems from quantum quenches *Phys. Rev. A* **100** (Dec, 2019) 063632.

[149] L. Villa, J. Despres, S. J. Thomson, and L. Sanchez-Palencia, Local quench spectroscopy of many-body quantum systems *Phys. Rev. A* **102** (Sep, 2020) 033337.

[150] M. C. Bañuls, J. I. Cirac, and M. B. Hastings, Strong and weak thermalization of infinite nonintegrable quantum systems *Phys. Rev. Lett.* **106** (Feb, 2011) 050405.

[151] K. Hódsági, M. Kormos, and G. Takács, Quench dynamics of the Ising field theory in a magnetic field *SciPost Phys.* **5** (2018) 027.

[152] O. A. Castro-Alvaredo, M. Lencsés, I. M. Szécsényi, and J. Viti, Entanglement oscillations near a quantum critical point *Phys. Rev. Lett.* **124** (Jun, 2020) 230601.

[153] S. Scopa, P. Calabrese, and A. Bastianello, Entanglement dynamics in confining spin chains *Phys. Rev. B* **105** (Mar, 2022) 125413.

[154] J. Vovrosh, R. Mukherjee, A. Bastianello, and J. Knolle, Dynamical hadron formation in long-range interacting quantum spin chains *PRX Quantum* **3** (Oct, 2022) 040309.

[155] S. Birnkammer, A. Bastianello, and M. Knap, Prethermalization in one-dimensional quantum many-body systems with confinement *Nature Communications* **13** no. 1, (Dec, 2022) 7663.

[156] O. Pomponio, L. Pristyák, and G. Takács, Quasi-particle spectrum and entanglement generation after a quench in the quantum Potts spin chain *Journal of Statistical Mechanics: Theory and Experiment* **2019** no. 1, (Jan, 2019) 013104.

[157] G. Delfino, Quantum quenches with integrable pre-quench dynamics *Journal of Physics A: Mathematical and Theoretical* **47** no. 40, (Sep, 2014) 402001.

[158] G. Delfino and J. Viti, On the theory of quantum quenches in near-critical systems *Journal of Physics A: Mathematical and Theoretical* **50** no. 8, (Jan, 2017) 084004.

[159] G. Delfino, Persistent oscillations after quantum quenches: The inhomogeneous case *Nuclear Physics B* **954** (2020) 115002.

[160] G. Delfino and M. Sorba, Persistent oscillations after quantum quenches in d dimensions *Nuclear Physics B* **974** (Jan, 2022) 115643.

[161] F. D. M. Haldane, Continuum dynamics of the 1-D Heisenberg antiferromagnet: Identification with the O(3) nonlinear sigma model *Physics Letters A* **93** no. 9, (1983) 464–468.

[162] F. D. M. Haldane, Nonlinear field theory of large-spin Heisenberg antiferromagnets: Semiclassically quantized solitons of the one-dimensional easy-axis Néel state *Phys. Rev. Lett.* **50** (Apr, 1983) 1153–1156.

[163] F. Balducci, A. Gambassi, A. Lerose, A. Scardicchio, and C. Vanoni, Interface dynamics in the two-dimensional quantum Ising model *Phys. Rev. B* **107** (Jan, 2023) 024306.

[164] M. Magoni, P. P. Mazza, and I. Lesanovsky, Emergent Bloch oscillations in a kinetically constrained Rydberg spin lattice *Phys. Rev. Lett.* **126** (Mar, 2021) 103002.

[165] F. M. Surace, P. P. Mazza, G. Giudici, A. Lerose, A. Gambassi, and M. Dalmonte, Lattice gauge theories and string dynamics in Rydberg atom quantum simulators *Phys. Rev. X* **10** (May, 2020) 021041.

[166] A. Lerose, F. M. Surace, P. P. Mazza, G. Perfetto, M. Collura, and A. Gambassi, Quasilocalized dynamics from confinement of quantum excitations *Phys. Rev. B* **102** (Jul, 2020) 041118.

[167] P. Vorndamme, H.-J. Schmidt, C. Schröder, and J. Schnack, Observation of phase synchronization and alignment during free induction decay of quantum spins with Heisenberg interactions *New Journal of Physics* **23** no. 8, (Aug, 2021) 083038.

[168] P. Reimann, P. Vorndamme, and J. Schnack, Nonequilibration, synchronization, and time crystals in isotropic Heisenberg models *Phys. Rev. Res.* **5** (Oct, 2023) 043040.

[169] N. Bogolûbov, *Lectures on Quantum Statistics, Vol. 2.* Lectures on Quantum Statistics. Gordon and Breach, 1970. https://books.google.co.uk/books?id=kEcf_v4RYCwC.

[170] K. Huang, *Statistical Mechanics, 2nd Ed.* Wiley India Pvt. Limited, 2008. https://books.google.co.uk/books?id=ZHl8HLk-K3AC.

[171] M. Bonitz, *Quantum Kinetic Theory.* Springer International Publishing, 2015. https://books.google.de/books?id=HZ8QswEACAAJ.

[172] A. J. A. James, F. H. L. Essler, and R. M. Konik, Finite-temperature dynamical structure factor of alternating Heisenberg chains *Phys. Rev. B* **78** (Sep, 2008) 094411.

[173] W. D. Goetze, U. Karahasanovic, and F. H. L. Essler, Low-temperature dynamical structure factor of the two-leg spin-$\frac{1}{2}$ Heisenberg ladder *Phys. Rev. B* **82** (Sep, 2010) 104417.

[174] F. H. L. Essler and R. M. Konik, Finite-temperature lineshapes in gapped quantum spin chains *Phys. Rev. B* **78** (Sep, 2008) 100403.

[175] B. Pozsgay and G. Takács, Form factors in finite volume II: Disconnected terms and finite temperature correlators *Nuclear Physics B* **788** no. 3, (Jan, 2008) 209–251.

[176] F. H. L. Essler and R. M. Konik, Finite-temperature dynamical correlations in massive integrable quantum field theories *Journal of Statistical Mechanics: Theory and Experiment* **2009** no. 09, (2009) P09018.

[177] B. Pozsgay and G. Takács, Form factor expansion for thermal correlators *Journal of Statistical Mechanics: Theory and Experiment* **2010** no. 11, (Nov, 2010) P11012.

[178] E. Granet, M. Fagotti, and F. H. L. Essler, Finite temperature and quench dynamics in the Transverse Field Ising Model from form factor expansions *SciPost Phys.* **9** (2020) 033.

[179] M. Fava, S. Gopalakrishnan, R. Vasseur, F. Essler, and S. A. Parameswaran, Divergent nonlinear response from quasiparticle interactions *Phys. Rev. Lett.* **131** (Dec, 2023) 256505.

[180] P. Reimann, B. N. Balz, J. Richter, and R. Steinigeweg, Temporal relaxation of gapped many-body quantum systems *Phys. Rev. B* **101** (Mar, 2020) 094302.

[181] Y. Xian, Spontaneous trimerization of spin-1 chains *Journal of Physics: Condensed Matter* **5** no. 40, (Oct, 1993) 7489.

[182] A. Läuchli, G. Schmid, and S. Trebst, Spin nematics correlations in bilinear-biquadratic $S = 1$ spin chains *Phys. Rev. B* **74** (Oct, 2006) 144426.

[183] M. Binder and T. Barthel, Infinite boundary conditions for response functions and limit cycles within the infinite-system density matrix renormalization group approach demonstrated for bilinear-biquadratic spin-1 chains *Phys. Rev. B* **98** (Dec, 2018) 235114.

[184] I. Affleck, T. Kennedy, E. H. Lieb, and H. Tasaki, Rigorous results on valence-bond ground states in antiferromagnets *Phys. Rev. Lett.* **59** (Aug, 1987) 799–802.

[185] C. K. Lai, Lattice gas with nearest-neighbor interaction in one dimension with arbitrary statistics *Journal of Mathematical Physics* **15** no. 10, (11, 2003) 1675–1676.

[186] B. Sutherland, Model for a multicomponent quantum system *Phys. Rev. B* **12** (Nov, 1975) 3795–3805.

[187] M. Fishman, S. R. White, and E. M. Stoudenmire, The ITensor software library for tensor network calculations 2020. `https://arxiv.org/abs/2007.14822`.

[188] S. Hermanns, K. Balzer, and M. Bonitz, Few-particle quantum dynamics–comparing nonequilibrium Green functions with the generalized Kadanoff–Baym ansatz to density operator theory *Journal of Physics: Conference Series* **427** no. 1, (Mar, 2013) 012008.

[189] F. H. L. Essler and R. M. Konik, Application of massive integrable quantum field theories to problems in condensed matter physics in *From Fields to Strings: Circumnavigating Theoretical Physics*, pp. 684–830. World Scientific, Feb, 2005.

[190] H. Kim and D. A. Huse, Ballistic spreading of entanglement in a diffusive nonintegrable system *Phys. Rev. Lett.* **111** (Sep, 2013) 127205.

[191] A. Lazarides, A. Das, and R. Moessner, Equilibrium states of generic quantum systems subject to periodic driving *Phys. Rev. E* **90** (Jul, 2014) 012110.

[192] D. Rossini, R. Fazio, V. Giovannetti, and A. Silva, Quantum quenches, linear response and superfluidity out of equilibrium *EPL (Europhysics Letters)* **107** no. 3, (Jul, 2014) 30002.

[193] C. Lei, S. Peng, C. Ju, M.-H. Yung, and J. Du, Decoherence control of nitrogen-vacancy centers *Scientific Reports* **7** no. 1, (Sep, 2017) 11937.

[194] K. Georgopoulos, C. Emary, and P. Zuliani, Modeling and simulating the noisy behavior of near-term quantum computers *Phys. Rev. A* **104** (Dec, 2021) 062432.

[195] P. Hauke, F. M. Cucchietti, L. Tagliacozzo, I. Deutsch, and M. Lewenstein, Can one trust quantum simulators? *Reports on Progress in Physics* **75** no. 8, (Jul, 2012) 082401.

[196] A. J. Daley, Quantum trajectories and open many-body quantum systems *Adv. Phys.* **63** no. 2, (2014) 77–149.

[197] L. Bonnes and A. M. Läuchli, Superoperators vs. trajectories for matrix product state simulations of open quantum system: A case study 2014. https://doi.org/10.48550/arXiv.1411.4831.

[198] J. Cui, J. I. Cirac, and M. C. Bañuls, Variational matrix product operators for the steady state of dissipative quantum systems *Phys. Rev. Lett.* **114** (Jun, 2015) 220601.

[199] A. H. Werner, D. Jaschke, P. Silvi, M. Kliesch, T. Calarco, J. Eisert, and S. Montangero, Positive Tensor Network Approach for Simulating Open Quantum Many-Body Systems *Phys. Rev. Lett.* **116** (Jun, 2016) 237201.

[200] H. Weimer, A. Kshetrimayum, and R. Orús, Simulation methods for open quantum many-body systems *Rev. Mod. Phys.* **93** (Mar, 2021) 015008.

[201] A. C. Li, F. Petruccione, and J. Koch, Perturbative approach to Markovian open quantum systems *Sci. Rep.* **4** (2014) 4887.

[202] L. M. Sieberer, M. Buchhold, and S. Diehl, Keldysh field theory for driven open quantum systems *Rep. Prog. Phys.* **79** no. 9, (2016) 096001.

[203] L. Bertini, A. De Sole, D. Gabrielli, G. Jona-Lasinio, and C. Landim, Fluctuations in stationary nonequilibrium states of irreversible processes *Phys. Rev. Lett.* **87** (Jul, 2001) 040601.

[204] L. Bertini, A. D. Sole, D. Gabrielli, G. Jona-Lasinio, and C. Landim, Stochastic interacting particle systems out of equilibrium *Journal of Statistical Mechanics: Theory and Experiment* **2007** no. 07, (July, 2007) P07014–P07014.

[205] L. Bertini, A. De Sole, D. Gabrielli, G. Jona-Lasinio, and C. Landim, Macroscopic fluctuation theory *Rev. Mod. Phys.* **87** (Jun, 2015) 593–636.

[206] M. Bauer, D. Bernard, and T. Jin, Stochastic dissipative quantum spin chains (I) : Quantum fluctuating discrete hydrodynamics *SciPost Phys.* **3** (2017) 033.

[207] D. Bernard and T. Jin, Open quantum symmetric simple exclusion process *Phys. Rev. Lett.* **123** (Aug, 2019) 080601.

[208] T. Jin, A. Krajenbrink, and D. Bernard, From stochastic spin chains to quantum Kardar-Parisi-Zhang dynamics *Phys. Rev. Lett.* **125** (Jul, 2020) 040603.

[209] D. Bernard, F. H. L. Essler, L. Hruza, and M. Medenjak, Dynamics of fluctuations in quantum simple exclusion processes *SciPost Phys.* **12** (2022) 042.

[210] S. Diehl, A. Micheli, A. Kantian, B. Kraus, H. P. Büchler, and P. Zoller, Quantum states and phases in driven open quantum systems with cold atoms *Nature Physics* **4** no. 11, (Nov, 2008) 878–883.

[211] B. Kraus, H. P. Büchler, S. Diehl, A. Kantian, A. Micheli, and P. Zoller, Preparation of entangled states by quantum Markov processes *Phys. Rev. A* **78** (Oct, 2008) 042307.

[212] F. Verstraete, M. M. Wolf, and J. Ignacio Cirac, Quantum computation and quantum-state engineering driven by dissipation *Nature Physics* **5** no. 9, (Sep, 2009) 633–636.

[213] S. Diehl, E. Rico, M. A. Baranov, and P. Zoller, Topology by dissipation in atomic quantum wires *Nature Physics* **7** no. 12, (Dec, 2011) 971–977.

[214] C.-E. Bardyn, M. A. Baranov, C. V. Kraus, E. Rico, A. İmamoğlu, P. Zoller, and S. Diehl, Topology by dissipation *New Journal of Physics* **15** no. 8, (Aug, 2013) 085001.

[215] K. Stannigel, P. Hauke, D. Marcos, M. Hafezi, S. Diehl, M. Dalmonte, and P. Zoller, Constrained Dynamics via the Zeno Effect in Quantum Simulation: Implementing Non-Abelian Lattice Gauge Theories with Cold Atoms *Phys. Rev. Lett.* **112** (Mar, 2014) 120406.

[216] V. Gorini, A. Kossakowski, and E. C. G. Sudarshan, Completely positive dynamical semigroups of N-level systems *J. Math. Phys.* **17** no. 5, (1976) 821–825.

[217] G. Lindblad, On the generators of quantum dynamical semigroups *Comm. Math. Phys.* **48** no. 2, (1976) 119–130.

[218] H.-P. Breuer and F. Petruccione, *The theory of open quantum systems*. Oxford University Press on Demand, 2002.

[219] W. F. Stinespring, Positive Functions on C*-Algebras *Proceedings of the American Mathematical Society* **6** no. 2, (1955) 211–216.

[220] T. Prosen, Third quantization: a general method to solve master equations for quadratic open Fermi systems *New J. Phys.* **10** no. 4, (2008) 043026.

[221] J. Eisert and T. Prosen, Noise-driven quantum criticality 2010. https://doi.org/10.48550/arXiv.1012.5013.

[222] T. Prosen, Spectral theorem for the Lindblad equation for quadratic open fermionic systems *J. Stat. Mech.* **2010** no. 07, (2010) P07020.

[223] S. Clark, J. Prior, M. Hartmann, D. Jaksch, and M. B. Plenio, Exact matrix product solutions in the Heisenberg picture of an open quantum spin chain *New J. Phys.* **12** no. 2, (2010) 025005.

[224] B. Horstmann, J. I. Cirac, and G. Giedke, Noise-driven dynamics and phase transitions in fermionic systems *Phys. Rev. A* **87** (Jan, 2013) 012108.

[225] M. Keck, S. Montangero, G. E. Santoro, R. Fazio, and D. Rossini, Dissipation in adiabatic quantum computers: lessons from an exactly solvable model *New J. Phys.* **19** no. 11, (2017) 113029.

[226] E. Vernier, Mixing times and cutoffs in open quadratic fermionic systems *SciPost Phys.* **9** (2020) 49.

[227] S. Maity, S. Bandyopadhyay, S. Bhattacharjee, and A. Dutta, Growth of mutual information in a quenched one-dimensional open quantum many-body system *Phys. Rev. B* **101** (May, 2020) 180301.

[228] V. Alba and F. Carollo, Spreading of correlations in Markovian open quantum systems *Phys. Rev. B* **103** (Jan, 2021) L020302.

[229] M. V. Medvedyeva, F. H. L. Essler, and T. Prosen, Exact Bethe ansatz spectrum of a tight-binding chain with dephasing noise *Phys. Rev. Lett.* **117** (Sep, 2016) 137202.

[230] D. A. Rowlands and A. Lamacraft, Noisy coupled qubits: Operator spreading and the Fredrickson-Andersen model *Phys. Rev. B* **98** (Nov, 2018) 195125.

[231] N. Shibata and H. Katsura, Dissipative quantum Ising chain as a non-Hermitian Ashkin-Teller model *Phys. Rev. B* **99** (Jun, 2019) 224432.

[232] N. Shibata and H. Katsura, Dissipative spin chain as a non-Hermitian Kitaev ladder *Phys. Rev. B* **99** (May, 2019) 174303.

[233] A. A. Ziolkowska and F. H. L. Essler, Yang-Baxter integrable Lindblad equations *SciPost Phys.* **8** (2020) 044.

[234] M. Nakagawa, N. Kawakami, and M. Ueda, Exact Liouvillian spectrum of a one-dimensional dissipative Hubbard model *Phys. Rev. Lett.* **126** (Mar, 2021) 110404.

[235] B. Buca, C. Booker, M. Medenjak, and D. Jaksch, Dissipative Bethe Ansatz: Exact Solutions of Quantum Many-Body Dynamics Under Loss 2020. https://doi.org/10.48550/arXiv.2004.05955.

[236] P. Ribeiro and T. Prosen, Integrable quantum dynamics of open collective spin models *Phys. Rev. Lett.* **122** (Jan, 2019) 010401.

[237] S. Lerma-Hernández, A. Rubio-García, and J. Dukelsky, Trigonometric SU(N) Richardson–Gaudin models and dissipative multi-level atomic systems *Journal of Physics A: Mathematical and Theoretical* **53** no. 39, (Aug, 2020) 395302.

[238] D. Yuan, H.-R. Wang, Z. Wang, and D.-L. Deng, Solving the Liouvillian gap with artificial neural networks *Phys. Rev. Lett.* **126** (Apr, 2021) 160401.

[239] M. de Leeuw, C. Paletta, and B. Pozsgay, Constructing integrable Lindblad superoperators *Phys. Rev. Lett.* **126** (Jun, 2021) 240403.

[240] J. M. Torres, Closed-form solution of Lindblad master equations without gain *Phys. Rev. A* **89** (May, 2014) 052133.

[241] V. Eisler, Crossover between ballistic and diffusive transport: the quantum exclusion process *J. Stat. Mech.* **2011** no. 06, (2011) P06007.

[242] B. Žunkovič, Closed hierarchy of correlations in Markovian open quantum systems *New J. Phys.* **16** no. 1, (2014) 013042.

[243] S. Caspar, F. Hebenstreit, D. Mesterhazy, and U.-J. Wiese, Dissipative Bose–Einstein condensation in contact with a thermal reservoir *New J. Phys.* **18** no. 7, (2016) 073015.

[244] S. Caspar, F. Hebenstreit, D. Mesterházy, and U.-J. Wiese, Dynamics of dissipative Bose-Einstein condensation *Phys. Rev. A* **93** (Feb, 2016) 021602.

[245] D. Mesterházy and F. Hebenstreit, Solvable Markovian dynamics of lattice quantum spin models *Phys. Rev. A* **96** (Jul, 2017) 010104.

[246] M. Foss-Feig, J. T. Young, V. V. Albert, A. V. Gorshkov, and M. F. Maghrebi, Solvable family of driven-dissipative many-body systems *Phys. Rev. Lett.* **119** (Nov, 2017) 190402.

[247] I. Klich, Closed hierarchies and non-equilibrium steady states of driven systems *Ann. Phys.* **404** (2019) 66–80.

[248] F. H. L. Essler and L. Piroli, Integrability of one-dimensional Lindbladians from operator-space fragmentation *Phys. Rev. E* **102** (Dec, 2020) 062210.

[249] F. Spitzer, Interaction of Markov processes *Adv. Math.* **5** no. 2, (1970) 246 – 290.

[250] T. M. Liggett, *Interacting Particle Systems*. Springer, New York, 1985.

[251] B. Derrida, An exactly soluble non-equilibrium system: The asymmetric simple exclusion process *Phys. Rep.* **301** no. 1, (1998) 65 – 83.

[252] G. M. Schütz, *Exactly Solvable Models for Many-Body Systems Far From Equilibrium*. in Phase Transitions and Critical Phenomena 19, pp. 1 - 251, C. Domb und J. Lebowitz (eds.) Academic Press, London, 2000.

[253] L.-H. Gwa and H. Spohn, Six-vertex model, roughened surfaces, and an asymmetric spin Hamiltonian *Phys. Rev. Lett.* **68** (Feb, 1992) 725–728.

[254] L.-H. Gwa and H. Spohn, Bethe solution for the dynamical-scaling exponent of the noisy Burgers equation *Phys. Rev. A* **46** (Jul, 1992) 844–854.

[255] D. Kim, Bethe ansatz solution for crossover scaling functions of the asymmetric XXZ chain and the Kardar-Parisi-Zhang-type growth model *Phys. Rev. E* **52** (Oct, 1995) 3512–3524.

[256] O. Golinelli and K. Mallick, Bethe ansatz calculation of the spectral gap of the asymmetric exclusion process *J. Phys. A: Math. Gen.* **37** no. 10, (2004) 3321.

[257] J. de Gier and F. H. L. Essler, Bethe ansatz solution of the asymmetric exclusion process with open boundaries *Phys. Rev. Lett.* **95** (Dec, 2005) 240601.

[258] J. De Gier and F. H. L. Essler, Exact spectral gaps of the asymmetric exclusion process with open boundaries *J. Stat. Mech.* **2006** no. 12, (2006) P12011.

[259] J. de Gier and F. H. L. Essler, Slowest relaxation mode of the partially asymmetric exclusion process with open boundaries *J. Phys. A: Math. Theor.* **41** no. 48, (2008) 485002.

[260] K. Mallick, Some exact results for the exclusion process *J. Stat. Mech.* **2011** no. 01, (2011) P01024.

[261] N. Crampé, E. Ragoucy, and D. Simon, Matrix coordinate Bethe ansatz: applications to XXZ and ASEP models *J. Phys. A: Math. Theor.* **44** no. 40, (2011) 405003.

[262] M. Bauer, D. Bernard, and T. Jin, Equilibrium fluctuations in maximally noisy extended quantum systems *SciPost Phys.* **6** (2019) 45.

[263] D. Bernard and T. Jin, Solution to the quantum symmetric simple exclusion process: The continuous case *Communications in Mathematical Physics* **384** no. 2, (Apr., 2021) 1141–1185.

[264] R. Frassek, C. Giardinà, and J. Kurchan, Duality in quantum transport models *SciPost Phys.* **10** (2021) 135.

[265] B. Derrida, M. R. Evans, and D. Mukamel, Exact diffusion constant for one-dimensional asymmetric exclusion models *Journal of Physics A: Mathematical and General* **26** no. 19, (Oct, 1993) 4911–4918.

[266] L. Bertini, A. De Sole, D. Gabrielli, G. Jona-Lasinio, and C. Landim, Macroscopic fluctuation theory for stationary non-equilibrium states *J. Stat. Phys.* **107** (2002) 635.

[267] T. Bodineau and B. Derrida, Current fluctuations in nonequilibrium diffusive systems: An additivity principle *Phys. Rev. Lett.* **92** (May, 2004) 180601.

[268] L. Bertini, A. De Sole, D. Gabrielli, G. Jona-Lasinio, and C. Landim, Current fluctuations in stochastic lattice gases *Phys. Rev. Lett.* **94** no. 3, (2005) 030601.

[269] B. Derrida, Non-equilibrium steady states: fluctuations and large deviations of the density and of the current *Journal of Statistical Mechanics: Theory and Experiment* **2007** no. 07, (Jul, 2007) P07023–P07023.

[270] J. de Gier and F. H. L. Essler, Large deviation function for the current in the open asymmetric simple exclusion process *Phys. Rev. Lett.* **107** (Jun, 2011) 010602.

[271] A. Lazarescu and K. Mallick, An exact formula for the statistics of the current in the TASEP with open boundaries *Journal of Physics A: Mathematical and Theoretical* **44** no. 31, (Jul, 2011) 315001.

[272] S. Moudgalya, A. Prem, R. Nandkishore, N. Regnault, and B. A. Bernevig, *Thermalization and its absence within Krylov subspaces of a constrained hamiltonian*, p. 147–209. World Scientific, Sept., 2021.

[273] T. Prosen, Third quantization: a general method to solve master equations for quadratic open Fermi systems *New Journal of Physics* **10** no. 4, (Apr, 2008) 043026.

[274] J. E. Santos, G. M. Schütz, and R. B. Stinchcombe, Diffusion–annihilation dynamics in one spatial dimension *J. Chem. Phys.* **105** (1996) 2399.

[275] P.-A. Bares and M. Mobilia, Solution of classical stochastic one-dimensional many-body systems *Phys. Rev. Lett.* **83** (Dec, 1999) 5214–5217.

[276] M. Mobilia and P.-A. Bares, Exact solution of a class of one-dimensional nonequilibrium stochastic models *Phys. Rev. E* **63** (Apr, 2001) 056112.

[277] N. Crampe, E. Ragoucy, V. Rittenberg, and M. Vanicat, Integrable dissipative exclusion process: Correlation functions and physical properties *Phys. Rev. E* **94** (Sep, 2016) 032102.

[278] A. Ziółkowska, *Tales of instability and decay: an integrable perspective*. PhD thesis, University of Oxford, 2021.

[279] M. Fagotti and P. Calabrese, Entanglement entropy of two disjoint blocks in XY chains *Journal of Statistical Mechanics: Theory and Experiment* **2010** no. 04, (Apr, 2010) P04016.